

IN-SITU TESTING OF A DARRIEUS HYDRO KINETIC TURBINE IN  
COLD CLIMATES

by

Shamez Kassam

A Thesis submitted to the Faculty of Graduate Studies of

The University of Manitoba

in partial fulfilment of the requirements of the degree of

MASTER OF SCIENCE  
in  
MECHANICAL ENGINEERING

Department of Mechanical and Manufacturing Engineering

University of Manitoba

Winnipeg, Manitoba, Canada

Copyright © 2009 by Shamez Kassam

**THE UNIVERSITY OF MANITOBA**  
**FACULTY OF GRADUATE STUDIES**  
\*\*\*\*\*  
**COPYRIGHT PERMISSION**

**In-Situ Testing of a Darrieus Hydro Kinetic Turbine in Cold Climates**

**By**

**Shamez Kassam**

**A Thesis/Practicum submitted to the Faculty of Graduate Studies of The University of  
Manitoba in partial fulfillment of the requirement of the degree**

**Of**

**Master of Science**

**Shamez Kassam©2009**

**Permission has been granted to the University of Manitoba Libraries to lend a copy of this thesis/practicum, to Library and Archives Canada (LAC) to lend a copy of this thesis/practicum, and to LAC's agent (UMI/ProQuest) to microfilm, sell copies and to publish an abstract of this thesis/practicum.**

**This reproduction or copy of this thesis has been made available by authority of the copyright owner solely for the purpose of private study and research, and may only be reproduced and copied as permitted by copyright laws or with express written authorization from the copyright owner.**

## Abstract

There is a significant potential for kinetic turbine technology in Canada. An estimated 225 GW of power have been identified in wave and tidal energy with river energy yet to be adequately assessed. Manitoba is an ideal location for river turbines, and thus this study was conducted to demonstrate the turbine's feasibility in cold climates. Frazil ice is a cause for concern in northern regions because it reduces the output power of larger hydro installations and can adversely impact kinetic turbine installations. Along with environmental concerns, a 5 kWe Darrieus turbine was evaluated for its performance. Sources of power loss were quantified in this study. It was found that the turbine's support arms contributed a significant loss of up to 66%. The non-ducted Darrieus design self-started in a flow of 2 m/s and saw a peak power coefficient of 0.35 while producing reliable and consistent power to the grid throughout the winter and summer months.

## Acknowledgements

I would like to acknowledge the tireless efforts of all those intimately involved with the testing performed at Pointe du Bois. I would like to thank Dr. Eric Bibeau and John C. Woods for their contribution towards the fruition of this work. Their physical efforts, both behind the desk and out on the site, made it possible to conduct our research. Their guidance and advice throughout the years has proven to serve as a great start towards my career as an engineer. Much credit must be given to the employees of New Energy Corporation Inc, who made many road trips from their head office in Calgary, Alberta to install, maintain, and test their turbines in the Winnipeg River. Their expertise and contributions facilitated our testing and without them, this project would not have been the success it turned out to be. I am greatly appreciative to the staff at the Pointe du Bois power generating station, from the operations personnel to the staff house service. To all those who supported our project, Manitoba Hydro, NSERC, and WED, I thank you for the opportunity to demonstrate kinetic turbine technology and its viability in Canada. Thank you to all of the technical support representatives who guided me through equipment troubleshooting and finally, to Mustang for their Survival Suits for keeping us warm and safe on the river during a Manitoba winter.



## Table of Contents

Abstract .....	i
Acknowledgements .....	ii
Table of Contents .....	iii
List of Tables.....	ix
List of Figures .....	x
Nomenclature .....	xiv
Nomenclature .....	xiv
Scientific Notation.....	xiv
Abbreviations.....	xv
Chapter 1: Introduction	
1.1 Hydro kinetic power .....	1
1.2 Current estimated capacity .....	2
1.3 Current state of technology.....	3
1.3.1 Extractable power .....	4
1.3.2 Turbine configurations.....	5
1.3.3 Installations and company profiles .....	6
1.4 Environmental challenges in Manitoba .....	9
1.5 Research objectives .....	11

## Chapter 2: Literature Review

2.1	Overview .....	14
2.2	Turbine performance .....	15
2.2.1	Tip speed ratio (TSR).....	16
2.2.2	Numerical models .....	18
2.3	Research and development .....	20
2.3.1	Horizontal axis hydraulic turbine.....	21
2.3.2	Vertical axis hydraulic turbine.....	23
2.3.2	Advantages and disadvantages of turbine configuration .....	25
2.4	Frazil ice .....	26

## Chapter 3: Experimental Setup

3.1	Overview .....	31
3.2	Permits .....	31
3.3	Pointe du Bois test site.....	32
3.4	Turbine and research vessel details .....	36
3.5	Anchoring .....	38
3.6	Data acquisition system (DAQ).....	45
3.7	Network .....	47
3.8	Hardware .....	48
3.8.1	DAQ box .....	48
3.8.2	Video .....	51
3.8.3	Power analyzer .....	52

3.8.4	Data taker .....	54
3.8.5	Sensors .....	54
3.9	Software.....	60
3.9.1	Video system.....	61
3.9.2	Power analyzer.....	62
3.9.3	Data taker .....	62
3.9.4	Scanfile software.....	64
3.9.5	Output.....	65

## Chapter 4: Testing and Deployment

4.1	Overview .....	69
4.2	Test matrix.....	69
4.3	Winter tests.....	71
4.4	Summer tests.....	72
4.5	Initial deployment of the research vessel .....	72
4.6	Turbine deployment.....	77
4.7	Research vessel removal.....	77
4.8	Research vessel redeployment.....	79

## Chapter 5: Turbine Performance

5.1	Overview .....	82
5.2	Performance calculations.....	82
5.2.1	Power measurement .....	83

5.2.2	Water to wire efficiency.....	84
5.2.3	Inverter efficiency .....	85
5.2.4	Rotor efficiency.....	85
5.2.5	Drivetrain power losses.....	86
5.2.6	Overall loss .....	87
5.2.7	Anchor load calculations.....	87
5.3	Flow estimation .....	89
5.3.1	Laboratory calibration.....	90
5.4	Winter testing results .....	93
5.4.1	Power output .....	94
5.5	Modeling power loss due to arms.....	97
5.6	Arm design tests .....	104
5.7	Summer testing results.....	105
5.7.1	Quantification of power loss.....	109
5.7.2	Rotor output .....	112
5.7.3	Anchoring loads .....	114
5.8	Conclusions .....	116

## Chapter 6: Icing

6.1	Testing in cold climates .....	118
6.2	Climate effects on instrumentation.....	121
6.3	Research vessel icing.....	123
6.3.1	Ice formation .....	124

6.3.2	Ice mitigation .....	127
6.3.3	Ice removal.....	129
6.4	Conclusions .....	130

## Chapter 7: ADV Flow Measurements

7.1	Acoustic Doppler velocimetry.....	135
7.2	ADV tests .....	135
7.3	ADV test apparatus.....	137
7.4	ADV deployment.....	138
7.5	ADV flow analysis .....	138
7.5.1	Seeding.....	139
7.5.2	Signal .....	143
7.5.4	Acceleration thresholding method .....	146
7.6	ADV field measurements .....	149

## Chapter 8: Turbine Durability

8.1	Overview .....	153
8.2	Hazardous floating debris.....	153
8.3	Effect on performance .....	159
8.4	Conclusions .....	161

## Chapter 9: Conclusions and Recommendations

9.1	Conclusions .....	162
9.2	Recommendations .....	163
9.3	Contributions.....	165
	References .....	166

## Appendix A: DAQ Start-Up Sequence

A1.1	Boat computer operation .....	172
A1.2	Power analyzer operation.....	174
A1.3	Data taker operation .....	178
A1.4	ATCO computer operation.....	181

## Appendix B: Sensor Specifications

B1	Load cell .....	182
	B1.1 4-wire .....	182
	B1.2 3-wire .....	183
B2	Vibration sensors .....	184
B3	Thermocouples .....	184
B4	Flow meter .....	185
B5	ADV specifications.....	186

	Appendix C: Journal Entries .....	1877
--	-----------------------------------	------

## List of Tables

Table 1: Installations and demonstrations.....	7
Table 2: Major companies developing hydro kinetic power.....	8
Table 3: List of sensors .....	55
Table 4: Thermocouple wiring location on DT85 .....	56
Table 5: Test matrix .....	70
Table 6: Performance results for the various arm designs .....	108
Table 7: Breakdown of power from generator to grid .....	111
Table 8: Power extraction breakdown .....	112
Table 9: Loads on main anchor line.....	115
Table 10: ADV test matrix.....	136
Table 11: ADV tests using milk to seed the flow .....	142
Table 12: ADV results using two spike replacement methods .....	147
Table 13: ADV final results .....	149
Table 14: ADV results by location and depth.....	150
Table 15: Assessment of the risk of impact .....	158

## List of Figures

Figure 1: Turbine configurations: a) horizontal axis, b) vertical axis.....	5
Figure 2: Ducted turbines: a) horizontal axis (Luna), b) vertical axis (Blue Energy) .....	6
Figure 3: Power outages due to cold weather .....	10
Figure 4: 5-kWe Darrieus turbine .....	12
Figure 5: Turbine set up and operation .....	13
Figure 6: Turbine performance with respect to a) RPM, b) TSR .....	17
Figure 7: Comparison of GH-Tidal and SERG-Tidal models with experimental results evaluating a) power, b) torque .....	19
Figure 8: CFD results compared to experimental values.....	20
Figure 9: Duct effects on flow through turbine a) non-ducted, b) ducted, and c) CFD results .....	22
Figure 10: Ducted design for a VAHT .....	24
Figure 11: Pointe du Bois kinetic turbine test site: a) ADCP measurements, b) location of research platform under walkway bridge, c) aerial view of the site, d) bathymetry profiles of the channel, e) ADCP mounted probe, and f) flow measurements .....	34
Figure 12: Velocity profiles at test location at various locations.....	35
Figure 13: a) Top view of the research platform b) 5 kWe Darrieus turbine .....	37
Figure 14: Anchor drilling method .....	40
Figure 15: Anchor drilling schematic .....	41
Figure 16: Anchoring system.....	44



Figure 17: a) Cross-section of imbedded anchor and b) drilling rig set up .....	45
Figure 18: Network schematic .....	47
Figure 19: Hardware connection schematic.....	49
Figure 20: Hardware arrangement inside DAQ box .....	51
Figure 21: Schematic of the current transformer box .....	53
Figure 22: Thermocouple wiring diagram .....	56
Figure 23: Vibration sensor wiring diagram .....	57
Figure 24: 4-Wire load cell wiring diagram.....	58
Figure 25: 3-Wire load cell wiring diagram.....	58
Figure 26: Flow meter wiring diagram .....	59
Figure 27: Real time sensor display using the DeLogger software .....	63
Figure 28: Output graphs of daily sensor data .....	66
Figure 29: Layout at Pointe du Bois .....	73
Figure 30: Research vessel deployed to final position.....	81
Figure 31: Losses within the dive train assembly .....	86
Figure 32: Load cell output graph voltage versus load.....	88
Figure 33: Graph of flow measurements throughout a day .....	90
Figure 34: Flow meter calibration results .....	91
Figure 35: Handheld flow meter error .....	92
Figure 36: Hourly averaged flow and power data over 1 day.....	95
Figure 37: Hourly averaged flow and power over 2 days.....	95
Figure 38: Raw data of the hourly averages presented in Figure 36.....	96
Figure 39: Free body diagram of turbine arm .....	98

Figure 40: Velocity diagram of turbine arm .....	100
Figure 41: Results from numerical estimation of performance loss .....	102
Figure 42: Power loss versus drag coefficient of the arms .....	103
Figure 43: Power loss over one revolution of a single support arm .....	104
Figure 44: Turbine support arm designs .....	105
Figure 45: Variations in flow per minute throughout an hour .....	106
Figure 46: Performance curves for the 5 kWe turbine.....	107
Figure 47: Power extraction, losses, and efficiencies .....	113
Figure 48: Temperature data at Pinawa, Manitoba for 2008 and the past 10 years.....	118
Figure 49: Inactive frazil ice flowing below pancake ice .....	120
Figure 50: Inactive frazil ice build up.....	122
Figure 51: Time lapse ice formation on research vessel.....	124
Figure 52: Ice formation between pontoons and on anchoring chain.....	126
Figure 53: Destruction caused by excessive ice on research vessel .....	128
Figure 54: Additional photos of icing.....	133
Figure 55: ADV stand deployed on deck.....	139
Figure 56: ADV probe check.....	140
Figure 57: Milk injected into the control volume of the ADV .....	141
Figure 58: ADV Test 7 raw signal full of spikes .....	144
Figure 59: ADV Test 7 filtered signal using the ATM method.....	145
Figure 60: ADV Test 6 signal after a) Mean replacement filtering, and b) Interpolation replacement filtering .....	148
Figure 61: Test 12 ADV data as turbine was stopped.....	151

Figure 62: Pipe holding the flow meter after iceberg impact .....	154
Figure 63: Log jam being cleared .....	156
Figure 64: Peaks in the vibration data indicating an impact .....	157
Figure 65: Turbine blades after winter testing .....	160

## Nomenclature

### Scientific Notation

$a$	Acceleration	$\eta_{w2w}$	Water to Wire Efficiency
$\theta$	Angle of Rotation	$d_o$	Outer Diameter
$\omega$	Angular Velocity	$AC_{out}$	Power Delivered to the Grid
$A$	Area	$PF$	Power Factor
$I$	Area Moment of Inertia	$S$	Reactive Power
$C_d$	Coefficient of Drag	$P$	Real Power
$C_p$	Coefficient of Power	$V_{rel}$	Relative Velocity
$I_A$	Current (line A)	$\eta$	Rotor Efficiency
$\rho$	Density of Water	$t$	Thickness
$D$	Drag Force	$\lambda$	Tip Speed Ratio
$F$	Force	$T$	Torque
$V_\infty$	Free Stream Flow Velocity	$Q$	Total Apparent Power
$d_i$	Inner Diameter	$V_{AN}$	Voltage (line A to neutral)
$\eta_{inv}$	Inverter Efficiency	$V_{l-l}$	Voltage (line to line)
$L$	Length	$V_{l-N}$	Voltage (line to neutral)
KE	Kinetic Energy	$\sigma_y$	Yield Stress
$V$	Measured Free Stream Velocity	$R$	} Radius
$U$	Modified Free Stream Velocity	$r$	
$M$	Moment		

## **Abbreviations**

ADV	Acoustic Doppler Velocimeter
ATM	Acceleration Thresholding Method
BEM	Blade Element Momentum
CFD	Computational Fluid Dynamics
CT	Current Transformer
CV	Control Volume
DAQ	Data Acquisition System
HAHT	Horizontal Axis Hydraulic Turbine
NECI	New Energy Corporation Inc
NRCAN	Natural Resources Canada
RPM	Revolutions per Minute
TSR	Tip Speed Ratio
VAHT	Vertical Axis Hydraulic Turbine

# Chapter 1

## Introduction

### 1.1 Hydro kinetic power

Hydro power is defined as the power derived from the energy of moving water. There are two areas from which hydro kinetic power can be derived: marine and river power. Marine hydro kinetic power deals with extracting energy in the ocean from tides and currents. Tidal energy comes from the predictable rise and fall of tides generated by the gravitational pull of the sun and the moon where as ocean currents are large convection systems generated by temperature differences. Hydro kinetic power extracted from the river comes from the kinetic energy of the flow. Unlike hydro dams that use potential energy from a stored reservoir and utilize the difference in elevation from inlet to outlet to create a hydraulic head, river kinetic hydro uses the energy from fast flowing water, thus extracting power from the kinetic energy within the flow using the same principles as wind energy. Extracting power in this way is still possible when the river is below critical flow.

Depending on the power output of the operation, Natural Resources Canada (NRCAN) has proposed a classification of various levels of hydro production. Large hydro implies a hydro dam when the total output of that operation exceeds 50 MW. Less than 50 MW is referred to as small hydro. In Canada, it is generally accepted that there are three categories of small hydro generation: small hydro, mini hydro, and micro hydro. Micro

hydro means any hydro electric generation less than 100 kW, mini hydro means hydro electric generation between 100 kW and 1 MW, and small hydro means hydro electric generation between 1 and 50 MW.<sup>1</sup> There are no classifications for river kinetic turbines but units under demonstration vary between a few kW to a MW.

Canada is a unique environment, abundant in both marine and river hydro kinetic power. Numerous sites in the Atlantic, Pacific and Arctic waters have been identified as economically suitable for marine power generation that also includes wave energy. River hydro kinetic power has yet to be fully investigated, but it has been identified in Canada as having the potential to extract river hydro kinetic power from the large network of river systems throughout the country.

## **1.2 Current estimated capacity**

Many studies have been carried out, for example by NRCAN and HATCH Energy, to quantify the power capacity of undeveloped sites throughout Canada. Multiple sites for developing marine and small hydro have been surveyed and analyzed, while the potential for river kinetic sites has yet to be assessed.

Preliminary studies conducted by NRCAN in 2008 concluded that there is a gross resource potential of 225 GW of wave and tidal current power. Tidal power estimates from sites all over the country account for in excess of 40 GW with most of this power

---

<sup>1</sup> [www.canmetenergy.nrcan.gc.ca](http://www.canmetenergy.nrcan.gc.ca)

coming from the Bay of Fundy. The other 160 to 180 GW can be obtained from wave power along the Atlantic and Pacific coast lines (Cornett 2006).

Hydro electric plants, which utilize hydraulic head, provide an installed capacity of over 72,500 MW in Canada with approximately 3,500 MW of small hydro across 359 sites.

There are still underdeveloped small, medium and large hydro sites; the potential of small hydro sites that could be developed is not well quantified in Canada. The potential of river hydro kinetic power has not been well understood due to the following factors:

- Until recently no commercial systems were available.
- It was uncertain that this technology could operate in cold climates due to ice impact.
- Impact of ice floes and logs in spring was not understood.
- No study to quantify this resource has been undertaken in Canada.

### **1.3 Current state of technology**

There are many new companies who work in the alternative energy sector with particular focus on hydro kinetic power generation. To offer a unique product, companies have identified specific design features that improve efficiencies and/or lower unit costs.

These unique designs have been patented and offer specific turbines for specific applications. This section will present an overview of the basic technology but not the specific enhancements made by individuals for a competitive edge in the marketplace.

Kinetic turbine technology is not just about the turbine itself, but about a host of issues



including simplicity in turbine deployment and retrieval, safety while handling the turbine, and the ability to reduce cost in spite of various issues: ice, logs, boating traffic, etc.

### 1.3.1 Extractable power

Kinetic turbines generate power by using mainly reaction type turbines with water flowing over hydrodynamic shapes to produce a pressure gradient that turns the rotor, which in turn rotates a generator. The amount of kinetic power available for extraction depends on the fluid velocity, rotor area and density of the fluid as expressed in Equation 1.

$$P = \frac{1}{2} \rho A V^3 \quad (1)$$

The total power available cannot be fully extracted. According to Betz limit, the maximum extractable power is 59% of the available power. An extra efficiency term needs to be added to incorporate mechanical and electrical losses within the turbine system. Typically the Betz limit and the electro-mechanical efficiency are combined to form a term called the coefficient of power,  $C_p$ , where the power becomes

$$P = \frac{1}{2} (0.59) \eta \rho A V^3 \quad (2)$$

$$P = \frac{1}{2} C_p \rho A V^3 \quad (3)$$

### 1.3.2 Turbine configurations

There are two types of turbines used to harness the power of the water's kinetic energy: horizontal and vertical axis turbines. Referred to as Horizontal/Vertical Axis Hydraulic Turbines (HAHT or VAHT), these turbines have existed for many years and have been used for extracting power from both wind and water. Their principles of operation are the same in both fluids. The fluid flows over the airfoils or hydrofoils, inducing aero/hydrodynamic forces that generate a torque with respect to the axis of rotation. The horizontal axis turbine has its axis in line with the flow while the vertical axis turbine has its axis of rotation orthogonal to the flow. Figure 1 shows the two types of turbines. Note that the vertical axis turbine depicted in Figure 1 b is a Darrieus type VAHT.

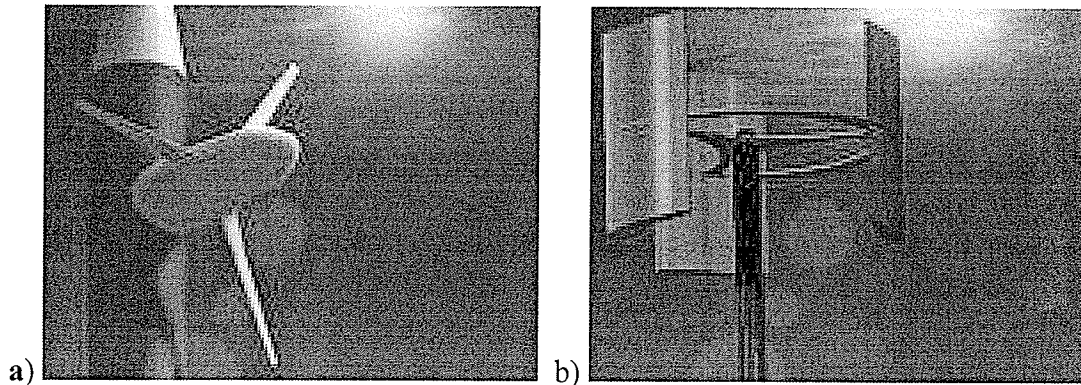


Figure 1: Turbine configurations: a) horizontal axis, b) vertical axis<sup>2</sup>

In order to increase the total power density, designs can incorporate a shroud to funnel more mass through the rotor area. Some companies claim that they can exceed the total extractable power beyond Betz limit however, they use value upstream of the shroud and apply them as if they were constant within the shroud. Ducted turbines increase the fluid

<sup>2</sup> "Marine Current Resource Technology and Methodology" website. [www.esru.strath.ac.uk](http://www.esru.strath.ac.uk)

velocity by means of the Venturi effect. Turbines that boast a larger than Betz limit output typically keep the upstream velocity constant when in reality it increases across the plane of the rotor. Ducts force more mass flow through the turbine and increase both the total available and total extractable power; however, the increase in drag can make deployment and retrieval more costly and less safe. Figure 2 shows a ducted horizontal and vertical axis turbine.

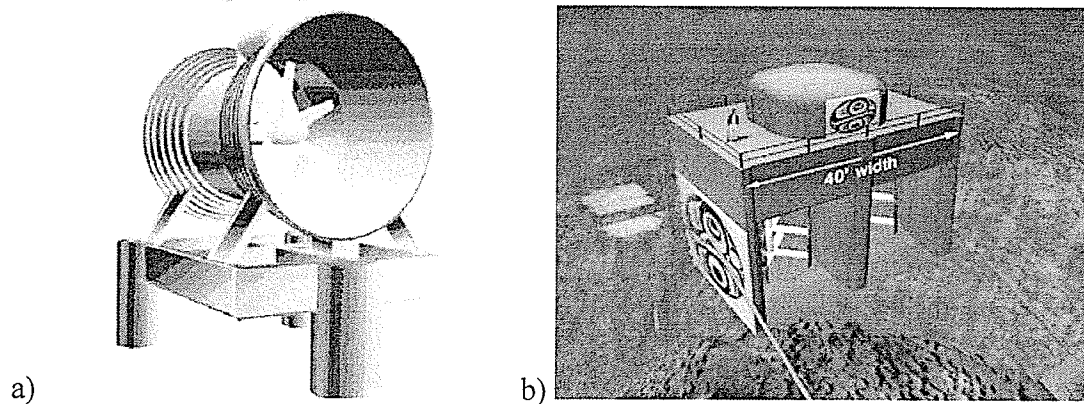


Figure 2: Ducted turbines: a) horizontal axis (Luna), b) vertical axis (Blue Energy)

### 1.3.3 Installations and company profiles

Much of the first activity in this sector of alternative energy took place after the energy crisis in the late 1970's. With the return of cheaper oil prices, this sector saw a quiet period until the next spike in gas prices. Recently, many new companies have been established, building upon the experience in the 1980's. Most companies are in the prototype and demonstration phases with the commercial implementation phase scheduled for 2010 and beyond. Adapted from Gaden (2007), Table 1 describe the

previous installations and demonstrations. Table 2 shows the major companies in the market.

Table 1: Installations and demonstrations

Name / Location	Year(s)	Resource	Type	Output
The Coriolis Program (Gulf Stream, USA)	1973–1978	Ocean current	Axial turbine	
ITDG/IT Power (River Nile, Sudan)	1976–1983	River	Darrieus turbine	
National Research Council and Nova Energy Ltd (St. Lawrence River)	1982	River	Darrieus turbine	25 kW
National Research Council and Nova Energy Ltd (Sheet River, Nova Scotia)	1983–1985	River	Darrieus turbine	10 kW
Nihon University (Kurushima Straits, Japan)	1983–1988	Ocean current	Darrieus turbine	3.5 kW
Nova Energy Ltd (Gulf Stream, USA)	1984–1985	Ocean current	Darrieus turbine	4 kW
Scottish Nuclear, IT Power, NEL (Loch Linnhe, Scotland)	1994	Tidal	Axial turbine	15 kW
Northern Territory University (Aspley Straits, Australia)	1994	Ocean current	Axial turbine	
Ontario Power Generation, UEK, St. Catharines, Ontario	2000	River	Axial turbine	< 30 kW
Pearson College, EnCana, Clean Current (Race Rocks, British Columbia)	2004–Present	Tidal	Axial turbine	
University of Manitoba, Manitoba Hydro (Point du Bois, Manitoba)	2008–Present	River	Darrieus turbine	5 and 25 kW

Table 2: Major companies developing hydro kinetic power

Company Name	Year(s)	Resource	Type	Output
Underwater Electric Kite (USA)	1981–Present	River, ocean current, Tidal	Axial turbine	Up to 120 kW
Florida Power Inc / Gulf Stream Technologies	1998–Present	Tidal	Axial turbine	Up to 200 kW
Blue Energy	1999–Present	Tidal	Darrieus turbine	Up to 250 kW
Marine Current Turbines Inc	1999–Present	Tidal	Axial turbine	300 kW
Verdant Power LLC	2000–Present	River, ocean current, Tidal	Axial turbine	60–80 kW
Exim and Seapower	2002–Present	Ocean	Savonius turbine	
Hydro Venturi Ltd	2002–Present	River, Tidal	Axial turbine	
Engineering Business Ltd Stingray Tidal Stream Generator	2002–Present	Tidal	Hydro- plane actuation	150 kW
Tidal Generation Limited	2003–Present	Tidal	Axial turbine	1 MW
Lunar system	2003–Present	Tidal	Axial turbine	1 MW
New Energy Corporation Inc.	2003–Present	River and tidal	Darrieus turbine	Up to 125 kW
Statkraft	2004–Present	Tidal	Axial turbine	

Kinetic turbine technology began to mature only recently. Most of the demonstrations and installations in the field are electrically loaded by load banks of heating elements and are not grid connected. The National Research Council and Nova Energy were the first in North America to connect an in-situ kinetic turbine to the power grid. After the tests by Faure *et al.* (1986) in the St. Lawrence River, field testing slowed down until the next grid connection was established by the University of Manitoba and New Energy Corporation Inc in 2008.

#### **1.4 Environmental challenges in Manitoba**

Kinetic turbine technology can reduce our “carbon footprint”, and bring stability to the energy grid by providing local energy production. With the sparse distribution of Canada’s population, there has been significant money put towards installing and maintaining of a large grid network to supply power to all communities. Off-grid communities currently use fossil fuels as their primary source of energy. The versatility of micro and mini hydro benefits remote communities by offering potentially low-cost, clean power.

Supplying distributed renewable power provides additional concerns when considering a northern location. The extreme cold climate causes strain on the power grid and power generation devices. For example, cold weather events lead to power outages. Figure 3 displays the number of outages with a peak of 1600 hours in Manitoba. Therefore, it is essential that for hydro kinetic power generating technology to be viable in Canada or

any other northern climate, it must be able to operate during extreme temperatures, common in this geographical area.

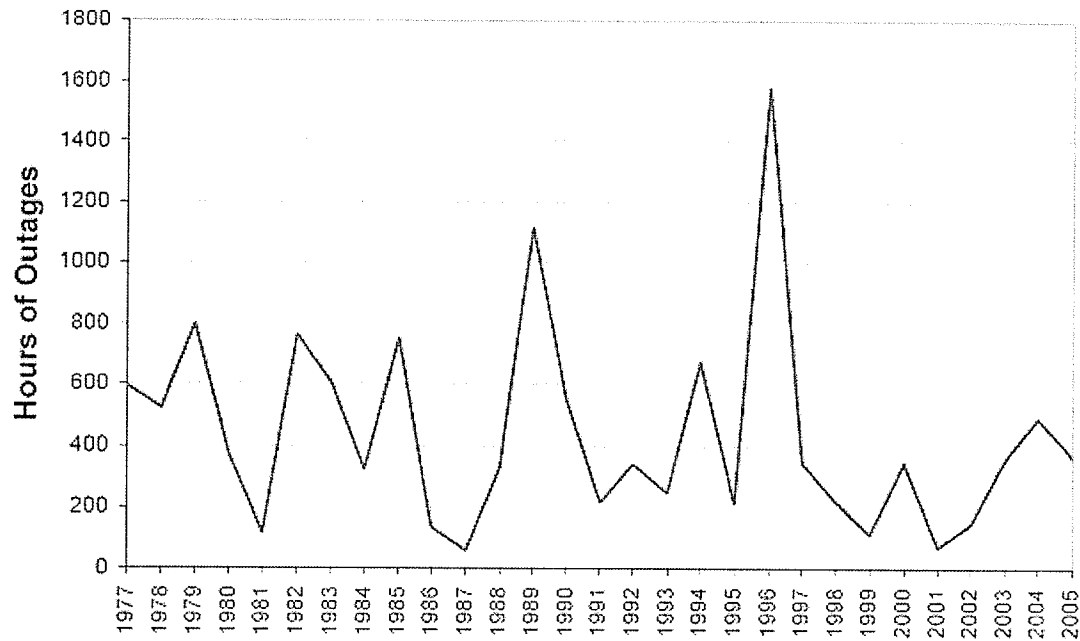


Figure 3: Power outages due to cold weather (courtesy of Manitoba Hydro)

There are many issues related to cold conditions that have an effect on output and performance, and that pose risks to equipment and personnel. The cold tundra of the Canadian Shield can reduce power production from hydro sources. Frazil ice, described as a sticky blizzard of ice particles within a flow, can have a serious impact on any device operating in supercooled water. Hydro dams around the world have seen this phenomenon block inlet gates and reduce overall performance by altering the head of the river. The seasonal cycles of northern climates also introduce a variety of floating debris in the form of icebergs and logs. Small and larger hydro structures are designed to withstand the forces of impacting debris and keep them from entering the turbine. Micro

and mini scale hydro systems become more vulnerable to these hazards because they are constructed with minimal protection to keep infrastructure costs reasonable and to minimize the impact on the local ecology. Costs will have a more profound effect on river hydro kinetic power generation because it is harder to justify the operational costs when revenues are much smaller for kinetic turbines compared to traditional hydro.

Because of these issues, utilities like Manitoba Hydro have not been able to ascertain whether river hydro kinetic power can be a reliable renewable technology in the future because of

- ice issues
- operational issues
- cost issues

All of these issues need to be quantified for cold climate applications.

## **1.5 Research objectives**

The objective of this research is to demonstrate the viability of river hydro kinetic power in cold climates and highlight the research areas that need to be addressed. To achieve this goal, a demonstration river was licensed and developed, and a 5 kWe and 25 kWe Darrieus vertical axis turbine designed and manufactured by New Energy Corporation Inc based out of Calgary Alberta, were deployed and operated. Figure 4 shows the 5 kWe unit on the deck of the research vessel.



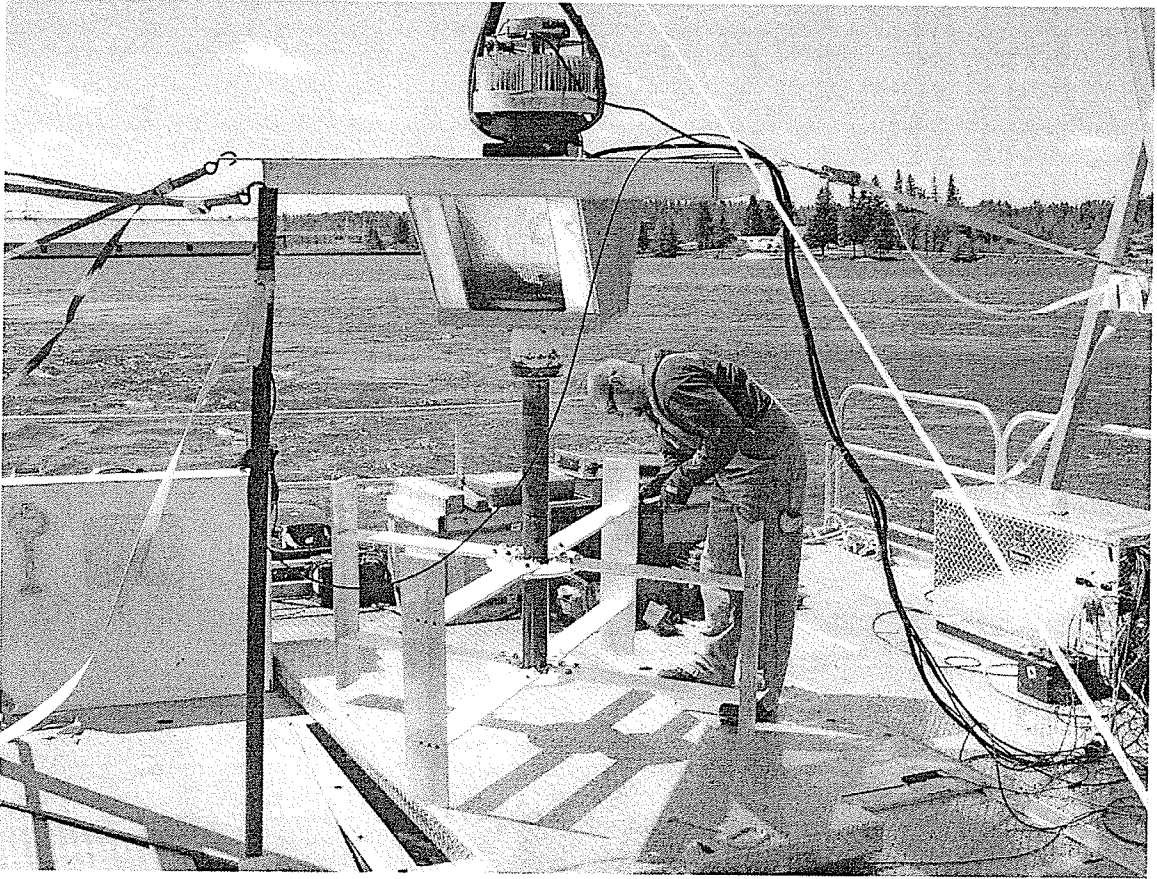


Figure 4: 5-kWe Darrieus turbine

The turbine's performance was monitored during winter and summer months of 2008 to assess the unit's efficiency and to quantify the amount of power lost in the conversion process. Long term in-situ testing yielded insight into the hazards and potential risks that the environment posed on the technology. Ice formation and foreign debris impacts on the unit were catalogued. This demonstration was grid-connected to supply renewable energy. Delivering power to the grid was a major and necessary component of this project to evaluate any additional issues of a permanent installation. This research project deployed a 5 and 25 kWe turbine into the Winnipeg River; however, only results

for the 5 kWe turbine are discussed in this thesis. Figure 5 gives additional photos of the turbine during installation and in operation.

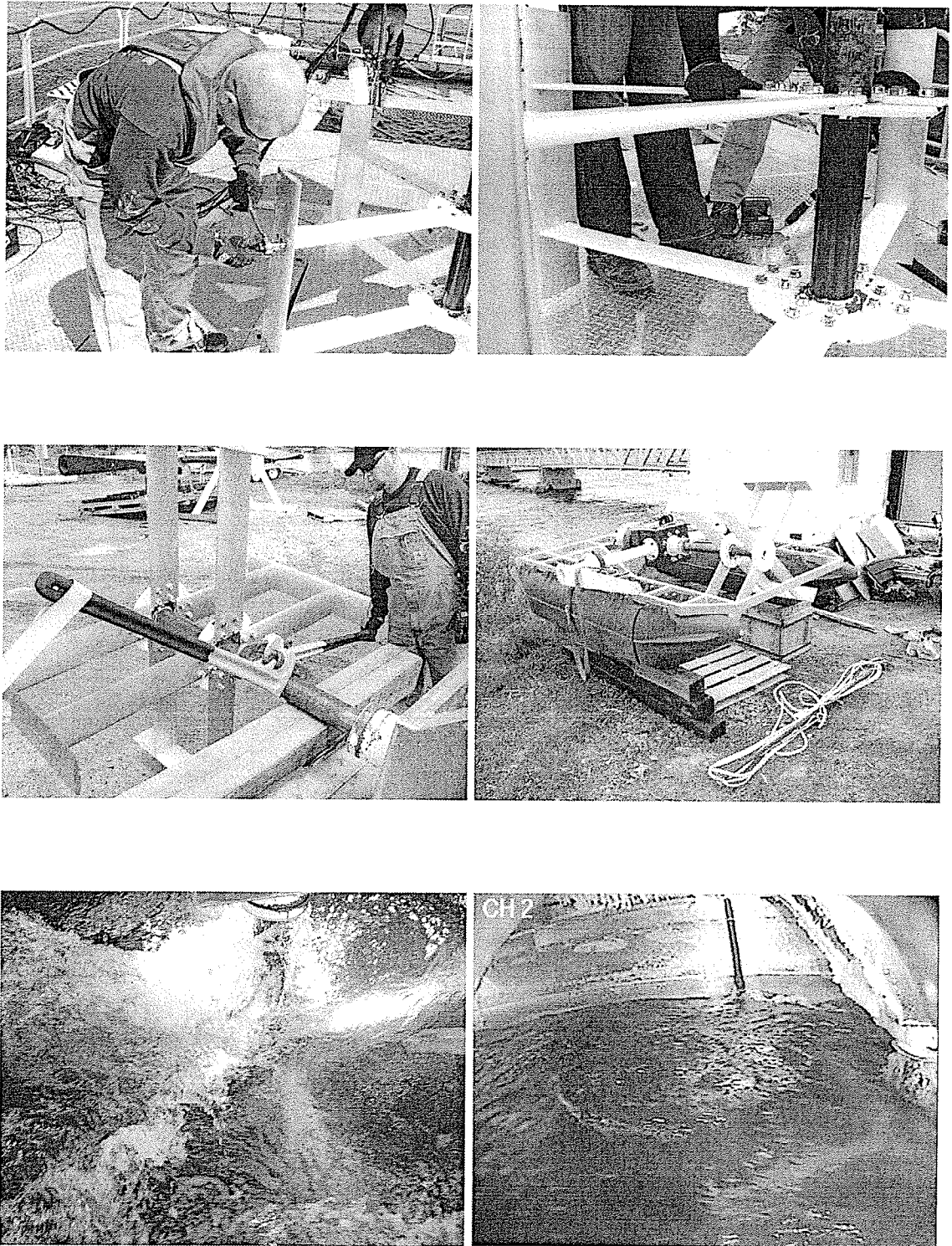


Figure 5: Turbine set up and operation

## Chapter 2

### Literature Review

#### 2.1 Overview

This chapter introduces literature covering the mathematical background and expertise developed for hydro kinetic turbines. Turbine performance and operational characteristics are outlined by introducing key concepts and formulations. The two turbine orientations presented in Chapter 1, vertical and horizontal, have similar performance characteristics with their own set of advantages and disadvantages. Efficiencies have been improved by implementing a duct structure to capture more of the river's mass flow. Aside from technical performance, this chapter also reviews the studies conducted on the frazil ice phenomenon because it is a pertinent issue that affects kinetic hydro power production in cold climates.

The research presented in this thesis focuses on the operation of a kinetic hydro site, from installation to sustained operation, in the Canadian climate. Throughout this process, no literature was available on the following important topics:

- effect of icing and logs on kinetic turbines
- deployment in fast flow river without the use of large equipment
- method of anchoring a kinetic turbine
- assessment of suitable for river sites kinetic turbine technology

This thesis presents results that contribute to some of these topics because they are the dominant issues that need to be addressed to adequately assess the viability of river kinetic turbines.

## 2.2 Turbine performance

The basic design of the VAHT consists of a rotor with 2 to 5 symmetric hydrofoil blades. In operation, the blades rotate around the shaft at 2 to 3 times the speed of the free stream. The relative velocity between the blade and the free stream induces hydrodynamic forces of lift and drag along the hydrofoil. The ratio between the blade velocity with respect to the free stream velocity is the Tip Speed Ratio (TSR). As the TSR changes, so does the angle of attack of the flow over the blades. The angle of attack varies with the blades' location along its circular path and thus an important operational characteristic of the VAHT emerges. The torque produced by the turbine is not constant throughout each revolution. Although the net torque through one revolution is positive, the instantaneous torque varies depending on its relative blade velocity to the incoming flow. Adjusting the angle of attack as the blade rotates has been investigated to increase efficiency, but this method is not practical. The shaft is connected to a gearbox that increases the RPM to match the generator's specifications. The TSR impacts the gearbox design. In general, gearboxes are available for a speed increase of less than 25:1 ratio so the rotor RPM, gearbox and generator have to be designed accordingly. Adding a second gearbox may not be practical for smaller turbine systems in river applications.

### 2.2.1 Tip speed ratio (TSR)

The TSR is an important non-dimensional number that turbine performance data can be evaluated against. There exists a non-linear relation that links the coefficient of power,  $C_p$ , with TSR. Equation 4 defines the TSR as the angular velocity of the shaft times the radius at which the blades are held, divided by the free stream velocity. The formula is further reduced to a function of RPM as expressed in Equation 5. The TSR is also used to compare turbines of different scales and design. Figure 6 shows that the performance curve of the coefficient of power extracted from the flow is unified when taken with respect to TSR rather than RPM.

$$TSR = \lambda = \frac{\omega R}{V_{\infty}} \quad (4)$$

$$\lambda = \frac{RPM * \left(\frac{2\pi}{60}\right) * R}{V_{\infty}} \quad (5)$$

The TSR shows how the turbine has consistent performance for different flow velocities. Performance curves such as the ones shown are unique to a specific design and configuration of the turbine. The performance of the turbine based on the TSR follows a curve with a point of maximum output and thus maximum efficiency. At low tip speeds, the fluid is allowed to pass freely with little power being extracted. Tip speeds in excess of the optimal point decreases efficiency as the rapidly rotating blades present a solid face to the fluid flow.

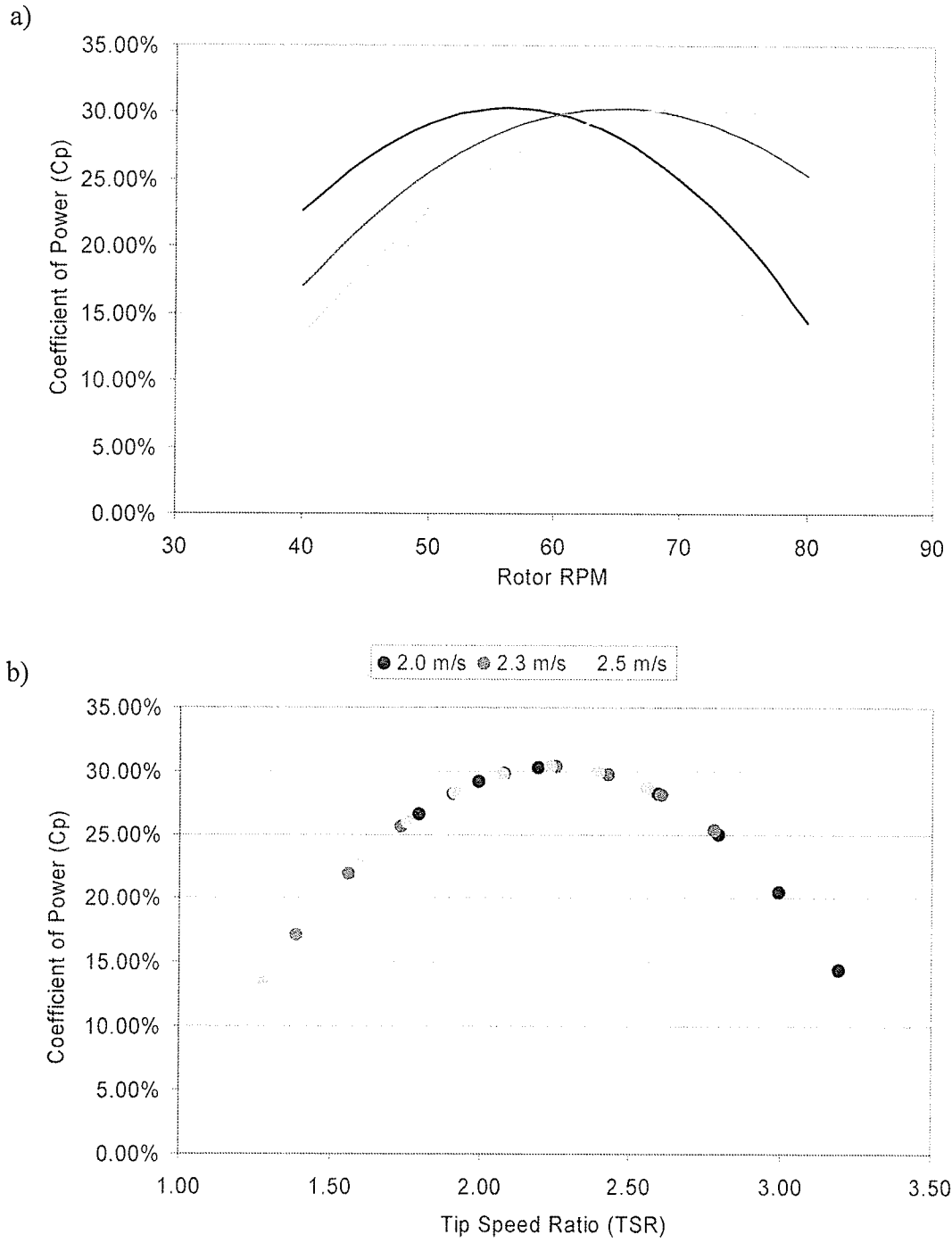


Figure 6: Turbine performance with respect to a) RPM, b) TSR for a flow of 2.0, 2.3 and 2.5 m/s

### 2.2.2 Numerical models

When modeling the performance of various turbine designs, the most employed method is the Blade Element Momentum theory (BEM). Batten *et al.* (2008) described this approach as the combination of momentum and blade element theories. The momentum theory is used to assess the axial and circumferential inflow factors, with an additional tip loss parameter to account for the finite number of blades. The blade element portion divides the blade into segments on which lift and drag forces are calculated. The amalgamation of both theories allows for the calculation of lift and drag along the blade when considering the fluid momentum at the various angles of attack during one rotation of the rotor. Integration of the loading on each element along the length of the blade allows for the derivation of torque, drag, and power coefficient for the rotor. This approach was used extensively by Batten *et al.* in 2006 and 2008 for predicting HAHT performance for various pitch and twist designs. The model was validated by wind and water tunnel tests with good agreement between theoretical and experimental values.

The BEM theory led the way to various commercial software packages. Bladed, a software package designed to assess horizontal axis wind turbines, was adopted by Mayers & Bajah (2006) to evaluate the turbines using water instead of air as the working fluid. Bajah *et al.* (2007) continued to use more advanced software packages to further their studies on pitch angles and turbine performance. The GH-Tidal Bladed software offers a full time-domain, hydroelastic treatment of the turbine response to environmental excitation. Included with this software are detailed flow environments such as combined wave and current loading, models of cavitation, added mass to the fluid/structure inertial

forces, and buoyancy forces. Another package, SERG-Tidal developed at the University of Southampton, offers specific improvements to the Tidal Bladed software that include improved interpolation, extrapolations for stall, and options for the tip loss factor. It was concluded that both software gave valid results over the range of TSR where power was optimal; however, at higher TSR they failed to predict the sharp drop in power. The GH-Tidal Bladed code tends to slightly over-estimate the power while the SERG-Tidal code under-estimates the thrust. Figure 7 shows the results obtained by Bajaj *et al.* (2007).

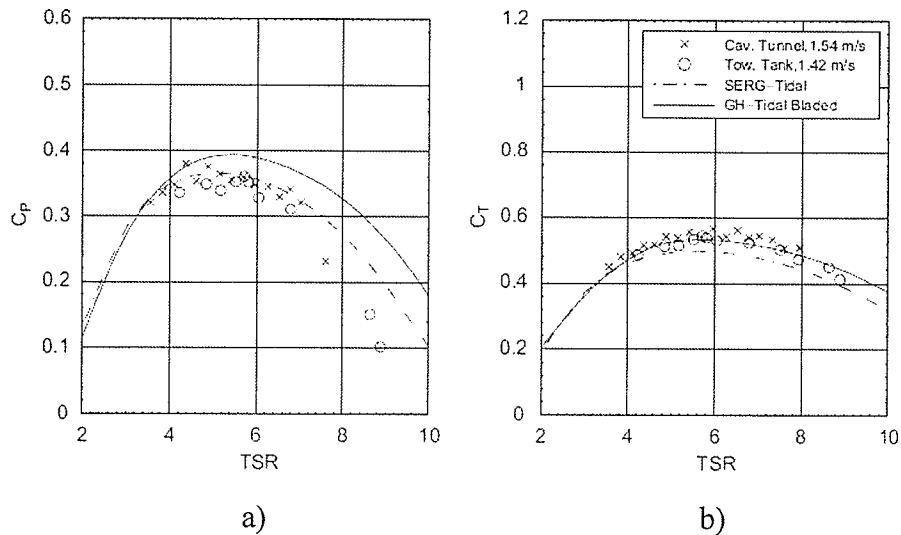


Figure 7: Comparison of GH-Tidal and SERG-Tidal models with experimental results evaluating a) power, b) torque (Bahaj *et. al* (2007))

The use of BEM theory models has been widely accepted by the fluid mechanical society and has been employed for many applications. The use of this theory in assessing aerodynamic and hydrodynamic forces on contoured blades has also been applied to Computational Fluid Dynamics (CFD) models. Antheaume *et al.* (2008) created a CFD



model that was solved using the Fluent CFD software package with a  $k-\epsilon$  turbulence model and a steady state formulation to simulate the performance of a VAHT. They found a good agreement between numerical and experimental values with particular interest in the agreement of values of TSR beyond the maximum power point as shown in Figure 8. In this section of the power curve, the flow is dominated by secondary effects corresponding to a viscous attached flow. However, before the maximum power point, a significant difference can be seen between numerical and experimental values. In this region, the dynamic stall phenomenon (also called primary effects) dominates the error in the results. Dynamic stall is exhibited by rotating blades because interaction between the trailing blades and shed vortices from leading blades causes a strong unsteady effect.

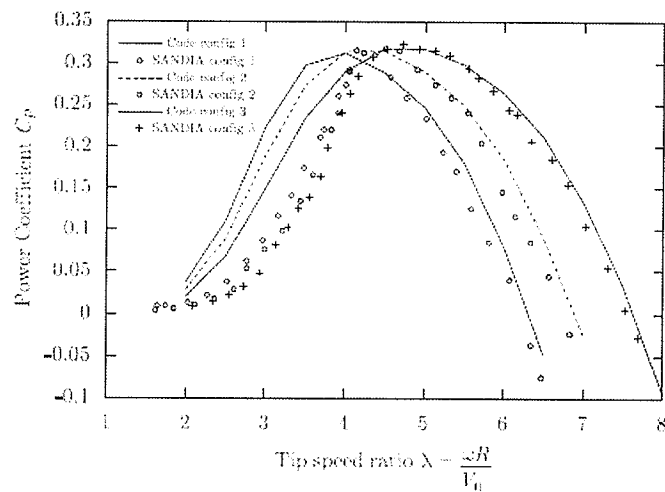


Figure 8: CFD results compared to experimental values (Atheaume *et al.* (2008))

### 2.3 Research and development

An excellent review of current technological progress was written by Khan *et al.* (2008).

A survey of literature revealed that the first publication of river current turbine

application came in 1978 and is attributed to Peter Garman. The technology was used for pumping water for irrigation. Within four years of this application, nine turbines were installed in Juba Sudan in the White Nile running for a total of 15,500 hours. In the early 80's, extensive work was done under the United States Department of Energy's ultra-low head energy program.

### **2.3.1 Horizontal axis hydraulic turbine**

The work conducted by the United States Department of Energy during the early 80's involved the testing of two HAHT configurations: a free standing rotor and a ducted rotor, both 3.05 m in diameter. The free standing rotor was designed to produce 15 kWe at 3.87 m/s and the ducted rotor was rated for 20 kWe in 2.13 m/s flow. Radkey and Hibbs (1981) concluded that ducted systems produced higher efficiencies ranging from 0.66 to 1.69, well beyond Betz limit. The purpose of a duct is to channel more mass flow through the turbine, thus effectively increasing the local fluid velocity across the turbine's face. By using the upstream velocity rather than the duct throat velocity to calculate efficiency, Betz limit could be surpassed. A shrouded HAHT was developed by UEK Corporation in the United States. The diffuser shape of the shroud changed the shape of the surrounding flow as described by Gaden (2007) and presented in Figure 9. His work conducted multiple CFD simulations to investigate the advantage of ducted turbines. His research confirms that a ducted design can more than double the fluid velocity.

Riegler (1983) concluded that using a low cost diffuser shroud on axial turbines increased the power coefficient to 1.96, 3.3 times the Betz limit. Gilbert and Foreman (1983) found a power increase of 4.25 times over the non-ducted design. Although the last two findings were based on experiments with wind turbines, this technology can be applied to a different fluid medium.

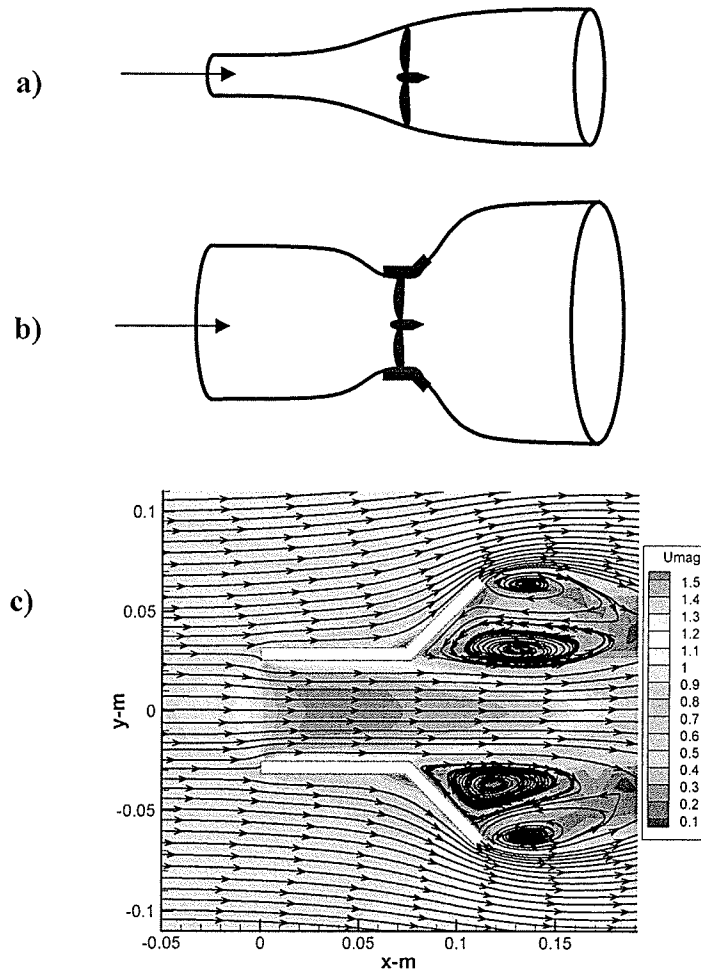


Figure 9: Duct effects on flow through turbine a) non-ducted, b) ducted, and c) CFD results (courtesy of Gaden, 2008)

Re-shaping the flow can increase the amount of extractable kinetic energy. Initial modeling by Gaden and Bibeau (2008) showed that it may be possible to re-shape the flow over and around a shaped anchor to optimize the flow for turbine interaction. The shaped anchor consists of a fabric mold sunk to the river bottom, into which mass is injected, providing a dense form made of concrete. The concept involved constructing a ramp-like object upstream of the turbine to funnel more fluid through the turbine.

The non-ducted turbine design has resulted in many models developed both privately and commercially. Batten *et al.* (2008) used a BEM theory approach, validated by a scale model test, to simulate the efficiency of a 20 m, 3 blade rotor at the optimal pitch in a 2 m/s flow. They found a power coefficient of 0.45. Note that at this value, a rotor efficiency of 45% will reduce after mechanical and electrical losses to the overall power generation system. Bajah *et al.* (2007) also found a maximum  $C_p$  in the range of 0.45 based on their numerical models, which were validated based on two experimental data sets.

### **2.3.2 Vertical axis hydraulic turbine**

Recognized by Khan *et al.* (2008), Blue Energy Canada made the largest contribution towards theoretical design for integrating Darrieus hydraulic turbines as a mainstream source of hydro energy production, but has yet to achieve a commercial demonstration. Using a ducted design, a range of turbines from 4 to 100 kWe were tested in the field yielding a power coefficient of nearly 0.45. Efficiencies reported by Kiho *et al.* (1996) were as high as 55%. Other tidal applications have found efficiencies in the range of

35% for a straight, non-ducted design as reported by Antheaume *et al.* (2008). Faure *et al.* (1986) also found efficiencies for a non-ducted design to be in the range of 33% – 35% when testing in the St. Lawrence River. Optimizing a submerged ducted system for a Darrieus turbine was carried out by Ponta and Jacovkis (2008) for a commercial system, as shown in Figure 10.

In all, 24 scale models were built and tested in the tow tank facilities at the USA's Department of Naval Engineering. The same results of accelerated flow were found in the vicinity of the turbine. An added conclusion, which developed from the Ponta and Jacovkis (2008) study, was that the flow speed within the ducted section became independent of upstream flow as the upstream current increased. For an upstream velocity of 2 m/s, the maximum flow through the turbine section was found to be approximately 3.1 m/s, increasing over 1.5 times. With an upstream flow of 2.8 m/s, the flow through the duct was found to stay relatively stable at around 3.2 m/s.

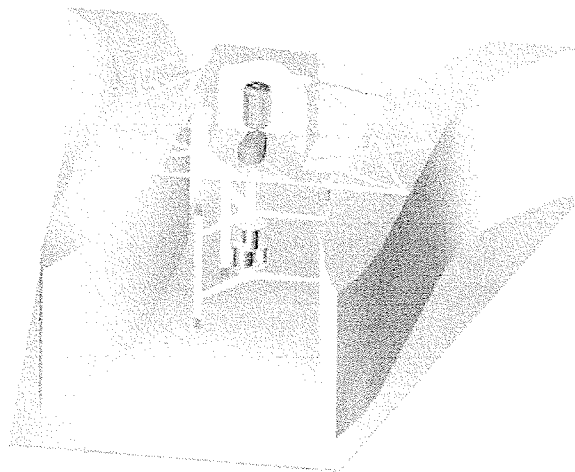


Figure 10: Ducted design for a VAHT (Ponta and Jacovkis, 2008)

Ducted systems show promise in maximizing the kinetic energy extraction from a flow. The added costs and design complexity of such a structure remain the major trade-off when designing a ducted kinetic turbine. Gaden and Bibeau (2008) and Khan *et al.* (2008) concluded that implementing a flow altering structure comes with an increased technical risk. The construction alone of such a structure in high flow areas adds to increase risk, expenses, and design and construction complexity. For river implementation, reduced depth availability may require ducted turbines because they are limited in size, but ducting adds safety risks during deployment and retrieval.

### **2.3.2 Advantages and disadvantages of turbine configuration**

The efficiencies publicized for non-ducted turbines are higher for HAHT because of their circular cross-section; they can capture more mass flow than a vertical axis hydro turbine (VAHT) of similar size. The horizontal axis of rotation allows each blade to produce a continuous torque throughout one rotation, outputting a smooth and constant power. The relative fluid velocity on VAHT blades oscillates in magnitude and direction throughout one rotation leading to an oscillating torque and power output. The HAHT can self start in lower flow velocities than the VAHT, but many features of the VAHT give it an advantage over the HAHT. The vertical shaft allows for direct linkage to the drive train which can be located above water. The simplistic design makes it cheaper than the HAHTs. It is capable of operating with the free stream entering from any direction while HAHT need to swivel in order to be directly perpendicular to the flow. The vertical axis of rotate can deflect incoming objects rather than injecting it.

## 2.4 Frazil ice

A literature review revealed a general lack of quantitative knowledge on the phenomenon of frazil ice, although it is critically important for hydro implementation in cold climates. Qualitative observations have been documented recently because of its negative effect on river and oceanic systems. Martin (1981) reviewed publications on frazil ice and defined it as small discs of ice measuring from 1 to 4 mm in diameter and 1 to 100  $\mu\text{m}$  in thickness that form in turbulent, supercooled water. Once formed, frazil ice crystals sinter to form larger structures through what is called “collision breeding”. The larger structures, comprising a collection of discs, are termed “flocs”. “Pans” are sheets of frazil ice that float to the surface. These have a diameter of about 1 m and a thickness in the range of 0.1 to 0.5 m. “Floes” are larger pans with diameters from 1 to 30 m and a thickness of 0.5 to 5 m. This study, refers to pancake ice to describe the thin layer of ice floating at the surface.

The mechanism through which frazil ice is created is the source of much debate. The literature offered differing opinions on the initial seeding source; however, aside from the seeding source, there are three main factors that need to be present: supercooled water, low ambient temperature (our own observations were documented at  $-20^{\circ}\text{C}$ ), and turbulence. In areas of fast flowing water, the lack of ice cover allows heat transfer between the fluid and the air, enabling the fluid to become supercooled. Nucleation is the mechanism through which ice forms initially. Primary nucleation can occur spontaneously or induced artificially. For pure water, which has been supercooled to  $-40^{\circ}\text{C}$ , spontaneous nucleation may occur. This is referred to as homogeneous

nucleation. However possible, it is not probable in nature. Ice is virtually always nucleated by induced means. Heterogeneous nucleation is the nucleation of supercooled water onto a foreign particle or surface. After primary nucleation, secondary nucleation is the mechanism from which ice propagates. The most accepted means of secondary nucleation is the shearing of potential crystals from their parent crystals when the parent crystals collided with a hard surface or other crystals. From this, frazil ice production can be deemed a secondary process. Turbulence is required to generate the shearing and collisions between parent crystals. Laboratory studies have produced frazil ice by introducing outside ice crystals into turbulent, supercooled water which then rapidly multiply into frazil ice via collision breeding. Although frazil ice formation is associated with turbulent flows, turbulence does not guarantee the presence of frazil ice. Sufficient intensity must exist for the growth of frazil ice. Clark and Doering (2008) carried out extensive studies into the relationship between turbulence intensity and frazil ice size. It was found that the mean and standard deviation of frazil ice particle sizes followed a parabolic curve when plotted against turbulence intensity. They hypothesized that “...increasing turbulence intensity allows larger particles to form due to a higher turbulent energy dissipation rate, until a point when the eddies physically limit that average size of the particles because of their relatively weak mechanical strength.” Although particle size may drop, the increased turbulence intensity increases the frequency of collisions and may in fact produce a higher density of smaller frazil ice particles. They also noted that high flow velocities may prevent the formation of frazil ice.



The presence of frazil ice in a flow has been observed to adversely affect power generation. All of these observations have been linked to hydro production from dams. An investigation into frazil ice effects on kinetic turbines has yet to be conducted. Fonseca and Roberts (1987) quantified the power loss at the Rivière-des-Praires power plant in Quebec to be up to 30% due to frazil ice blockage. This loss was primarily due to a buildup of ice on the inlet vanes; however, rivers such as the Niagara River have experienced an abrupt reduction in flow as large as 25% due to frazil ice accumulation. Bergander (1988) commented on small scale hydro dams in cold climates, stating that frazil ice and spring break up caused the most concern to the dam. He suggests that the best way of dealing with the issue of frazil ice blockage is to prevent frazil ice from forming. Daly (1987), Bergander (1988), and Gimperline (1991) suggested that the best solution to control frazil ice is to prevent its formation by promoting the growth of a stationary ice cover over the upstream river section. The ice acts as insulation, keeping the waters from becoming supercooled. This eliminates the growth of active frazil ice locally under the cover, and reduces incoming active frazil into passive frazil which is far less harmful, but still poses a concern because it can adversely affect power production. Passive frazil is derived from its active form when the waters warm above the supercooled values. The passive frazil ice particles are slush like in appearance and texture and do not exhibit the strong adherence characteristics of the active form. Rather than attaching to foreign substrates, passive frazil clumps together with other passive frazil clusters to form blockages. Gimperline (1991) stated that this form of frazil can clog hydraulic structures, reducing conveyance and increasing head losses. One of the most common solutions for preventing the presence of frazil ice is to have a fore bay with

constant ice cover. Ice booms could also be employed to slow down the flow and promote rapid growth of an ice cover before the waters become breeding grounds for frazil ice in early winter. For river kinetic turbine applications in cold climates, kinetic sites are found by looking for areas that do not form ice covers because this indicates high flow.

Anchor ice was another phenomenon of great concern since an underwater anchoring system would be used for this experiment. When active frazil attaches to the river bottom, it forms anchor ice and this affects the hydraulic characteristics of the flow. Arden and Wigle (1972) attributed a 20% to 30% flow reduction in the Niagara River to anchor ice, consistent with the findings of Fonseca and Roberts (1987). Anchor ice is known to attach itself to rocks at the river bed and transport them hundreds of meters downstream of their initial position. Anchor ice can also release from its substrate and float to the surface, posing a threat of impact as it surfaces. Qu and Doering (2007) described the anchor ice growth process in great detail. This type of ice accumulation can pose a serious risk from impacts and abrasion on the main underwater anchor lines. Clark and Doering (2008) investigated the relation between anchor ice and the Froude number of the flow and concluded a relation between the two. Their data shows a maximum anchor ice growth, in a gravel bed size of 5 mm, occurring when the Froude number reached 0.27, and that the density of the ice increases with increasing Froude number. Terada *et al.* (1998) documented frazil and anchor ice in the Niuppu River in Japan and observed that anchor ice did not form for Froude numbers of less than 0.2. Doering *et al.* (2001) also concluded that the Reynolds number determines whether

anchor ice remains attached to the bottom or is released and floats to the surface. They found that the anchor ice would release for a Reynolds number under 42,000. Therefore, in a river with a high Reynolds and Froude number, the ice would stick to the substrates in the river bed until the waters warmed.

## Chapter 3

### Experimental Setup

#### 3.1 Overview

This chapter describes the installation of the grid-connected 5 kWe Darrieus type kinetic turbine into the Winnipeg River in Manitoba, Canada. Discussion of the site along with permits, site layout, and anchoring are presented. Data gathering was remotely performed using various instruments, data acquisition systems, two computers, and multiple data storage locations. The research platform was instrumented with sensors to track the performance and condition of the turbine. Hardware and software aspects of this project are outlined in this chapter.

#### 3.2 Permits

Various permits are required to install a kinetic turbine in a river. There are no established protocols for operating a river kinetic turbine in Canada.

- **Manitoba Parks**

The Manitoba Parks permit regulates and issues permits for use on Manitoba land. A land permit was not required; however, a scientific permit was issued and requires a yearly renewal.

- **Manitoba Water Resource Branch**

This branch administers the Manitoba Power Act. Temporary installations to gather data do not require a permit from this governing body; however, formal clearance was given.

- **Fisheries & Oceans Canada**

The primary concern of this agency is the protection of wildlife within the water. A legal authorization is required where the Fisheries Act applies and this department provides advice where the act does not specifically apply. Drilling sediments and fish spawning months were the primary concerns which were addressed. Fish mortality was not seen as an issue due to the temporary nature of the installation.

- **Manitoba Conservation Environmental**

This permit regulates environmental assessment in Manitoba. It is only necessary for permanent installations and hence was not required for this project.

- **Navigable Waters Protection**

This agency does not issue permits for anchored boats. As this project pertained to an R&D research platform, the main issue is public access and mooring lines to insure that they do not obstruct other water traffic. Proper signage was required to reflect the obstruction imposed by the project.

- **Manitoba Power Act**

This agency does not regulate temporary research devices that are grid connected.

### **3.3 Pointe du Bois test site**

Manitoba Hydro operates a 78 MW hydro dam located in the town of Pointe du Bois near the border between Manitoba and Ontario on the Winnipeg River. This location was

selected as the site for testing the kinetic turbine for many reasons. Located in the Whiteshell Provincial Park area, the Canadian Shield offers an excellent river bed for anchoring the unit. The flow upstream of the hydro dam provides fairly steady flow rates, because the power plant is undersized due to changes in water flow after the plant was built. This ensures that water is almost always spilled except during a drought, which results in steady flows through the plant. However, it was later found that the plant often shuts down turbines and reduces the flow through the plant due to unscheduled maintenance resulting from crack formations of the dam infrastructure. The infrastructure of the power plant offers safety personnel and equipment and a walkway bridge, roads, high voltage lines, an enclosed protected access, and heavy lifting equipment, all of which were essential components for a project of this magnitude.

Figure 11 shows the Pointe du Bois test site, both physically and regarding flow profiles. An ADCP profile of the river was mounted on a boat, as seen in Figure 11 e, and the results can be viewed in Figure 11 a. Figure 11 c gives a satellite image of the area while Figure 11 b shows the anchored location of the research vessel. Figure 11 d and f respectively give the bathymetry profiles and flow measurements through the depth of the channel. A velocity and river bottom profile of the site using an ADCP measurement probe secured to a boat shows a maximum flow at the site of over 2.2 m/s between piers 2 and 3 of a walkway bridge upstream of the power plant. The water depth is 9.1 m (30 feet) at that location. The bridge piers also provide ample turbulence eddies to test the influence of turbulence levels by moving the research platform laterally.

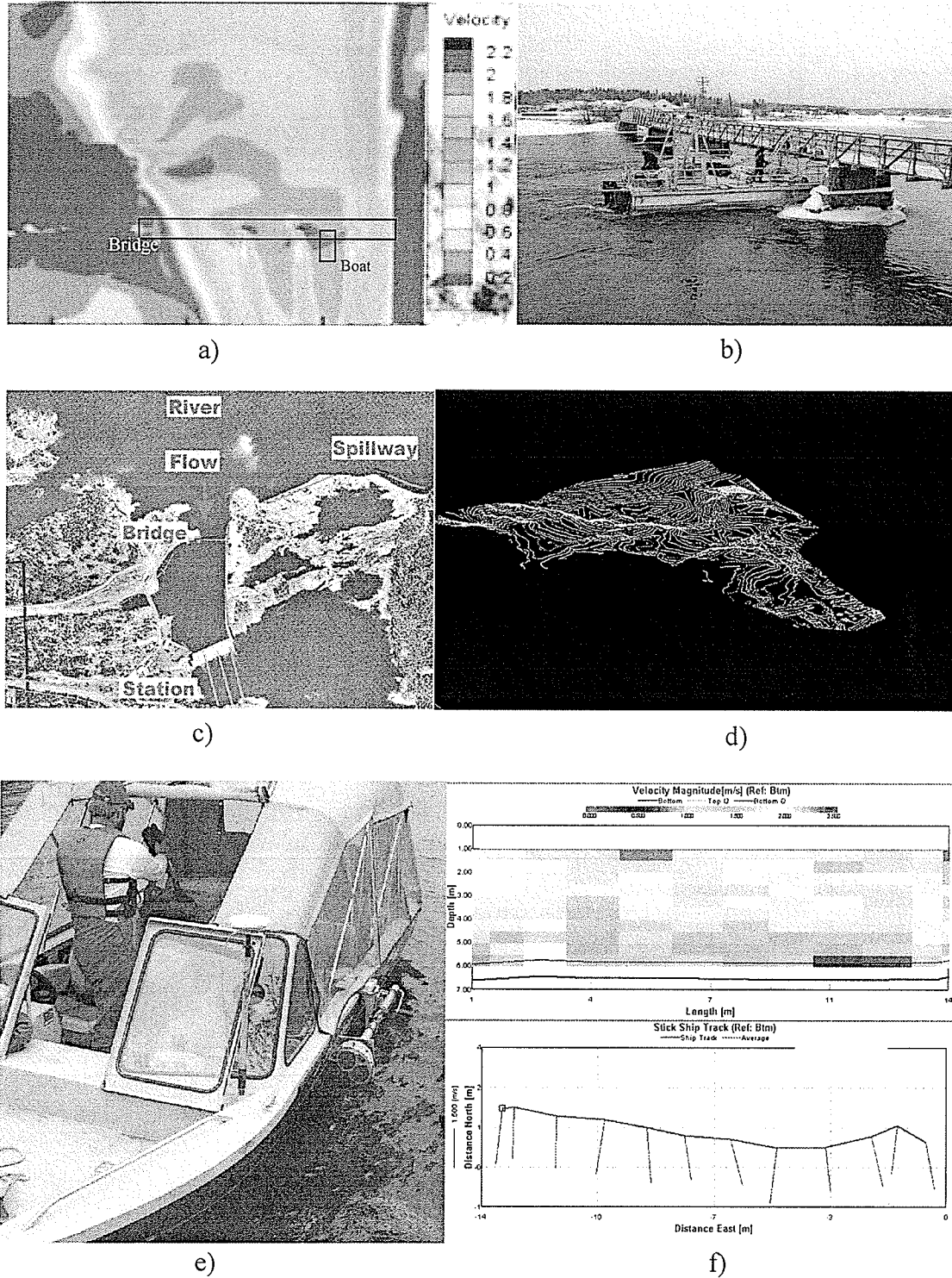


Figure 11: Pointe du Bois kinetic turbine test site: a) ADCP measurements, b) location of research platform under walkway bridge, c) aerial view of the site, d) bathymetry profiles of the channel, e) ADCP mounted probe, and f) flow measurements

In addition to ADCP measurements, two calibrated turbine flow meters were used to verify the flow measurements under the bridge and to obtain the velocity profile. A special cable system with a large weight and connected to an ATV was used to lower the turbine flow meters in the high current. The two turbines measured the flow velocity within 1% error of each other. The turbulent velocity profile is shown in Figure 12.

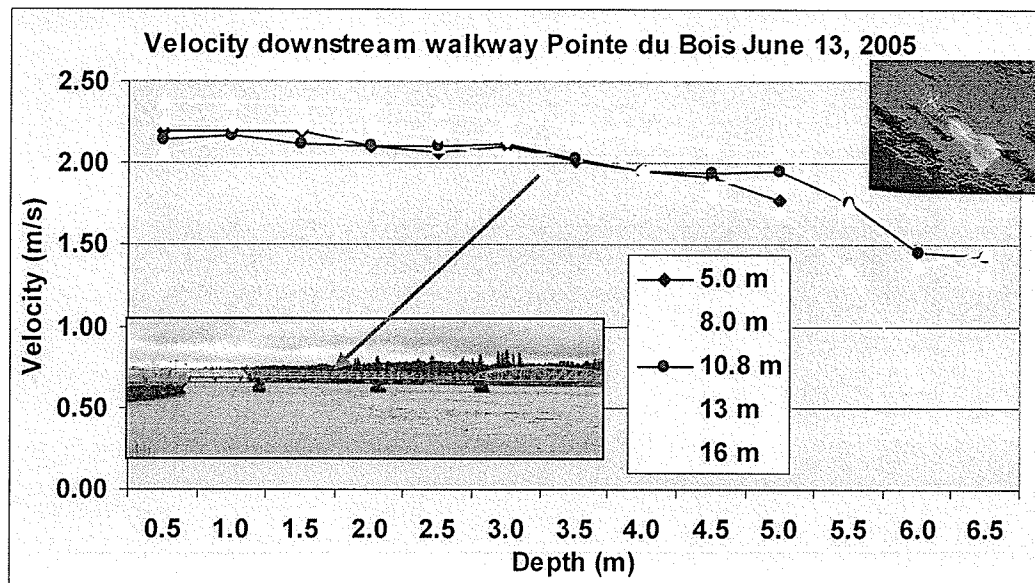


Figure 12: Velocity profiles at test location at various locations under the walkway bridge

The walkway bridge provides access to the spill gates and to the research platform located just beneath. Power to the spill gates is delivered by a single phase 240 V power line, which comes off a hydro pole located at the west edge of the river, and travels the length of the foot bridge to the spill gates. A control center was established inside an ATCO trailer located at the base of this hydro pole, making a 220 V three-phase grid connection convenient with the installation of a reverse metering system. The close proximity of the control center to the bridge kept cable lengths to a minimum. Power



(240/120 VAC) was supplied to the research vessel from the opposite shore and another 3-phase 600 VAC power line delivered the power generated by the turbine to the inverters located in the trailer. A hard line data connection linked the research vessel with the control center. Because the power fed to the control center from the turbine and the power used on the research platform were from opposite shore lines, the grounds on the research vessel were not the same, often tripping ground faults on the data acquisition system leading to power outages.

A staff house located downstream of the bridge close to the power dam housed and fed the workers. This amenity was welcome as New Energy Corporation Inc (NECI) employees and University of Manitoba researchers spent days on assembly, deployment, testing, troubleshooting, and removal. The commute from Winnipeg to Pointe du Bois was approximately 2 hours, so the availability of local lodging was a benefit to the project.

### **3.4 Turbine and research vessel details**

The research vessel and turbine was supplied by NECI and this section presents some of the details. The research vessel is an 8,000 lb all aluminum pontoon boat with a deck measuring 30 ft by 18 ft. The pontoons are 3 ft wide and 3 ½ ft deep allowing for a maximum payload of 10,000 lb. The deck consists of five panels, 8 ft by 4 ft, which sit on two main struts running the length of the vessel. These panels are removable and can slide along, thus exposing a one-panel-width gap between the pontoons to the water below. NECI manufactured a cradle for the 5 kWe turbine, which occupied the place of

one panel. With the vessel's design, the turbine could then be located anywhere along the deck in place of any of the five panels.

The turbine, designed and manufactured by NECI, has 4 blades that mount to a rotor measuring 1.52 m in diameter and 0.76 m in height using 8 support arms (two arms per blade). Rated for 5 kWe in a water velocity of 3 m/s, the rotor rotates at 90 RPM. With a gearbox ratio of 13.5:1, the generator outputs 0 to 198 V. All together, the system measures 2.25 m high and weighs 340 kg. Figure 13 shows the research vessel layout along with a picture of the turbine.

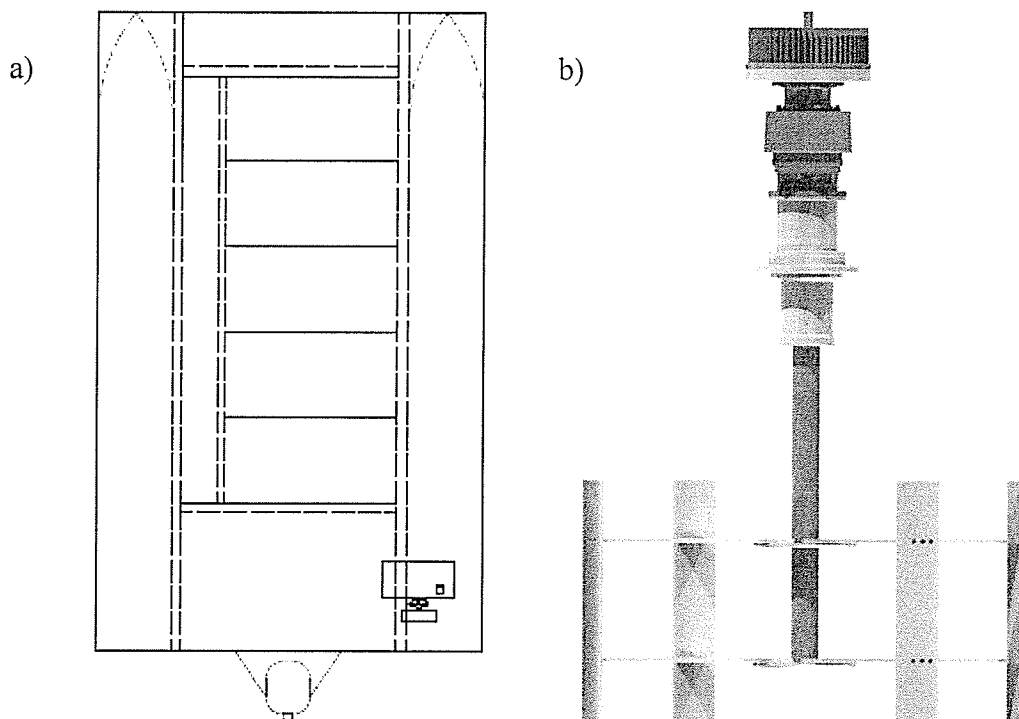


Figure 13: a) Top view of the research platform b) 5 kWe NECI Darrieus turbine

(courtesy of NECI)

### 3.5 Anchoring

This project tested the concept that a tethered turbine can be economically feasible if the anchoring costs can be kept low. Anchoring is a major factor in determining a suitable installation site. The rivers of the Canadian Shield offer a solid rock riverbed that can secure an anchor reliably.

Bibeau *et al.* (2008) stated that many rivers in Manitoba had suitable locations; however, those within the Red River valley have a soft muddy riverbed, which result in ever-changing river bottom configurations and suspended particles (which would be expected to be abrasive). The geographical make up of the Canadian Shield provides a desirable terrain: a granite river bed for installing river bottom anchors. However, techniques to drill in fast flowing rivers 30 feet below the water's surface could not be found. The goal was to develop an anchoring system that would cost less than \$35,000. Most installations of this type use a barge with legs secured to the bottom. The cost to move such a barge to the site or retrofit an existing barge exceeded the anchoring budget because the legs needed to exceed 10 m and withstand the high flow rates.

Various methods were considered during the development stages, including an artificially created reef to anchor the turbine to the bottom, using cable retention from the shoreline. This option would be a significant undertaking with risk and it would require a considerable amount of additional effort in construction. Even under low flow conditions, this approach would require an extensive construction cost. However, if kinetic hydro were to be incorporated into a larger project such as the construction of a

bridge, the additional construction cost may be worth the long term financial benefits.

Many ideas needed to be discarded because of their impact to the hydro dam downstream, and because any anchor placed in the channel upstream of the dam that had volume would need to be removed later, which would add to the cost.

The solution decided upon was to anchor the turbine to the river bottom with steel rods, drilled and set into the rock using a cement compound, and protruding 0.25 m above the river bed. For the installation of the test platform at Pointe du Bois, two anchors were installed 91 m (300 feet) upstream of the bridge in the slower currents, as previously shown in the yellow area in Figure 11 a. These anchor points were designed to manage a total load exceeding well above 200,000 lbs; once the anchors were connected by  $\frac{3}{4}$ " chains to a common ring and forming a  $60^\circ$  angle, the rating of the anchor assembly decreased to 50,000 lbs. The ring was then used to connect the main cable that secured the research vessel and the turbine. The layout of the site can be found in Figure 14.

To place the two river bottom anchors, barge anchor points were first established on both sides of the shoreline at points A and B using 25 mm diameter steel rods drilled and fastened into place with cement. A flattop barge was fitted with a compressor (for drilling and pneumatic winches), three 2-ton positioning winches, and a drilling rig. The positioning winches were located at the downstream end of the barge, and  $\frac{1}{2}$ " steel cable ran through a pulley at each upstream corner and out to the anchor points on the shoreline.

Using this system, the barge could be located and held fixed at any position across the width of the river, by adjusting the line lengths. The two cable positioning system provided a full range of 2-D motion for locating the barge. A tug boat was used to move the barge back and forth from the dock to the site, and two open boats with outboard motors were towed alongside for emergency backup.

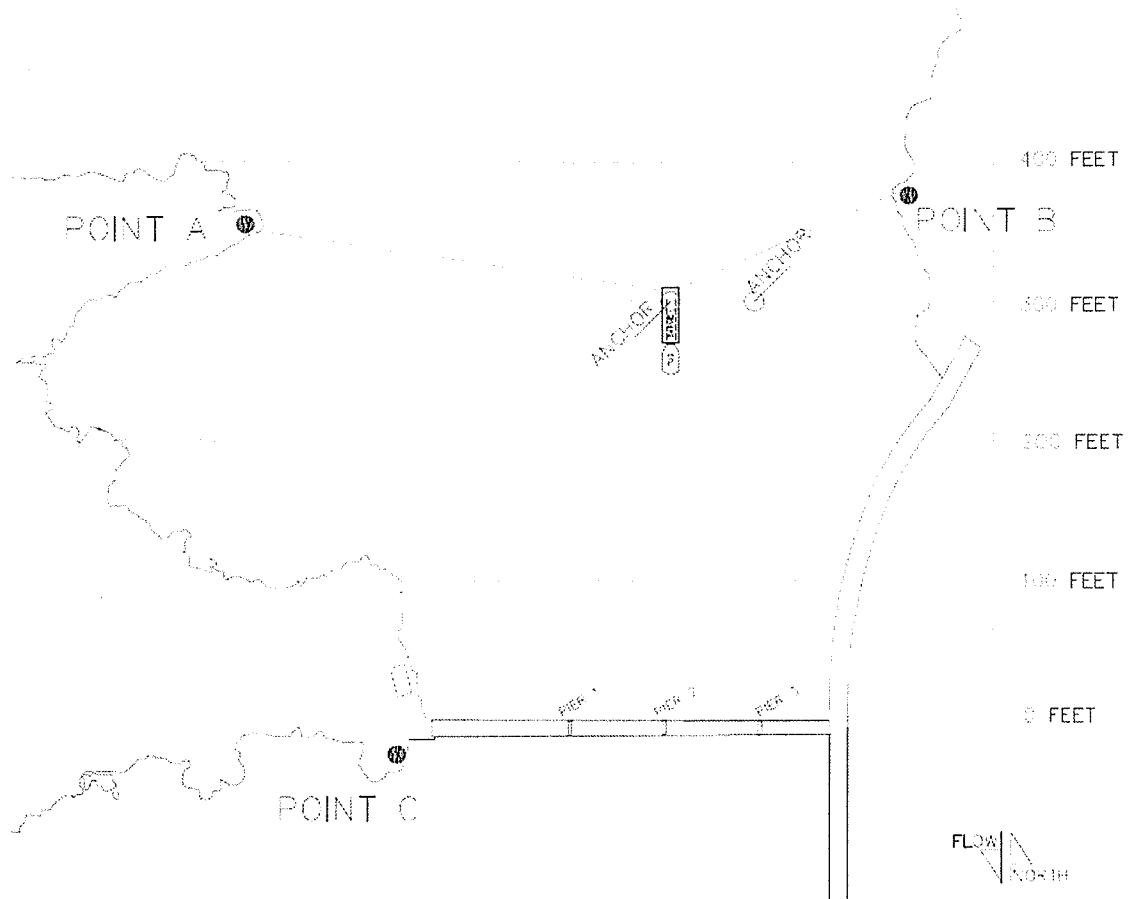


Figure 14: Anchor drilling method (courtesy of John Woods)

Drill rods were fitted with a sacrificial bit, and the bit end was welded onto each rod. Once the rods were embedded into the rock they were sacrificed and left in the rock to act as attachment points. The rods were hollow, so that a grout mixture could be pumped into

the hole, through the rods, filling up the void created in the rock and the rod itself. The rods and bits are similar to those used in highway projects to stabilize rock cliffs. Since the rods were in 10 feet lengths, and the water was over 20 feet deep, the drill bits were unable to gain a sufficient initial bite due to the shaft wobbling. A heavy drilling plate with a collar was designed, which was lowered to the bottom with the drill rod, in order to hold the rod in place and start the drill hole. Figure 15 shows the overall schematic of the system.

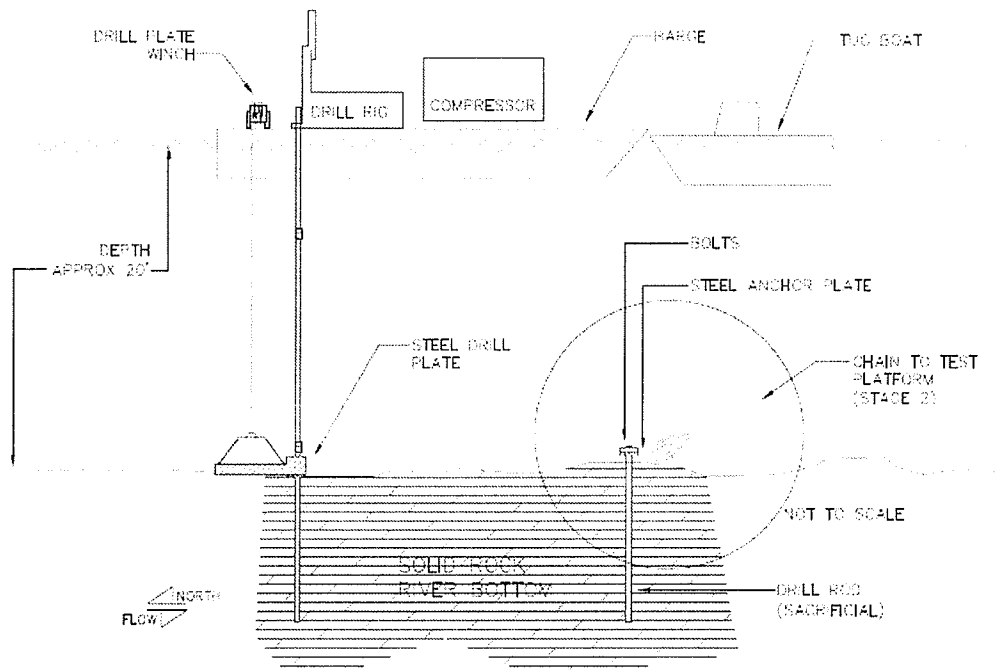


Figure 15: Anchor drilling schematic (courtesy of John Woods)

Once the rods were in place and filled with grout, a tethered scuba diver was lowered to the bottom to cut off the excess rod and place a steel plate over the rods. Cold water prevented the drill operator from decoupling the cemented rod as planned. Two nuts

were threaded onto the rods, in a lock-nut configuration. To these anchors, 3/4" chain was fastened using a threaded pin shackle.

Two anchors points were placed perpendicular to the river's flow direction, and 30 feet of 3/4" chain was attached from each to a center yolk, from which the turbine would be supported. The above technique constituted a unique installation method, and required concurrent design input to meet the original design objectives. The anchoring system of the turbine required a minimal amount of structural components and labour to put it in place. This reduced capital costs and minimized environmental impact. The use of a barge with 30 feet legs would have significantly simplified the anchoring but it was too costly.

The final anchoring system can be viewed in Figures 16 and 17. Two chains connected the two anchor points drilled into the bed rock to a common point referred to as the master link. Large buoys were tethered to the master link. The buoys needed to be large because of the weight of the chains, and because the speed of the flow would easily suck them under the free surface, making them difficult to locate during deployment. The main cable was shackled to the master ring and ran from there to the load cell link downstream. From the load cell link, two cables anchored the port and starboard sides of the research vessel. The cables were shackled to eyelets that were bolted and welded to the frame of the research vessel just above each pontoon.

For added security, a safety line was anchored on the downstream shore of the foot bridge at point C. The anchor was drilled and cemented into a large rock. The safety line was then shackled to the anchor at one end and connected to the rear shore side of the research vessel. It was connected to a similar eyelet that was used at the bow to connect the main cable. The safety line was not designed to withstand the full load of the research vessel in the high flow area. Therefore the line used was of a smaller diameter, only ½” steel cable. The design of the safety line was a contingency plan. Should ever the main cable be compromised, the research vessel and turbine would not end up impacting the dam downstream. The safety line would get taut causing the drifting research vessel to swing radially inward towards the downstream bay area where it would settle. The safety cable ensured a smooth and gentle capture of the research vessel should it ever be released from the main anchoring line.



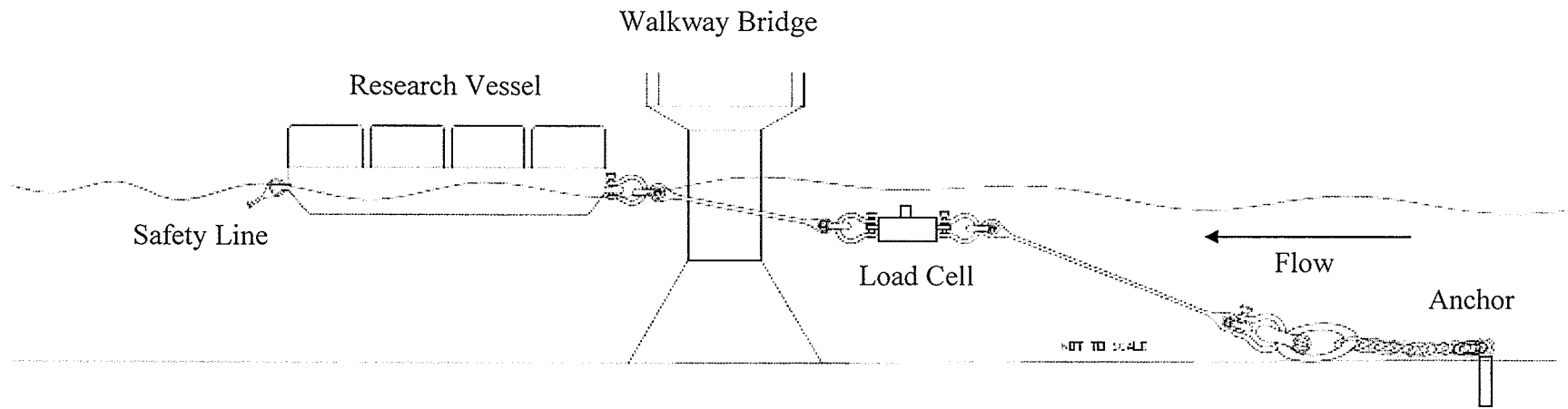


Figure 16: Anchoring system

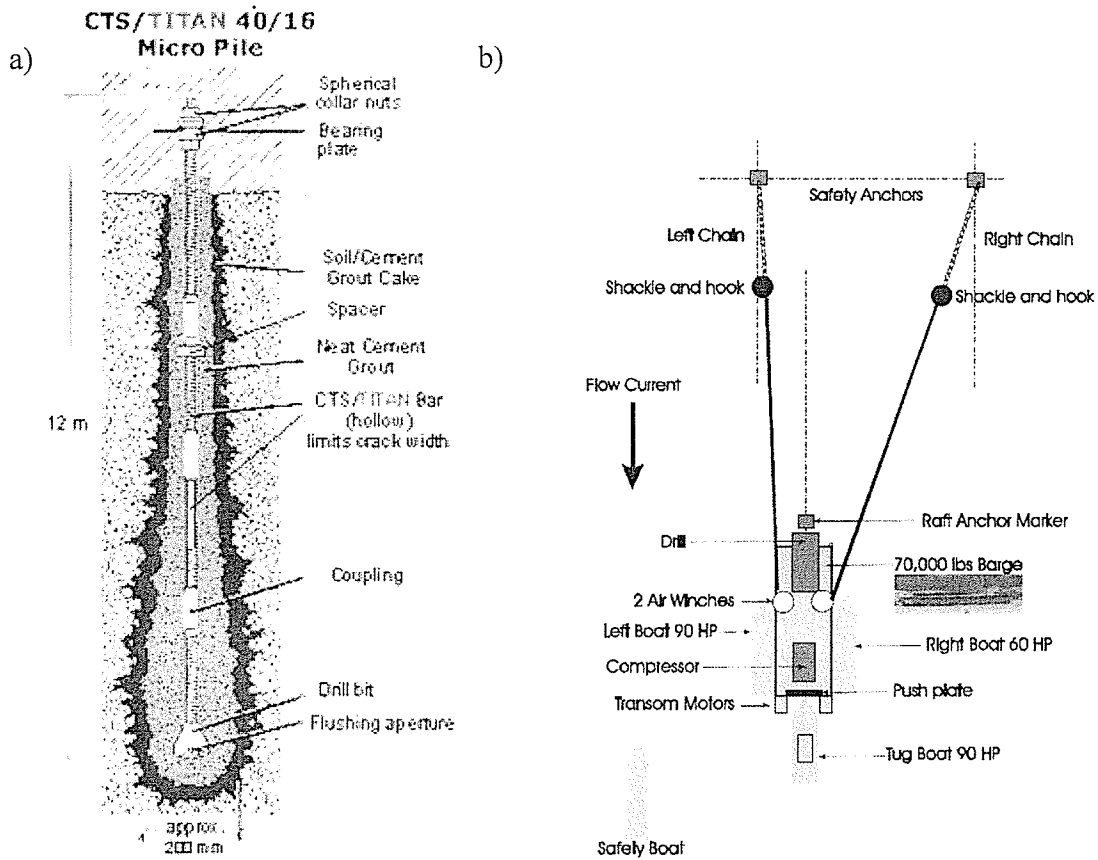


Figure 17: a) Cross-section of imbedded anchor and b) drilling rig set up on the water

### 3.6 Data acquisition system (DAQ)

Data on turbine performance and environmental conditions were captured by various sensors and cameras. The research platform was equipped with four thermocouples, two vibration sensors, one load cell, one flow meter, three current transformers, three outdoor cameras and one underwater infrared camera. Video was logged continuously by the Digipro4 software package and broadcast over the internet via client software. Power data was recorded by an Arbiter 930-A power analyzer that measures up to 600 Hz. The sensor readings were logged by a DT85 data taker. Log files from the two data systems

(power meter and data taker) were analyzed, graphed, and posted online by Scanfile software developed in the Perl language) for routine viewing by the groups involved with this project. All of the sensors were checked against an alarm value indicating an issue with the turbine's operation. When triggered, an email alert system initialized to warn of the sensor readings.

The DAQ was controlled by two computers; one computer resided in the control center in the ATCO trailer, and the other computer was mobile. The mobile controller was the boat computer because it resided on the research platform during testing. There were three main systems that functioned independent of each other: the DT85 data taker, the 930-A power analyzer, and the Digipro4 software. Data was logged by the first two systems and the third system captured important events and monitored the project remotely. The DT85 recorded sensor readings every minute; therefore, an hour block consisting of 60 data points was unloaded for each sensor. The 930-A power analyzer had a maximum sampling frequency of every 10 seconds. Every five minutes the log file was copied into a common file. Each day the power analyzer's log was deleted and started anew. These log files were then accessed by the Scanfile software on the ATCO computer for final consolidation and analysis. The three data capturing systems actively ran on the boat computer while the ATCO computer controlled the data management. Both computers gathered, processed, stored, and presented the data.

### 3.7 Network

The network schematic shown in Figure 18 depicts the information pathways that are in place at the Pointe du Bois site as they were designed by Manitoba Hydro. The top level firewall directs the remote desktop connection on port 3389 to the ATCO computer while the boat computer is free to access via ports 2000, 2001, and 2003 only. No other ports were allowed to enter this network while all ports could exit.

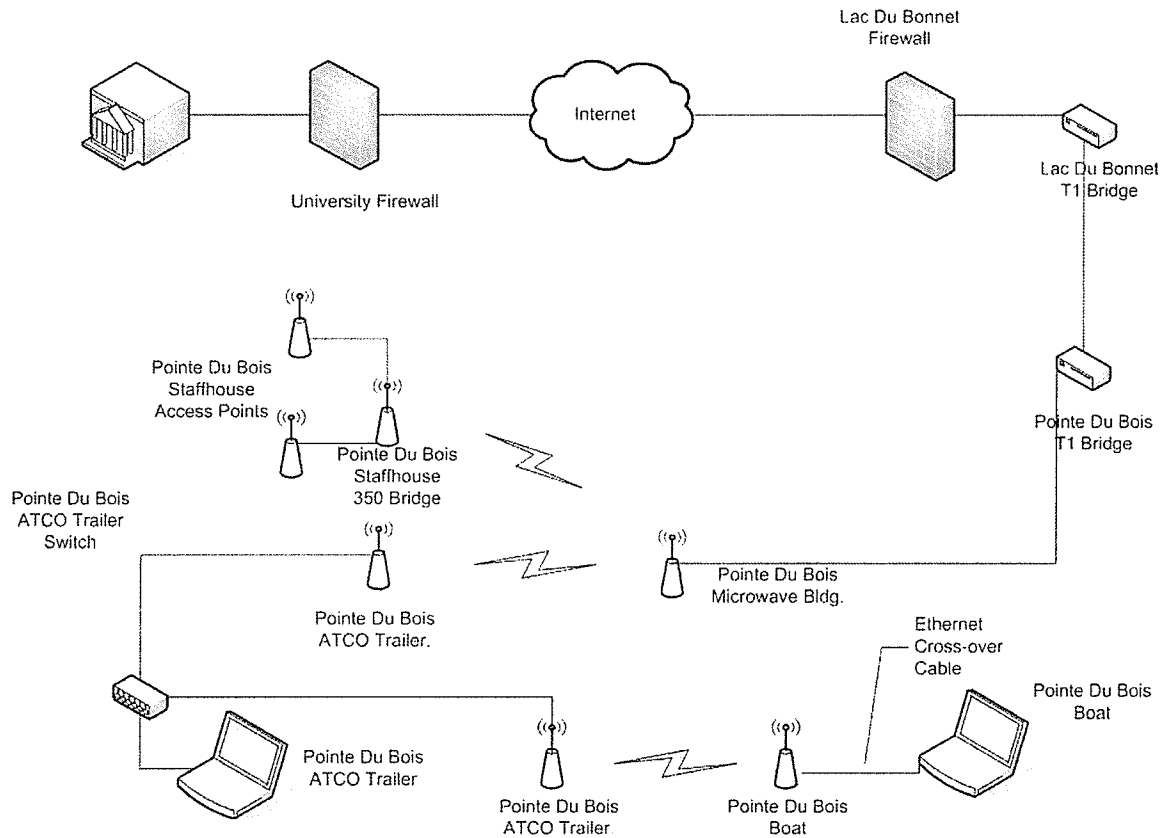


Figure 18: Network schematic

The boat computer used the three ports to share the video feed online through the Digipro4 Server. The boat computer could only be accessed remotely from the ATCO computer. The ATCO computer was accessible remotely from any internet access point. At first, the two computers were networked via a wireless connection; however, reflection of the wireless signal off the water and through the steel bridge frame caused many issues. The signal was not getting across cleanly or consistently, so the connection was then switched to a hardwire connection using 300 ft of CAT 5 Ethernet cable to ensure reliable communication.

### **3.8 Hardware**

The DAQ had multiple components located on the boat and on shore. Figure 19 gives the overall schematic, hardware and connections of the DAQ.

#### **3.8.1 DAQ box**

All data acquisition equipment located on the research vessel was housed in an aluminum trailer hitch box for protection from the elements and organizational purposes. This box housed the boat computer along with its mouse and keyboard, current transformer (CT) box, DT85, and the 930-A power analyzer. There were two power bars to spread the incoming 120 VAC shore power to all of the systems within. To keep the box cool, a small CPU fan was mounted at the back of the box to expel warm air. On the outside of the box there were multiple inputs for the various sensors and cameras.

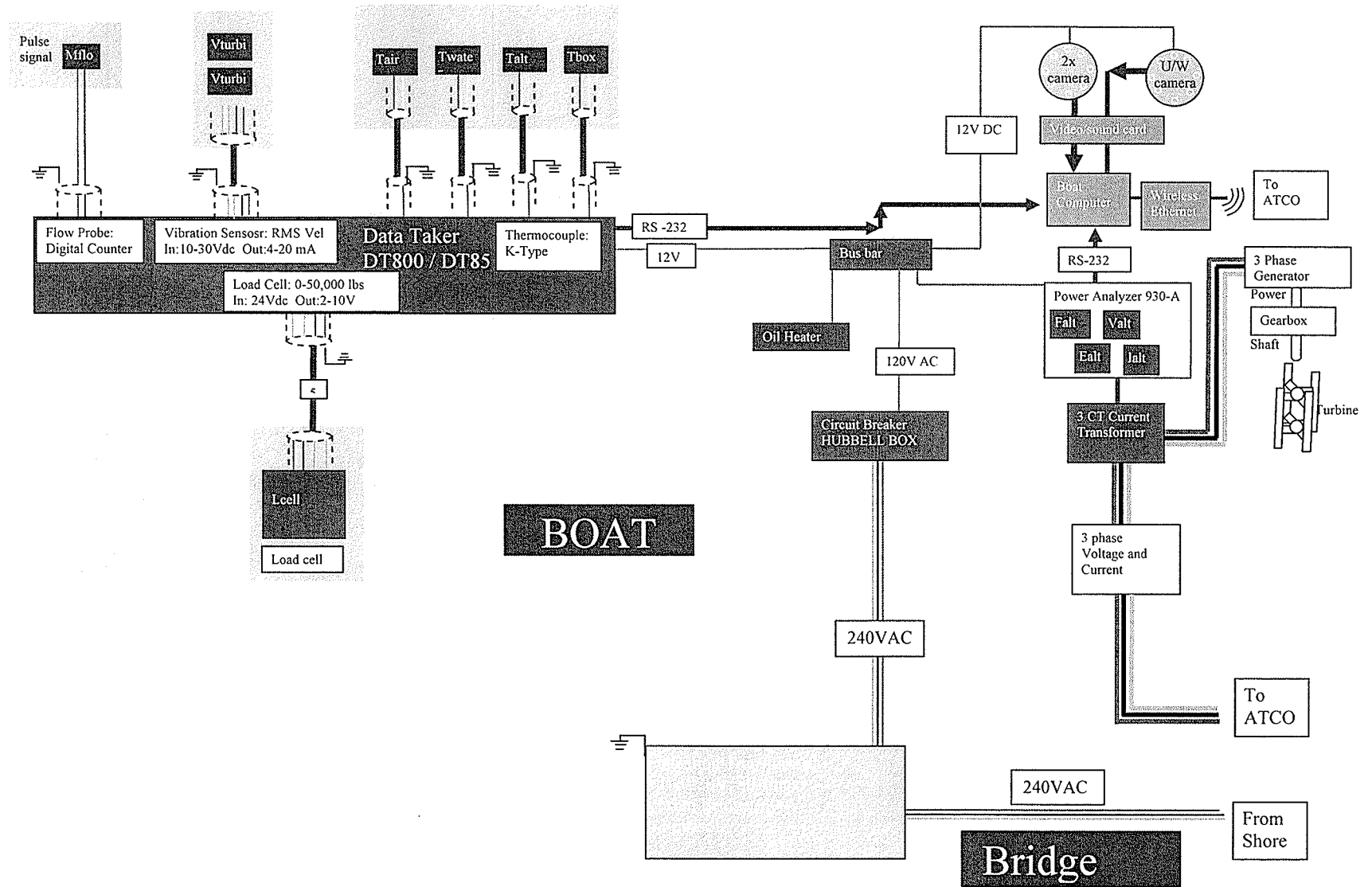


Figure 19: Hardware connection schematic

Cont'd on next page

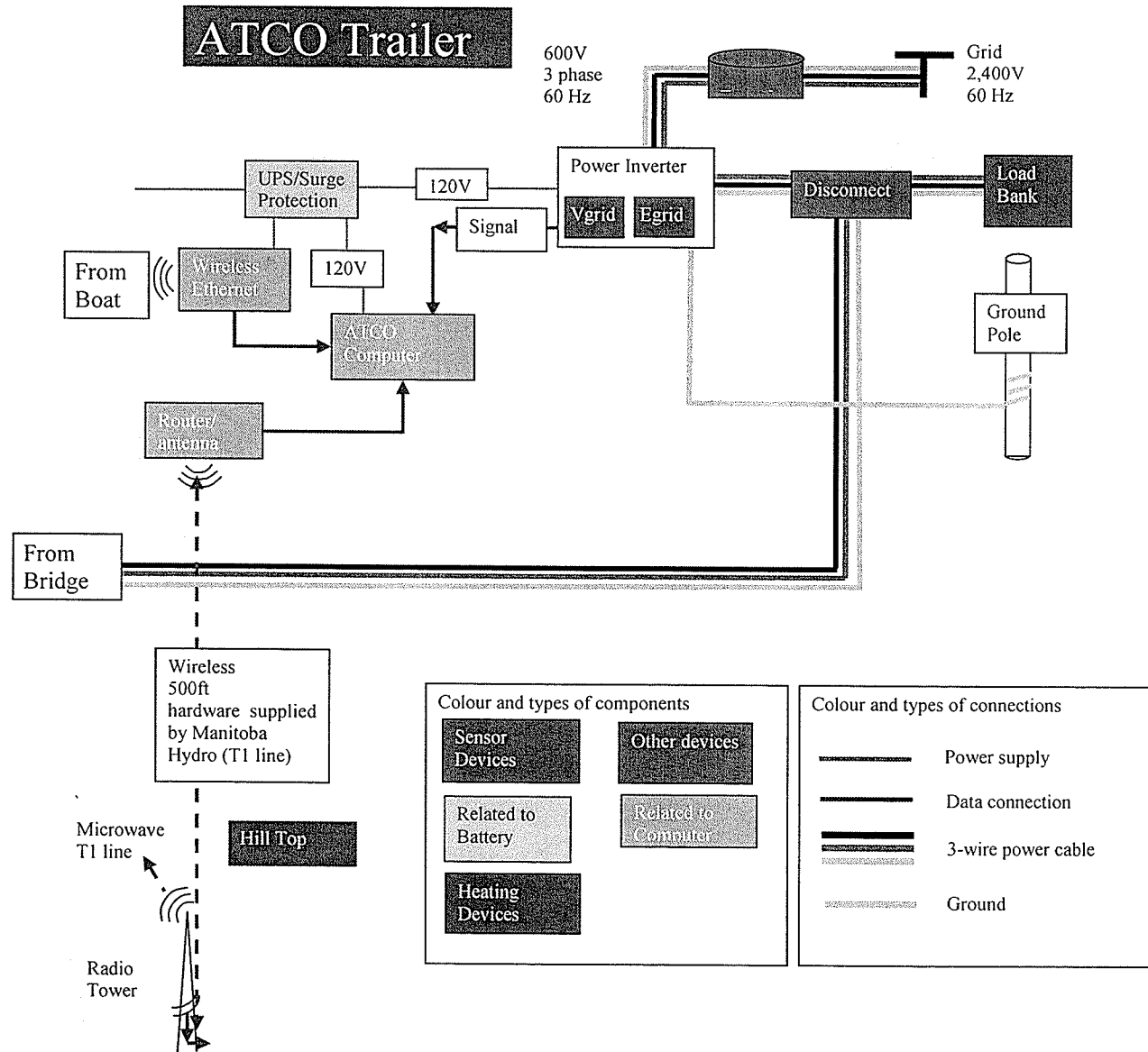


Figure 19: Hardware connection schematic (cont'd)

All inputs for the DAQ were designed to have connectors outside the box for a quick disconnect. During deployment and redeployment, the DAQ box proved to be a valuable space and time saver because relocating the box and re-connections the sensors were straightforward.

### 3.8.2 Video

Four cameras were mounted on the research platform and on the bridge. Three outdoor, motion sensing, infrared cameras were used to record the site above water and one underwater camera was used to view the turbine under the water line. One camera on the bridge showed the research vessel and was essential in viewing the overall system.

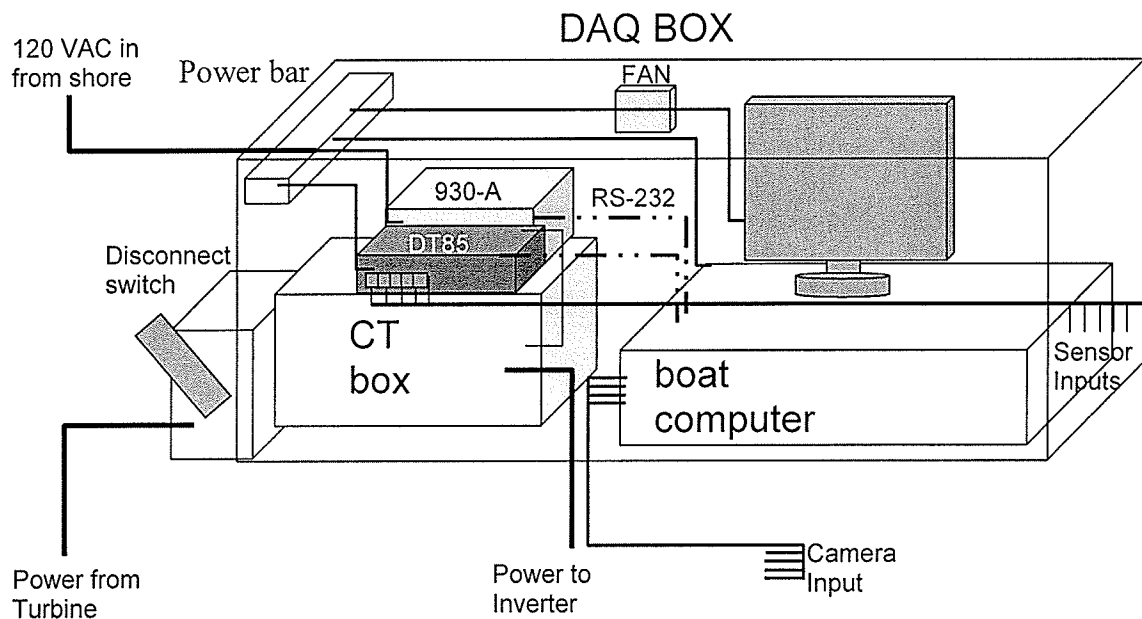


Figure 20: Hardware arrangement inside DAQ box



During the winter, this camera was used to assess the ice buildup and show the location of the turbine between the piers. Two cameras on the platform, one above and one below gave a closer look at the turbine drivetrain and the water's free surface respectively. The drivetrain camera showed operational motions and direct impacts while the camera below showed if the turbine was in operation or stalled. The camera below deck gave a clear picture of ice accumulation between the pontoons. The underwater camera shows the turbine in operation during the winter. In the summer, sediments in the water created poor visibility. The cameras were mounted using aluminum brackets, self-tapping screws, and mounting hardware supplied with the cameras.

The video capture hardware was installed into two of the boat computer's PCI slots. It could record up to 4 channels and it had digital outputs available on one of the PCI boards. These outputs were controlled using the Digipro4 Server software. The cameras requires their own independent power source, a 9 VDC adaptor plugged into a 120 VAC circuit. RCA video cables connected to the Video In terminals on the boat computer and led outside the DAQ box for easy connection to the cameras on the research vessel. All cameras, connectors, and cables were exposed to the extreme cold temperatures during winter.

### **3.8.3 Power analyzer**

The power came from the 3-phase AC generator on the turbine via an 8 gauge Tec cable capable of transmitting 600 V. It was directly wired into a disconnect switch on the side of the DAQ box. From there, the wiring entered the CT box (Figure 21) where each

phase is wrapped around a 200:5 amp current transformer. Leads from the CT and voltage connect directly to the 930-A power analyzer. Phase-to-phase voltage readings were picked up from a junction box just ahead of where the line splits into the individual phases for the CT's. From the CT box, the power line connects to another Tec cable that runs down the length of the bridge to the inverters located in the ATCO trailer. The inverters directed the power onto the grid after adjusting the power signal so that it matched the grid at 240 V and 60 Hz.

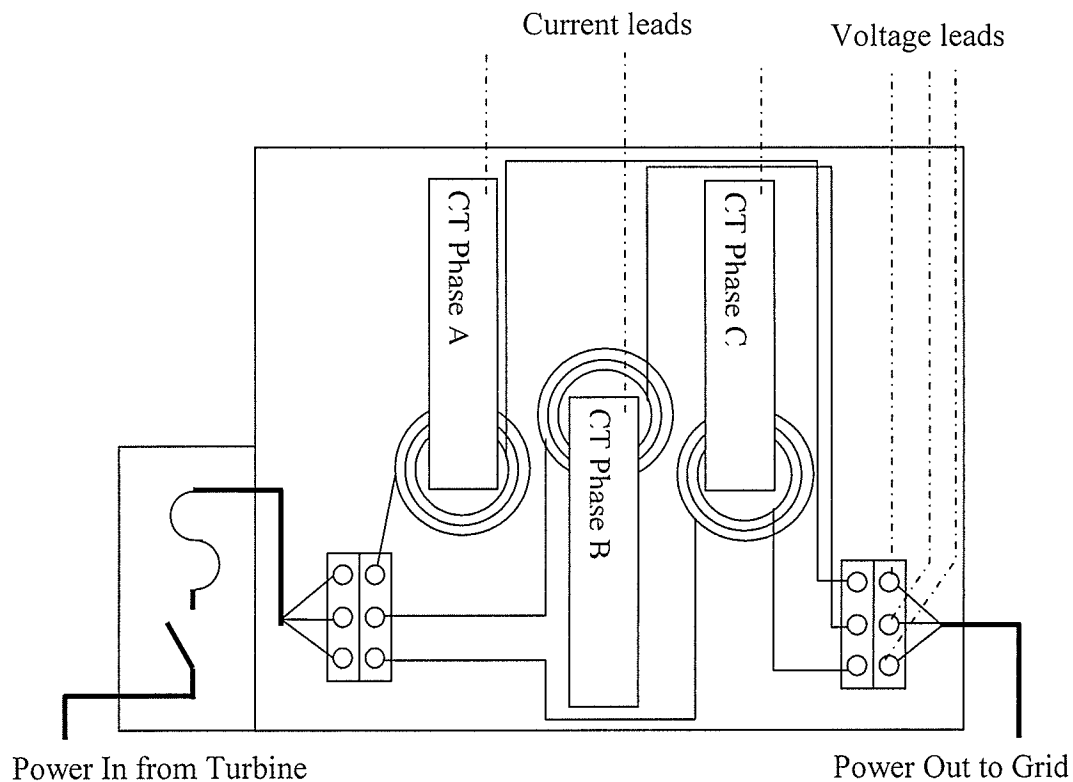


Figure 21: Schematic of the current transformer box

The Arbiter 930-A power analyzer was set up in a 3-phase, 4-wire, 3-element configuration and the data port was connected to the boat computer via an RS-232 serial cable. It was set up on COM 4, which resides near the bottom of the PCI expansion slots.

To access the data coming from the 930-A, Tera Term software was used to connect to COM 4. By coding a macro into Tera Term, the software was able to establish a connection, record the data, pause for 20 seconds every 5 minutes while the raw file was being copied, and then resume logging. Power to the analyzer was supplied through a typical CPU power cord that plugs into any 120 VAC circuit.

#### **3.8.4 Data taker**

The DT85 data taker was versatile and could be used in many configurations. The configuration used for this testing had the DT85 connected to the boat computer via RS-232 serial cable plugged into COM 1 on the motherboard. It is powered through a 12 VDC adaptor plugged into any 120 VAC circuit. The sensors connected to the appropriate wires with bullet connectors located on the front of the DAQ box as per their labels. Inside the box, the sensor wires connected to the appropriate input channels on the DT85. The leads off the sensors connected to green junctions, which were the input ports for the DT85. This design allowed the junction boxes to be disconnected from the DT85 so that the wiring remained in place while the DT85 can be moved.

#### **3.8.5 Sensors**

The sensor inputs to the DT85 were prearranged and fixed in location as detailed in Table 3. This section outlines the specifications of each sensor along with its connection schematic to the DT85.

Table 3: List of sensors

Sensor	Channel	Wiring Type	Reading Type
Ambient Thermocouple	1	Thermocouple	instantaneous
Water Thermocouple	1*	Thermocouple	instantaneous
Generator Thermocouple	3	Thermocouple	instantaneous
CPU box Thermocouple	REFT	DT85 Reference Temperature	instantaneous
Vibration 1	7+	Current Loop	Maximum
Vibration 2	7-	Current Loop	Maximum
Load Cell	9	Voltage	Maximum
Flow Meter	4	Digital High Speed Counter	Counts per minute

Table 3 lists the channels of the DT85 to which each sensor was wired. Multiple sensors occupied one channel. This was achieved by using all four inputs on each channel: the +, -, \*, and # inputs. The two sensors were differentiated as Channel 1 (between + and - inputs) and Channel 1\* (between \* and # inputs). For a shared input using a current signal, the channels were differentiated by Channel 7+ (between + and #) and Channel 7- (between - and #).

### 3.8.5.1 Thermocouples

Thermocouples used for this project were K-type, purchased from Omega Canada. These were chosen because they are the most common and inexpensive thermocouples for general use. The signal was converted to a temperature

reading by the DT85 internal calculations. The readings were validated by using both the DT85 and a handheld multimeter that supported K-type thermocouples. Both thermocouples (one connected to DT85 and the other to the multimeter) were exposed to ambient, hot water, and cold water environments and their readings were checked against each other for validation.

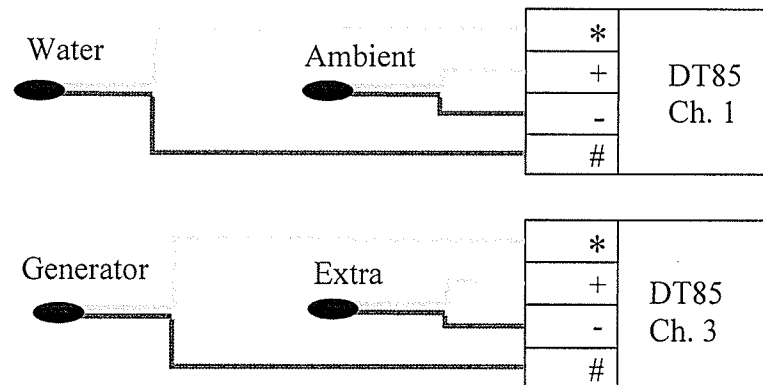


Figure 22: Thermocouple wiring diagram

Table 4: Thermocouple wiring location on DT85

Thermocouple	DT85 Channel
Ambient	1
Water	1*
Generator	3
Extra	3*

### 3.8.5.2 Vibration sensors

Vibration sensors (Figure 23) measured the RMS velocity as the sensors vibrate. The sensors had a maximum threshold of 50 g, required a 12 VDC input, and output a 4 to 20 mA current that related to a percentage of the maximum value. These sensors were unidirectional, so two sensors were needed to capture vibrations within a plane. The two sensors were mounted in a streamwise and cross-stream orientation.

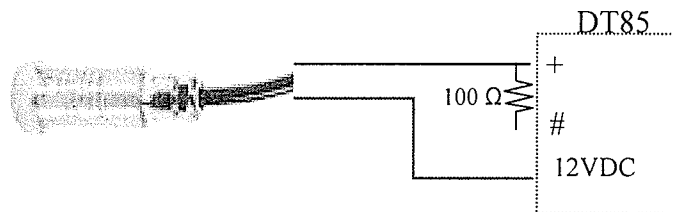


Figure 23: Vibration sensor wiring diagram

### 3.8.5.3 Load cell

The load cell, purchased from Honeywell Sensotec Sensors, was submersible. Two 50,000 lb load cells were purchased for this project, both with different input/output settings. Their certificates of calibration detail their specifications (see Appendix B). One had 4 wires and required a 10 VDC input while giving a 1.37 mV/V output. Thus the maximum load would output 13.7 mV.

The other load cell is of a 3-wire configuration. This sensor requires a 15 to 40 VDC input and gives a 4 to 20 mA output for the load ranging from 0 to 50,000 lbs. The physical wiring schematics and how they connected to the data taker are shown in Figures 24 and 25, respectively.

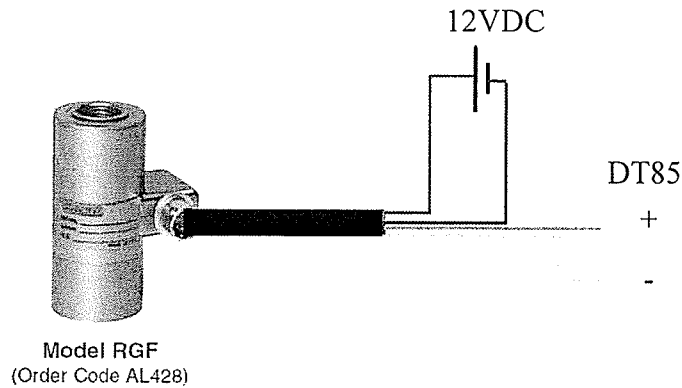


Figure 24: 4-Wire load cell wiring diagram

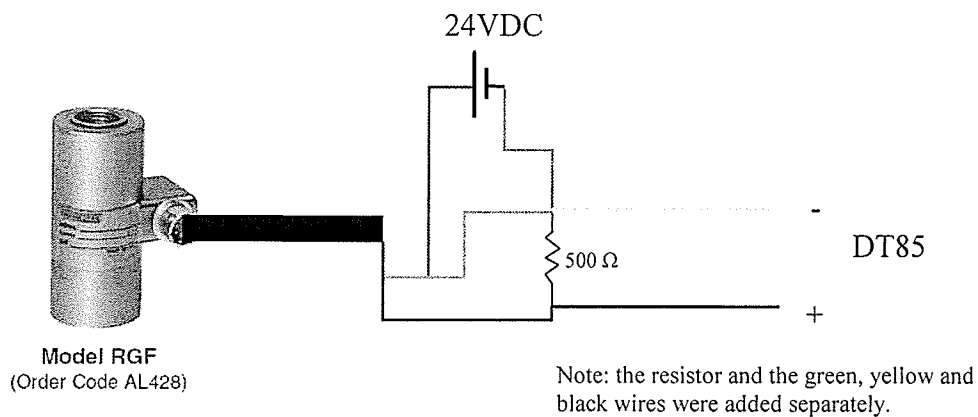


Figure 25: 3-Wire load cell wiring diagram

### 3.8.5.4 Flow meter

This probe is a propeller style counter and is shown in Figure 26. As the flow rotates the propeller, a magnet at the tip of a blade caused a contact to close within the internal circuitry and gave a resistance between the bare wires of  $1 \Omega$ . Each rotation gave a closed circuit pulse. The DT85 high speed counter added the number of pulses in a minute and then the flow rate could be calculated by Equations 6 and 7.

$$316 \text{ RPM} = 1 \text{ ft/s} \quad (6)$$

$$1036 \text{ counts/min} = 1 \text{ m/s} \quad (7)$$

This model of flow meter had a short tube that created an entry boundary layer. Also because it had two propeller blades and one magnet to trigger one count per full revolution, this meter was found to be inaccurate. See Section 5.3.1 for details on flow meter calibration.

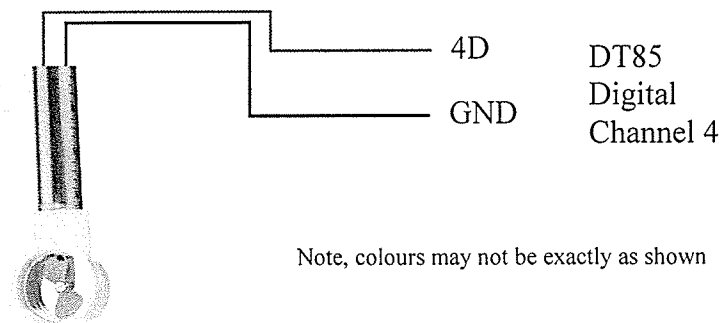


Figure 26: Flow meter wiring diagram



### 3.9 Software

The functions on the boat computer were initiated using Windows Scheduled Task.

There were three programs that ran on scheduled intervals:

- Deload – Invoked Deload.exe which logged the latest data from the DT85 since the last de-loading. The file was named by a date and time stamp and stored on the data drive on the boat computer.
- Power Copy – Invoked PowerCopy.pl, a Perl script, written to copy the power analyzer's log file to a common file named aPower.csv. The data was renamed to a common file name so that it could be read by the Scanfile software.
- Power Copy Day – Invoked Date.pl. This program ran one second before midnight every day. It deleted the power analyzer's log file so that each day captured a new log. Before deleting the file, it was renamed as that day's date and stored on the boat's data drive for the archives.

The ATCO computer was networked with the boat computer's data drive via CAT5 Ethernet cable. With the two computers networked, the ATCO computer could access all the files logged by the data taker and the power analyzer.

- Scanfile.pl – Ran on the ATCO computer. This program accessed all the logged data and analyzed it. It ran continuously, searching the boat's data drive for any new .csv files. Once a new file was found, the software scanned and analyzed data from all of the sensor and power readings. A daily file was compiled from

the hourly sensor data and backed up to the ATCO's data drive. The power data was also backed up onto this drive in the same manner. The data was then graphed, stored locally on the ATCO drive and posted online via an FTP protocol. The software could also send email alerts if the values scanned in exceeded the alarm criteria. All alarm values were logged while emails about the specific alarm were sent out immediately at a maximum of once per day.

### **3.9.1 Video system**

Video was recorded using the Digipro4 Server software. This program allowed video to be recorded on a predetermined schedule or when motion sensitive cameras detect motion. For this project, the cameras were set to continuous capture and set to broadcast over the internet, viewable with the Digipro4 client software. Accessed through port 2000, video could be accessed by any client software via the internet using the IP address of the network. Video could be stored through the client software or by retrieving it from the hard disk on the boat where the server records. Review of the footage could only be done using the Digipro4 Search software because the video was recorded in a proprietary format. Remote access to the boat computer's video archive could be obtained; however, the large size of the video files made this a slow and difficult task. If anyone attempted to access this program while it was in the remote desktop environment, the program crashed and shut down. Each daily file ranged in size up to 20 GB. The video drive on the boat computer was 200 GB in size and held up to 2 weeks of continuous video before deleting the oldest file. The software continued to overwrite old files to accommodate new ones.

### 3.9.2 Power analyzer

The Tera Term software logged the data coming from the 930-A power analyzer into a file named by the user. A macro was written to initialize the connection and logging procedure. It was set up to write all data to a file called log.csv located in the Tera Term program folder. The macro recorded data for 4 minutes and 40 seconds before a 20 second downtime. While the file log.csv was being accessed by the Tera Term program, it could not be manipulated; hence, a small window of 20 seconds was programmed in. Therefore, the program had to be started in sync with any 5 minute interval such as 5:05 or 10:15. It was during this 20-second window that the file could be copied by the Power Copy task. It was copied to aPower.csv located in the data drive under the DT800/Data subfolder. The file, log.csv was continuously appended to, so it increased until it was deleted. The Power Copy Day task copied the log.csv file to the same location as aPower.csv and named it as the current day's date, and then log.csv was deleted to be started anew the next day. This allowed daily files of the power data to be kept in order.

### 3.9.3 Data taker

The DT85 data taker was controlled via the DeLogger software package. Available on the boat computer's desktop, the DeLogger program was the gateway to the DT85. This program was used to define the sensors, display readings, manipulate and control data logging, and other functions. The software was versatile, user friendly, and was used to set all logging parameters. The data from each sensor was logged at the specified rate and in the order in which it was defined. As the data was logged, it could be displayed

within the DeLogger software in real time. Figure 27 is a snapshot of the screen where real time data is displayed.

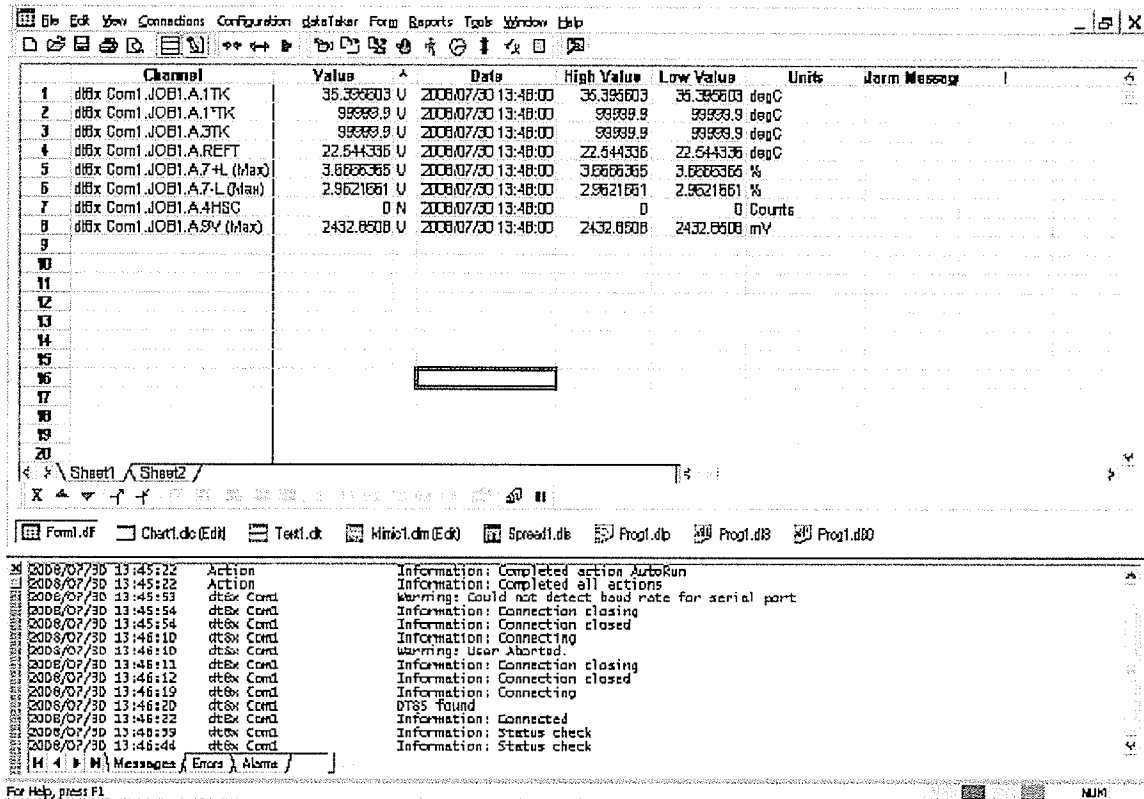


Figure 27: Real time sensor display using the DeLogger software

For the 5 kWe turbine testing, the data was set to log each channel once every minute.

The thermocouples logged the instantaneous reading for each minute while the vibration and load sensors recorded the maximum value within that minute sampling at around 6 Hz. The flow meter recorded the number of counts in a minute and reset.

### 3.9.4 Scanfile software

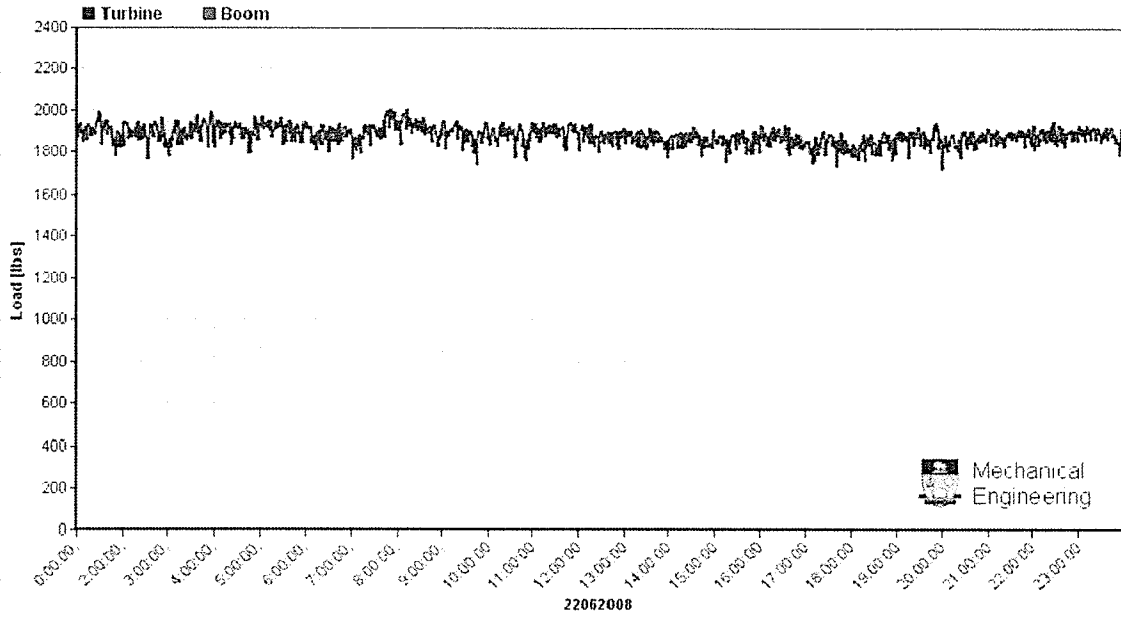
The Scanfile software was programmed using the Perl language and was developed for this project. Its capabilities included sending out email alarms, graphing data, and updating a web site with those graphs. The program was set to run in an infinite loop, constantly looking for a new .csv file to appear in the DT85 sub-directory. Hence this program did not analyze any data until the DT85 unloaded a new data set. Once found, the software renamed the .csv file with an “a” in front to indicate that it had already been analyzed. A one minute delay was incorporated into the program so that the DeLoad software could complete unloading the data taker of all its recent data before the Scanfile software accessed the files. The program then proceeded to analyze the data from the data taker first. Line by line it scanned and sorted the data into its respective arrays for each sensor. With each scan, the value was compared to a defined alarm value. After going through the 60 lines representing one hour of data, the stored array for each sensor was plotted using Perl Chart Director. This software is an addition to Perl. The graphs of the most recent hour’s data were saved locally on the ATCO computer’s C:\ drive. Scanfile checks the date on the .csv file name to determine whether to start a file for the new day, or to append the data to the current day’s file. This function allowed the hourly data to be compiled into daily files. When the hourly data had been analyzed, the software repeated the scan and sort of the sensor data but for the daily file. Thus a daily graph was also made and copied to a subfolder named by date under the Graphs folder in the ATCO computer’s data drive.

The program then continued to access the power data stored in the file aPower.csv. The Scanfile program then sorted the data into time, current, voltage, and frequency arrays. From these arrays, the power output in Volt-Amps of the turbine was calculated. The data was once again graphed and stored locally.

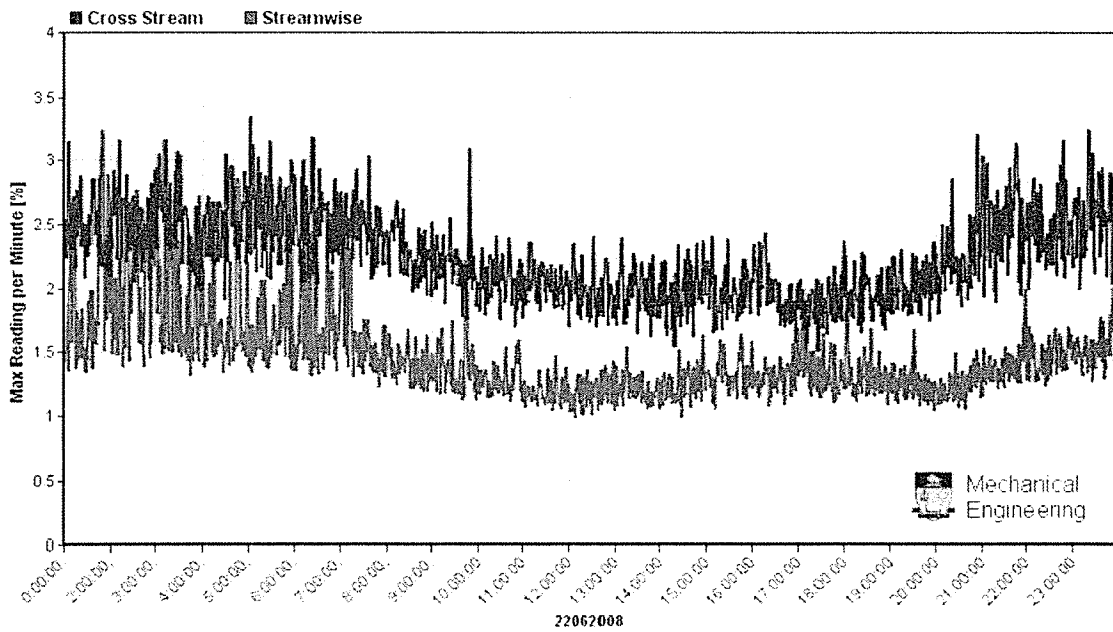
If an alarm was triggered, a message was sent to the alarm subroutine where it was logged in an alarm file (Alarm.csv) and the message was then embedded into an email. Programming was put in place where an email message was sent out immediately but allowed only that one email out per sensor per day; however each alarm triggered was logged in the alarm log file despite repetitiveness. This prevented having multiple emails for a continuous alarm.

### **3.9.5 Output**

The graphs output by the Scanfile software were stored locally and broadcast online for interested parties to view and assess. This section presents all of the graphs that were created and output.

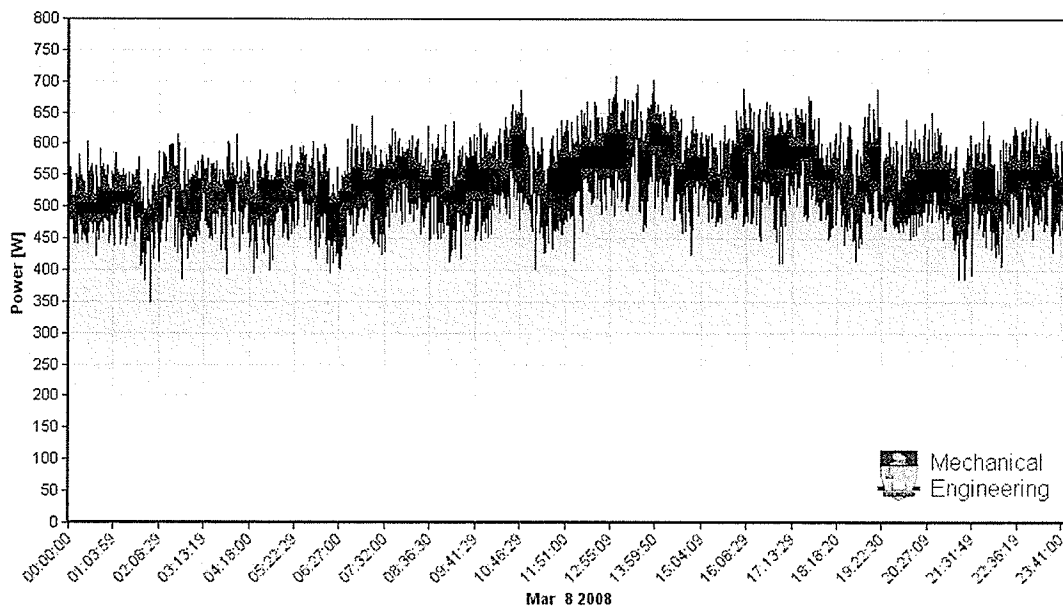


a) drag force

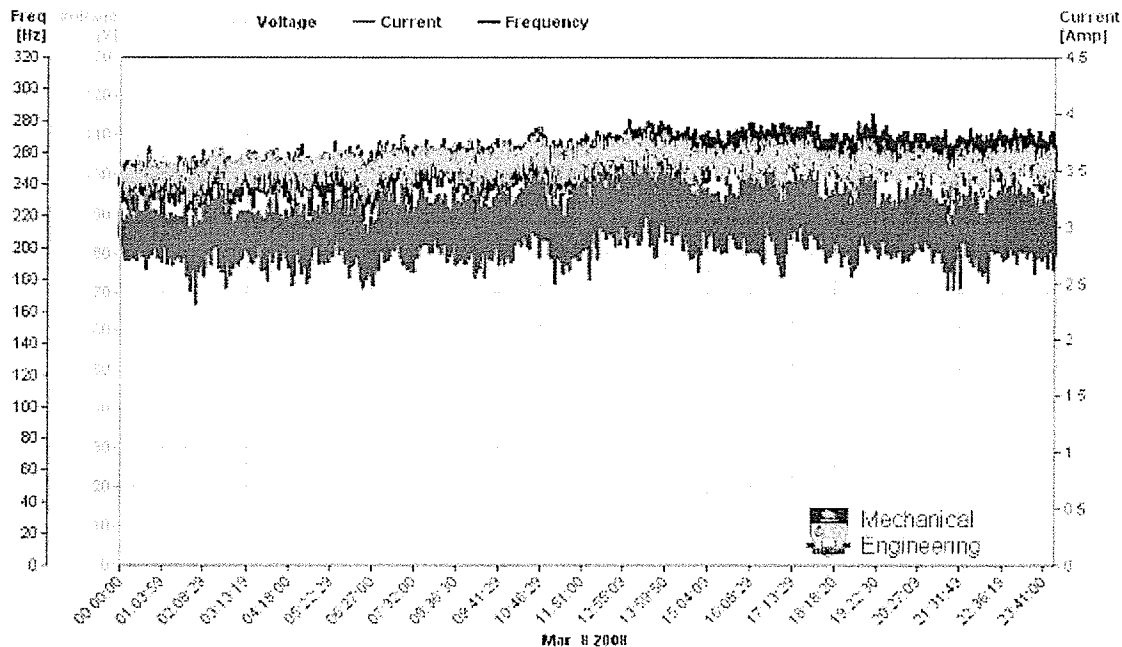


b) vibration

Figure 28: Output graphs of daily sensor data



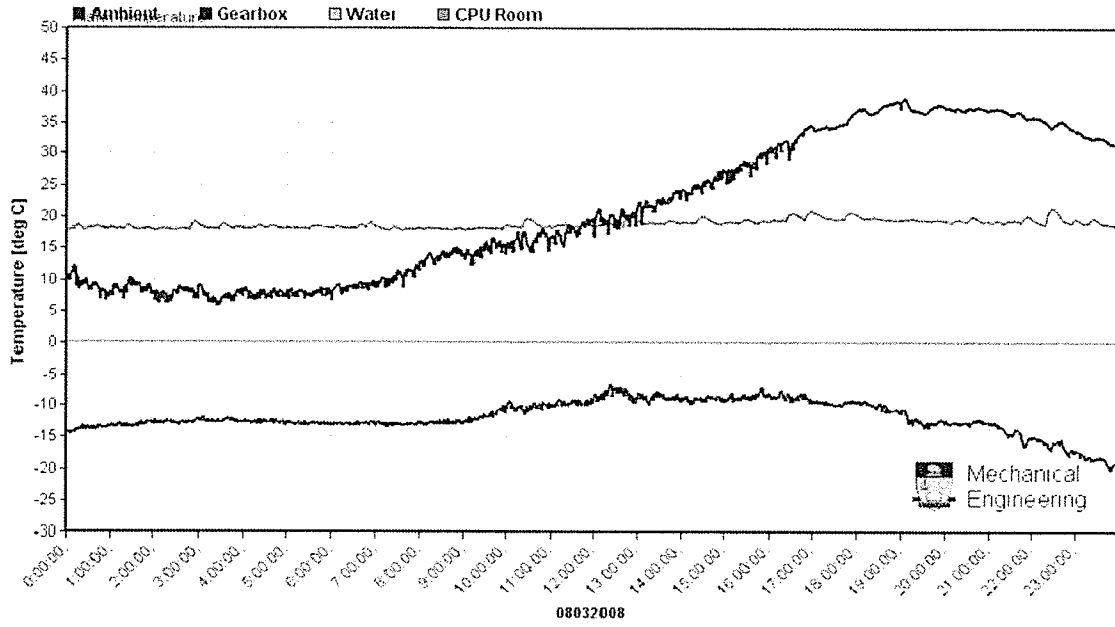
c) power output



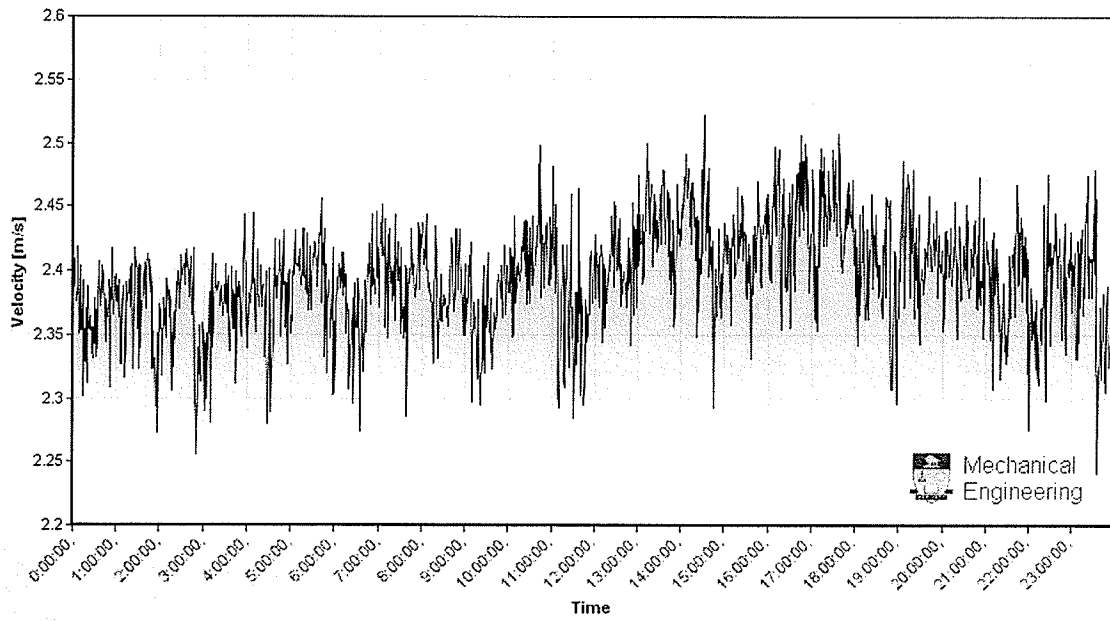
d) generator output

Figure 28: Output graphs of daily sensor data (cont'd)





e) temperatures



f) free stream velocity

Figure 28: Output graphs of daily sensor data (cont'd)

## Chapter 4

# Testing and Deployment

### 4.1 Overview

The objective of this thesis was to assess the performance of the vertical axis hydraulic turbine (VAHT) in Manitoba's climate to determine if this technology could be used in cold Canadian climates. The assessment of such parameters called for specific tests, and general observations. This chapter outlines the tests that were carried out: turbine operation during winter, flow measurements using the Acoustic Doppler Velocimeter (ADV) to validate flow meter readings, and turbine power loss due to the shape of the supports arms of the Darrieus turbine.

Deployment of the research vessel into a high velocity river required detailed planning and safety precautions. Initial deployment required that the vessel be launched upstream of the walkway bridge. After initial placement, the turbine was removed and redeployed to a downstream location. The steps taken to deploy and remove the research vessel are also outlined in this chapter.

### 4.2 Test matrix

Table 5 outlines the various experiments and objectives as they pertain to this thesis.

Table 5: Test matrix

Date	Experiment	Objective
Jan. 1–Mar. 18, 2008	Cold climate operations	<ul style="list-style-type: none"> <li>• Assess icing and associated cold climate issues with turbine operations</li> <li>• Obtain turbine performance in cold climate</li> <li>• Assess independence of turbine operations in a remote location</li> </ul>
June 6, 2008	Turbine performance	<ul style="list-style-type: none"> <li>• Obtain turbine performance in warm climate</li> </ul>
June 6, 2008	ADV measurements	<ul style="list-style-type: none"> <li>• Take ADV measurements for accurate flow rate</li> </ul>
June 6, 2008	Flat bar support arms	<ul style="list-style-type: none"> <li>• Evaluate performance using a blunt support arm</li> </ul>
June 7, 2008	Profile support arms	<ul style="list-style-type: none"> <li>• Evaluate performance using a profiled support arm</li> <li>• Evaluate performance based on location along research platform</li> </ul>
June 8, 2008	Hydrofoil support arms	<ul style="list-style-type: none"> <li>• Evaluate performance using a hydrofoil support arm</li> </ul>

### 4.3 Winter tests

Winter tests assessed the viability of installation and operations of a kinetic turbine in extreme cold conditions. The research platform was initially deployed in December of 2007. The turbine was operational and monitored by sensors during the winter months. The research vessel was removed from the test site at the end of the winter to avoid damage during the spring break up of the ice.

During the testing phase, the turbine was loaded using an Aurora inverter capable of handling 6 kW. The inverter uses a predefined curve to set the load that is delivered. This loading profile curve was created by NECI so that the load ramped up from the backside of the TSR performance curve, increasing from freewheeling to maximum power output. The power generated by the turbine was delivered to a battery bank and heaters. To verify power output, heaters were also directly connected to the generator on the research platform.

Winter testing looked at icing issues through the use of a load cell and video cameras. Due to the harsh environment, the load cell did not survive long because of ice that formed on the output cables and thus the evaluation of icing issues was made from images and on-hand experience. Along with icing, turbine performance was captured and is presented in Chapter 5

#### **4.4 Summer tests**

Re-deployment of the turbine in the summer tested the seasonal variation in performance. Turbine operation in warm climates was measured and assessed to quantify the effect of the cold season on power output. For this testing, the load on the generator was created by the grid. The Aurora inverter was grid-connected and loaded following the pre-defined curve.

To obtain the most accurate performance numbers, the ADV was employed to validate the flow rate measured by the year-round installed propeller style flow meter. Thirteen ADV measurements were taken to obtain a flow profile across the channel at various depths and locations between piers 2 and 3.

Power output was found to be affected by the design of the support arms. Testing of the power output based on the various cross-sections took place in the summer over 3 days. During this test, the location of the turbine was moved to the front end of the research platform to quantify the amount of power lost due to the wake off the pontoons of the research vessel.

#### **4.5 Initial deployment of the research vessel**

To discuss the procedure for deployment, removal and redeployment, the site layout is presented in Figure 29 with important locations marked on the map.

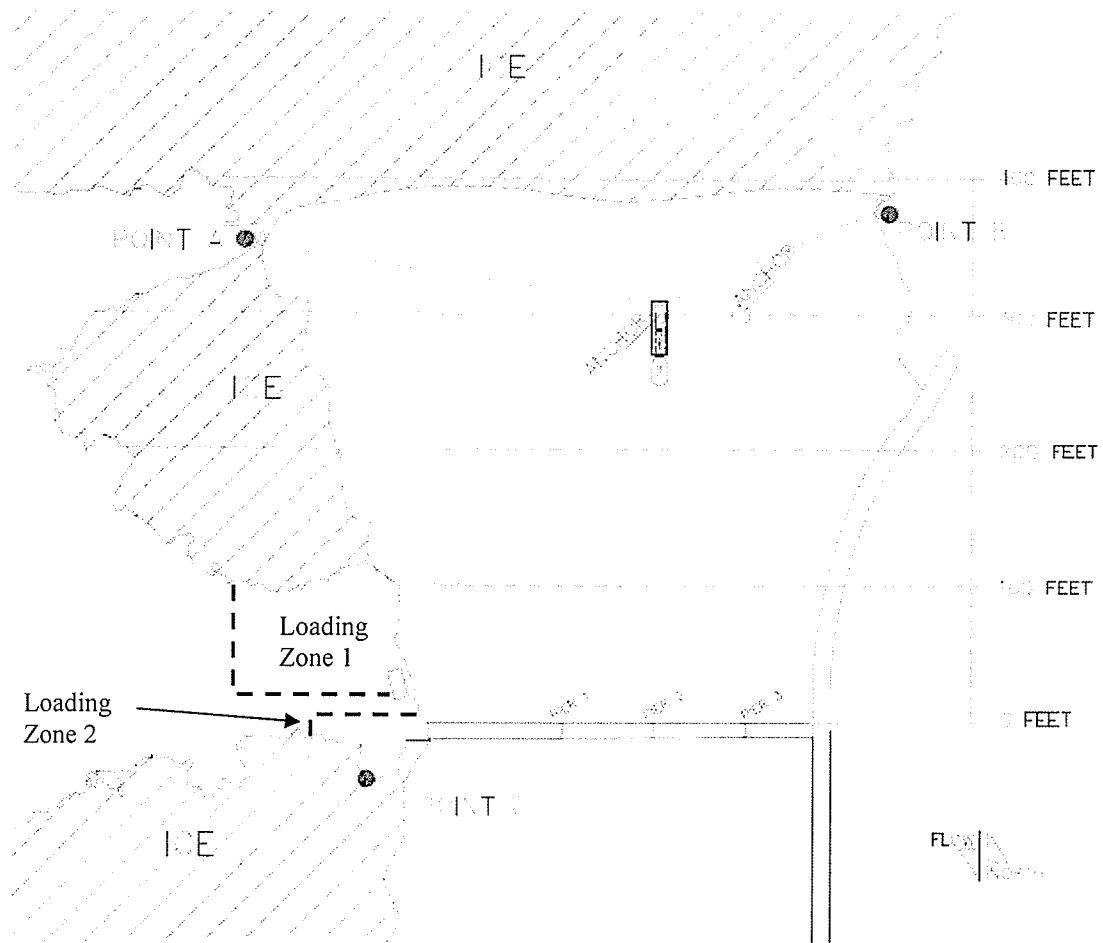


Figure 29: Layout at Pointe du Bois

The research vessel and turbine were transported via flat bed trailer from Calgary to the Pointe du Bois site by NECI. It was not shipped as a whole system and required assembly on-site at Loading Zone 1. This took place within 4 days in mid-December 2007. At this time of winter, the upstream river is frozen over. The upstream and downstream bays close to shore had ice cover 1 to 2 feet thick. The initial deployment procedure called for launching the research vessel into the upstream bay just north of the Loading Zone towards Point A.

The research vessel needed to be launched upstream of the bridge because the main cable lines had to be installed upon initial deployment. Therefore the upstream bay was chosen as the launching site. There was a 4-foot drop from the shore to the ice shield below. A ramp of snow was constructed to ease the pontoons onto the ice. Phase 1 was to move the research vessel from Loading Zone 1 to Point A. All large components of the turbine, along with the 1 ¼" main anchoring cable, were loaded onto the research platform prior to launch. The research vessel was lined up with Point A and the snow ramp with a front end loader. Once in the launch position, a steel cable line was taken from the front winch to the anchor at Point A. The winch line was let out and the free end was walked around the bay and taken over to Point A where it was fastened to the anchor. The winch pulled the research vessel down the snow ramp and onto the sheet of ice in the upstream bay.

The ice was quick to give way to the pressure of the tips of the pontoons. The ice cracked and the pontoons dug in through the ice and rested on the river bed. Breaking through the ice shield with the nose of both pontoons presented a difficult situation. The research vessel would not slide easily across the ice as anticipated, but rather the pontoons dug into the ice sheet; the research vessel was stuck making forward progress very slow and difficult. Sitting at an angle with the bow through the ice and the stern on shore, the 12,000 lb winch was unable to free the research vessel or pull it up onto the ice. To improve the launching angle, the snow ramp was manually removed from under the pontoons using shovels. Using the winch line, the research vessel was nudged forward and sideways in an attempt to free the pontoons from the river bed. The winch was the primary application of force to pull the research vessel forward. Twelve foot

C-channels were used as levers to pry up the pontoons from the bottom, and trucks were used to push the research vessel into the bay. The ice shield finally gave way and broke off clean from Loading Zone 1 to Point A clearing most of the ice cover in that bay.

When the ice in this corridor was removed, the research vessel was able to winch through the free flowing water over to Point A where it was anchored down in anticipation of Phase 2.

The next phase of deployment involved spanning a safety line across the river from Point A to Point B. To take the research vessel out onto the river where the currents run high, it was an established procedure that two points of safety be taken. Therefore, it was required that two systems be relied upon simultaneously for control and stability of the research vessel while deploying. The research vessel always operated with a main and back up safety measure. Onboard engine power was the primary means of control and security while a safety cable, typically a winch line, was used as the backup measure when the vessel was being moved. The shores were too far apart for the winch line to reach; therefore, an additional cable was strung between Points A and B and was used to winch from. This additional cable that ran the width of the river section allowed the research vessel to slide across the channel with ease and security because there was no need to reattach the winch line during travel. The safety line between Points A and B was erected using a zodiac boat and a two man crew. With one end fastened to the anchor at Point A, the zodiac traversed the river and connected the free end to the anchor at Point B. Slack in the line was by taken up by hand on shore at Point A.



Phase 3 saw the research vessel make its way to the master link, already in the water from when the anchors were installed. Slack was given from the winch line because this was the secondary safety measure. The engines were used to maneuver the research vessel out of the bay and into the free stream. Once the research vessel reached its target location above the master link, the winch line was made taut to ensure stability. The buoys were picked up and the master link was raised to the surface. The main line was shackled to the master link and Phase 4 began the process of easing the research vessel into its final position just downstream of the foot bridge between piers 2 and 3. Since the main line was connected, the winch line became unnecessary and thus was disconnected by zodiac. Relaxing the main engines, the vessel drifted down stream, allowing the main anchor line on deck to slowly pay out as the research vessel eased into its final position. Once in place, the safety line was then connected from the rear.

The safety line, which ran from the anchor at Point C to the rear of the research vessel, was pulled along the shore, then along the bridge. It was imperative that the cable did not rest in the water as the drag force on the 200 feet of cable would be too great for hand strength to control. The cable was strapped with tie raps to the outside of the bridge until it was fastened to the research vessel. Passing the cable from the bridge onto the research platform, it was shackled to an eyelet at the stern of the vessel. Once secured, the tie raps were cut free and the cable dropped into the water. The research vessel was then secured by the main line and a downstream safety line. The engines were then shut off and the research vessel was successfully deployed.

## **4.6 Turbine deployment**

The research platform was equipped with an A-frame, which was erected after deployment as bridge height restrictions would not allow the research vessel to be deployed with an erect A-frame. The A-frame had a manual chain driven, 2-ton hoist, which was free to slide across the width of the platform. The 5 kWe unit was small enough that the A-frame could support its entire weight, and the frame was tall enough that it could hold the entire turbine assembly above the platform. A cradle was designed and built by NECI that allowed the turbine to fit within an open section on the platform. The turbine was assembled on the research vessel after deployment. The hoist was used to hold the turbine upright during assembly and then lowered and fastened into place in the rear quarter of the research platform. The A-frame was able to slide along the length of the deck. The turbine cradle was the size of the panels that made up the research platform, so at any time the turbine could be moved by replacing a panel with the cradle.

## **4.7 Research vessel removal**

Removal and redeployment of the research vessel took place downstream of the bridge at Loading Zone 2. Since the main lines were already in place, there was no need to travel upstream of the bridge again. Removal began with a safety meeting, outlining everyone's task and location. Those who required safety equipment such as life jackets, survival suits, harnesses, radios, etc. were equipped. The zodiac engine was fired up and was launched as a safety and recovery vessel. Before anything could be disconnected on the research vessel, the engine was started and checked over for proper functionality and

sufficient fuel. With the engine running, there were three points of safety: the main line, safety line, and onboard engine.

The first phase of removal was to disconnect the safety line. Because it was located downstream and traveled the span of the river, it posed the danger of getting caught up in the propeller of the onboard motor. The safety line was disconnected and allowed to sink to the bottom. It was later pulled out by a skidder or front end loader. The second phase involved unfastening the main cable line. However, to do this, a second safety measure had to be initiated.

During removal, a winch line from the bow was handed to personnel on the bridge who secured the free end to the bridge as a temporary measure. Before putting the load of the research vessel fully onto the engines, the turbine was raised out of the water to reduce the drag force significantly. With just the drag of the vessel itself, the motor was used to thrust the research vessel forward, giving slack to the main cable and the temporary safety line on the bridge. Phase 2 was the disconnection of the main line. Once disconnected, the main cables were strung up to the bridge temporarily. If the research vessel was to be removed for extended periods of time, then the free ends of the main cable were fastened to a large buoy and left to float in the water.

Free of the main cable, relying on engine power, and using a winch line for back up, Phase 3 took the research vessel from between piers 2 and 3 to the shore of Loading Zone 2. The winch line was slacked and unfastened from the bridge; however, the hook

on the winch line was kept near to the railing. This procedure gave excessive slack on the winch line so that if the engine ever cut out, there would be some time to reconnect the winch hook to the bridge's railing and thus complete the safety backup. It was necessary to unfasten the winch hook from the bridge so that the line could follow the research vessel across the width of the river. The hook was handed to one crew member who was always accompanied by another. They held the hook close to the bridge ready to reattach at a moment's notice. As the research vessel used engine power to slide across the river, the crew followed along the length of the bridge. At the end of the bridge, the winch line was secured to a strong railing as a tie-off point.

Timbers were used to make a gangway between the shore and the research platform. If it was in for servicing, the research vessel was left in shallow waters and work commenced on deck. If the research vessel was being removed, a crane was called in to remove the turbine from the deck and the research vessel was dragged onto Loading Zone 2. Once ashore, the safety line could be reeled in and coiled up on shore awaiting future redeployment.

#### **4.8 Research vessel redeployment**

For redeployment of the research vessel into the testing location, additional winches were required after a failed attempt. The research vessel was then equipped with a total of five winches: one at the bow of each pontoon, one in the center of the bow, one at the rear of the port side pontoon, and one in the center of the stern. For redeployment, the bow winches were used. To prepare for redeployment, the main cables were extended by

using a 1-inch floating nylon rope with small buoys at the end of them. Each of the two main cable ends was held up by the bridge. To make these ends accessible to the research vessel, 40 feet of nylon rope was used to extend these lines into the water.

In a reversal of Phase 3 from the removal procedure, Phase 1 of the redeployment used engine power and a following winch line along the bridge as the primary and secondary means of control and safety. Using engine power, the vessel motored into position behind the floating nylon rope. The small buoys were picked up by the crew and anchored to the eyelets at the bow. Phase 1 was then complete as the research vessel was secured in the water just downstream of the final location.

Phase 2 required the use of the other two bow winches. The winch lines were slacked and passed to the crew on the bridge. Using ropes and floats, the hooks of the winch lines were passed up from the research platform and fastened to the ends of the main cable. Once secured, the ends of the main cable were released from the bridge and allowed to fall into the water. The winch lines were then retracted and the research vessel pulls up until the ends of the main line were at the bow. The connections to the bow eyelets are swapped from the nylon rope to the main cable and Phase 2 was complete.

Phase 3 finished the job as the onboard engine was relaxed and the vessel was allowed to drift back into its final position as shown in Figure 30. Before cutting off the motor

entirely, the downstream safety line was reconnected in the same manner as in the initial deployment.

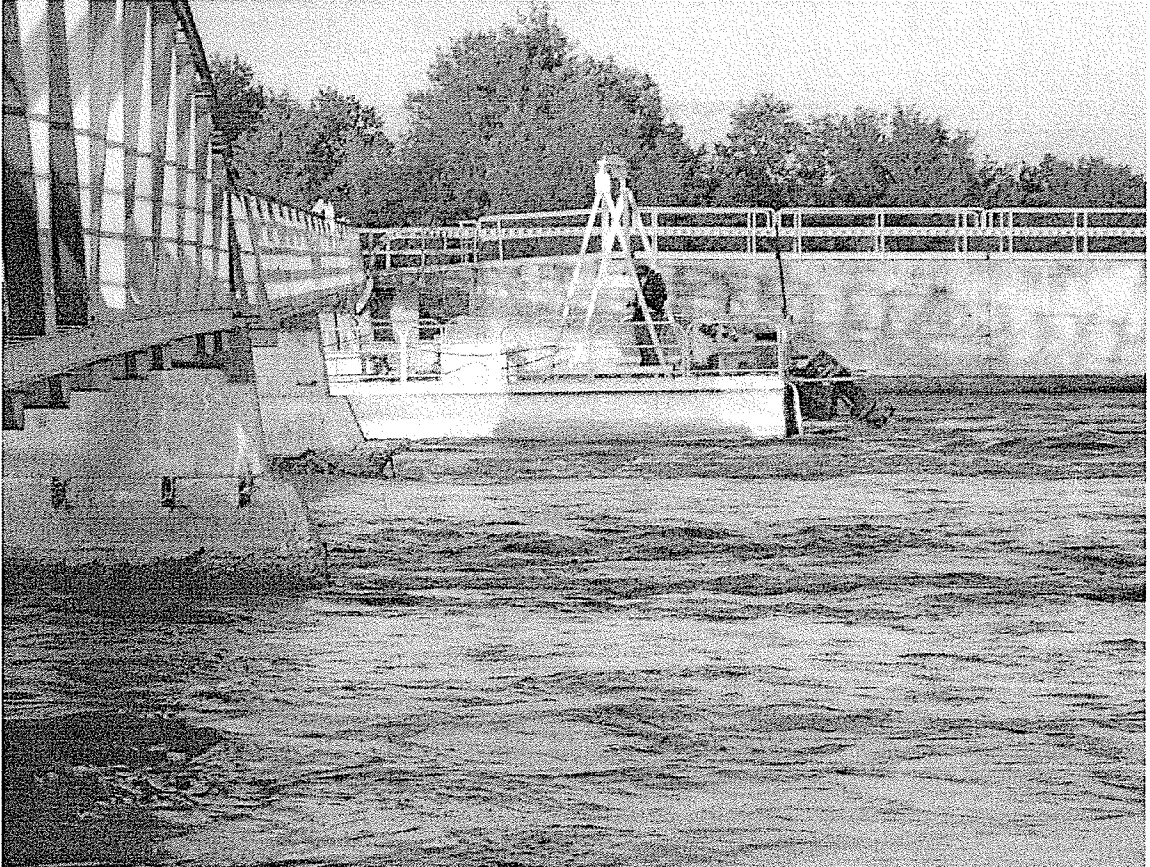


Figure 30: Research vessel deployed to final position

# Chapter 5

## Turbine Performance

### 5.1 Overview

This chapter presents the approach used to evaluate the turbine's performance along with the results of the winter and summer testing. The first section presents the theory and equations on which performance parameters were evaluated. Operating efficiencies vary significantly with the change in free stream velocity since the equation of power involves a cubic of the velocity term; hence, flow measurement is critical. The flow meter that was installed for constant monitoring was calibrated in a water tunnel against a pitot tube and the ADV. Winter testing resulted in a less-than-expected power output. A closer investigation into the issue launched a study into the design of the turbine's support arms. A numerical model for evaluating power loss due to the arms is presented in this chapter along with in-situ testing of three different support arm cross-sections.

### 5.2 Performance calculations

This section presents the formulations and procedures used to analyze the data gathered from various sources.

### 5.2.1 Power measurement

Power is measured by two instruments: the power meter located directly aft of the generator and the Aurora inverter. The power meter measures total power in volt-amps (VA) using the following relations laid out in this section.

The power meter was configured in a 3-phase, 4-wire, and 3-element setting. This resulted in measurements of  $V_{an}$ ,  $V_{bn}$ ,  $V_{cn}$ ,  $I_a$ ,  $I_b$ , and  $I_c$ . The voltage is that of phase to neutral for phases a, b, and c. The average voltage and current of all three phases are recorded by the unit and those values are used for all power calculations. The current transformer (CT) imposes an additional factor. Coiling around the CT magnifies the current read by the CT by the number of time the current flows through the center of the CT. The transformer itself then reduces that value to a millivolt output for the power meter to recognize. A physical measurement of the current showed that the true current was greater than the recorded value by a factor of 8.333. Thus the total power in VA is calculated by Equation 8. The relation between real and reactive power are given in Equations 9 and 10.

$$Q = V_{l-N} (I * 8.333) * 3 \quad (8)$$

$$Q^2 = P^2 + S^2 \quad (9)$$

$$S = \sqrt{Q^2 - P^2} \quad (10)$$

where Q is the total power, P is the real power in watts and S is the reactive power in volt-amps.



The power factor indicates the phase shift between voltage and current and represents a ratio between real and total power. Typically the power factor would be used to calculate how much real power,  $P$ , is being generated; however, as it pertained to this research, the power factor was calculated to appreciate the phase shift induced by the rectifier which delivers DC power to the inverter. The DC real power input to the inverter is logged by the Aurora unit and thus this value is used to obtain an overall power factor going into the inverter (see Equation 11).

$$PF = \frac{DC_{in}[W]}{Q [VA]} \quad (11)$$

### 5.2.2 Water to wire efficiency

The water to wire efficiency, calculated by Equation 13, is the overall efficiency. It was evaluated as the percentage of the power output to the grid with respect to the total available kinetic power, thus presenting the usable output as a percentage of the total available. The area in this calculation was taken as the cross-sectional area of the turbine orthogonal to the flow.

$$\eta_{w2w} = \frac{AC_{out}[W]}{KE [W]} \quad (12)$$

$$\eta_{w2w} = \frac{AC_{out}[W]}{\frac{1}{2}\rho AV_{\infty}^3} \quad (13)$$

### 5.2.3 Inverter efficiency

The inverter recorded the power coming in and out of the unit. Coming in after a rectifier, the DC input to the inverter recorded real power in watts. The inverter took this signal and converted the power into an AC signal at 240 V and 60 Hz as required by the grid. Therefore the efficiency of the inverter is obtained using the ratio of the power out to the power in.

$$\eta_{inv} = \frac{AC_{out}[W]}{DC_{in}[W]} \quad (14)$$

### 5.2.4 Rotor efficiency

The rotor efficiency, or the turbine's coefficient of power ( $C_p$ ), quantifies the amount of power extracted from the flow by the rotor of the turbine. The power output from the rotor shaft did not include any losses downstream such as drivetrain or inverter losses, but rather it measured the amount kinetic energy extracted from the flow by the rotor alone. This is calculated by adding up the losses along the line from rotor to grid and adding it to the power delivered to the grid. The efficiency is taken with respect to the available kinetic energy within the flow.

$$\eta = C_p = \frac{AC_{out}[W] + Losses [W]}{KE [W]} \quad (15)$$

### 5.2.5 Drivetrain power losses

Drivetrain losses include turbine bearing, gearbox (gear tooth, viscous, bearing, and seal losses) and generator losses. The turbine RPM was ramped up and then ramped back down in order to determine the overall losses produced by the gearbox and the generator. Two unique but similar curves are obtained by using a 2<sup>nd</sup> degree polynomial trend line through the data points. An average of the two equations is taken as the drivetrain losses for any given RPM. The experimental data obtained by NECI for quantifying the drivetrain loss is shown in Figure 31.

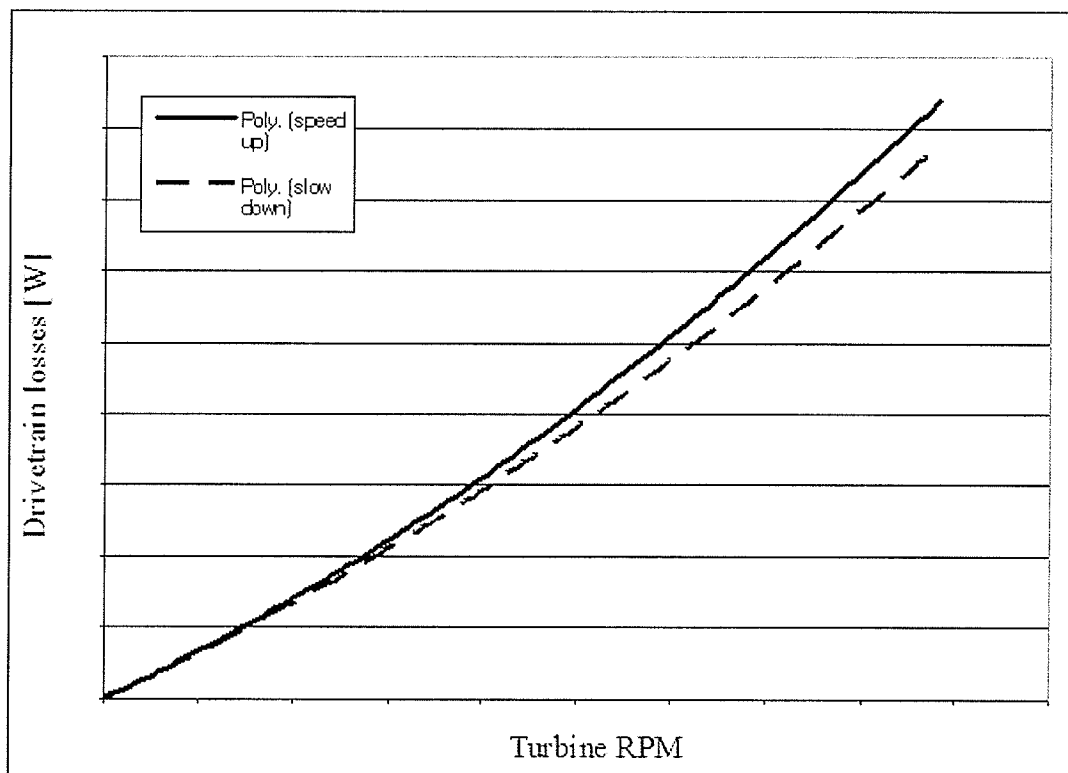


Figure 31: Losses within the dive train assembly (courtesy of NECI)

$$\text{Drive Train Loss [W]} = A(\text{RPM})^2 + B(\text{RPM}) \quad (16)$$

### 5.2.6 Overall loss

An overall power loss term was introduced to quantify the amount of unaccounted power and is evaluated using Equation 17. The turbine, when operating at a specific mean flow rate and TSR, has a specified power output as per design. This value is taken as the turbine's rated output. The difference between the rated and actual outputs is therefore a result of net losses. Thus the term for overall power loss is created to quantify this drop as the percentage of power lost from the expected output.

$$\text{Overall Power Loss} = \frac{(\text{Rated Power} - AC_{out})}{\text{Rated Power}} \quad (17)$$

### 5.2.7 Anchor load calculations

The output of the load cell used gives a current signal of 4 to 20 mA, which is proportional to 0 to 50,000 lbs of axial loading. A 500  $\Omega$  resistor was used to close the current loop and the voltage drop across that resistor fed a voltage signal into the data taker. This voltage signal is used to calculate of the instantaneous load using Equation 20.

$$V = IR \quad (18)$$

$$V = I(500) \quad (19)$$

Therefore the output voltage range for a 4 to 20 mA signal became 2 to 10 VDC. Hence the load is calculated using the slope of the linear relationship between load and voltage

as graphed in Figure 32. The slope of the line is used to determine the load on the main anchoring cable.

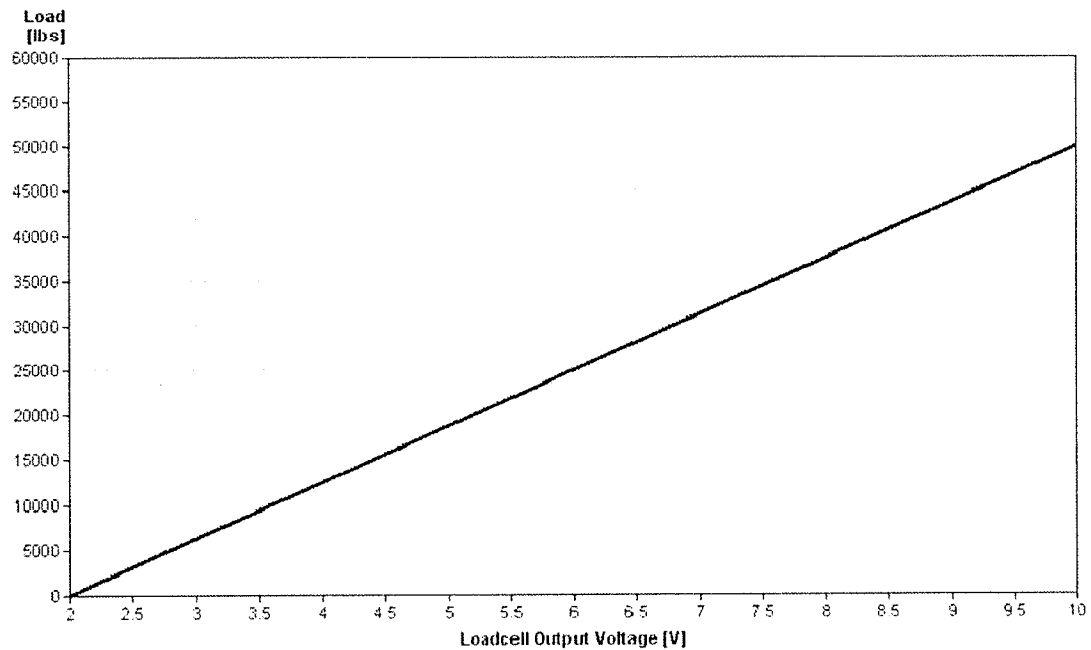


Figure 32: Load cell output graph voltage versus load

$$Load = (V - 2) * 6250 \quad (20)$$

The coefficient of drag for the turbine and pontoon vessel is determined using the fluid dynamic relation of

$$D = \frac{1}{2} \rho A V^2 C_d \quad (21)$$

The load generated by the research vessel is subtracted from the measured value to obtain the net force caused by the rotor. The load, measured in pounds, is converted to the

metric scale because the density, area and velocity parameters were all measured in metric. The formula then finalizes to Equation 22.

$$C_d = \frac{Load * 4.448}{\left(\frac{1}{2} \rho A V^2\right)} \quad (22)$$

### 5.3 Flow estimation

The propeller style flow meter was the primary instrument used to record the flow. The revolution counter method that it employed was advantageous for continual logging by the DT85, in contrast with the ADV, which required considerable effort in setup, data acquisition, and analysis. Flow estimation was a challenge due to the unsteadiness of the flowing river, along with interference from wakes. Figure 33 shows a day long record for flow captured by the flow meter. Turbulence, in combination with the design of a propeller style flow meter, resulted in measurements being consistent but unsteady. The mean flow rate remained constant on an hourly basis as the flow was regulated by the downstream dam; however, temporal variations in instantaneous flow caused the average per-minute readings to be unsteady. To verify the readings from the meter, a hand-held version from the same manufacturer was used in parallel with the meter installed on the research platform. The two meters were identical in function and it was found that they displayed the same results. A third means of verifying the flow on-site was the use of the Acoustic Doppler Velocimeter. Both the ADV and the flow meter were tested in the laboratory and compared to pitot tube results to validate the readings obtained by each.

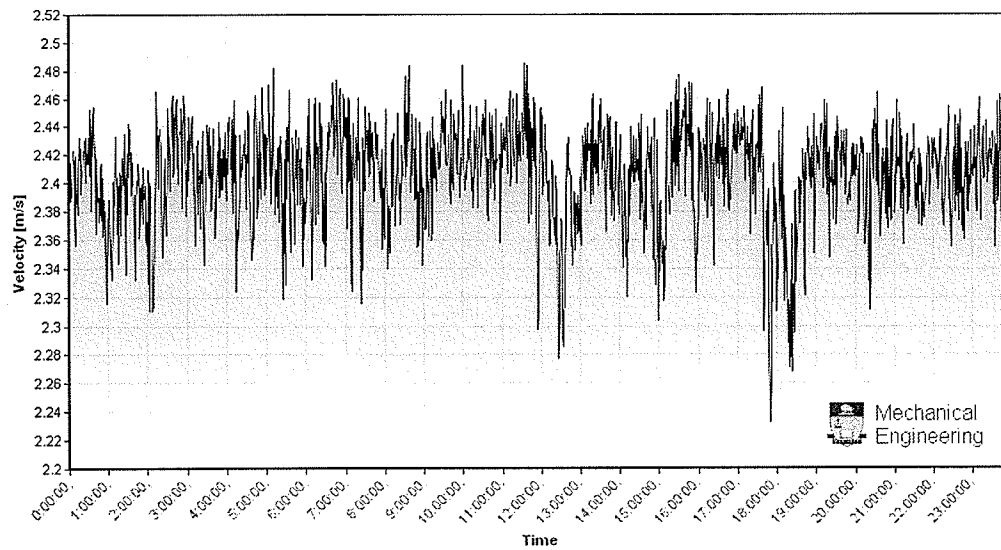


Figure 33: Graph of flow measurements throughout a day

### 5.3.1 Laboratory calibration

The ADV and the hand-held meter were both calibrated against a pitot tube in the water tunnel at the University of Manitoba. The three measurement devices were centered along all three axes within the water tunnel test section. The velocity of the water tunnel was controlled by adjusting the frequency of the main motor. The pitot tube readings were taken off a manometer using a vernier caliper to measure the inches of water. The flow was then ramped up and readings were taken at 25 Hz, then 30, 40, 50 and finally 60 Hz (60 Hz is the maximum setting rated at 1 m/s). The settings started at 25 Hz because at lower settings, the fluid velocity creates a visually negligible difference in the manometer. The flow was then ramped down in the reverse order and readings were recorded again. This ramp up and down procedure was repeated to test the consistency of

the tunnel. The water tunnel was able to reproduce the flow for a specific frequency input to an accuracy of 1.5%.

The ADV and the flow meter sampled the flow at four additional frequencies: 20, 15, 10 and 5 Hz. The 200 Hz sample rate of the ADV allowed for measurements at low velocities. The hand-held meter comes equipped with an attached computer display that showed both instantaneous and time averaged velocities. The hand-held meter was reset and allowed to run until the time averaged value became steady to within 0.01 m/s. The results are presented in Figure 34.

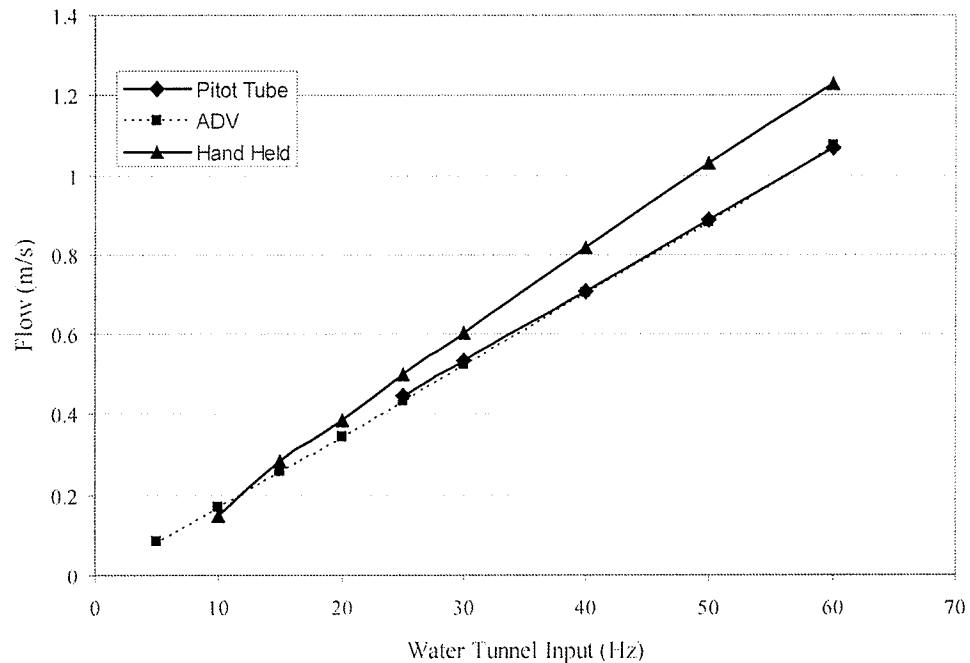


Figure 34: Flow meter calibration results

The ADV and the pitot tube yield similar results. The two results differ at the most by 3% at 25 Hz. Water tunnel calibrations indicate that the hand-held meter over-estimates



the fluid velocity. In the field, ADV and DAQ flow meter readings were taken simultaneously. These data points were incorporated into the following graph to investigate if the error is linear with flow velocity. From Figure 35, a conclusion could not be drawn about the behavior of the error, but rather a mean trend is observed. Taking the average resulted in a nearly consistent relation of a 14% error. Therefore, the data recorded by the DAQ is re-computed by the Scanfile software to take the 14% overestimation into account.

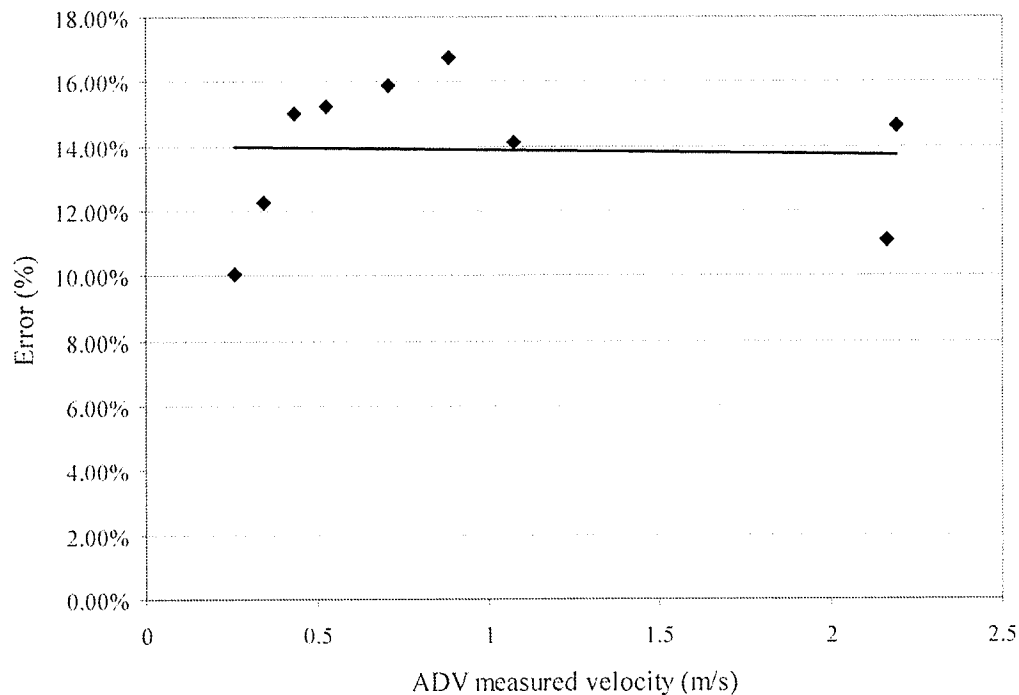


Figure 35: Handheld flow meter error

The data taker logged the number of counts per minute, which relates to the number of rotations of the propeller of the flow meter. The corrected flow rate for that minute is

calculated using Equation 23. The manufacturer specifies a constant of 1036 counts per minute for 1 m/s.

$$V_{\infty} = 0.86 * \left[ \frac{\text{counts/min}}{1036 \text{ counts}/(\text{min})(\text{m/s})} \right] \quad (23)$$

#### 5.4 Winter testing results

The 5 kWe unit was in the Winnipeg River for 69 days continuously through the months of January to March of 2008. Power data was logged intermittently because the early days of the DAQ system had many technical issues to address. Power outages to the research vessel and trailer, software updates, and maintenance are some of the reasons why data logging was halted for intermittent periods of time. When the turbine was in operation, the inverter attempted to place an electrical load based on a pre-programmed curve dependent on the generator frequency. The loading profile was found to be over estimating the capabilities of the turbine and thus would either stall the turbine, or cut out and allow the rotor to free wheel. The over-estimation was attributed to the flat bar support arms as the programmed loading curve was designed for support arms with a profiled cross-section. The inverter was not the only reason why the turbine stalled in the water; ice was also an issue. Ice formation between the pontoons grew to fill the area above the turbine and began to interfere with the tops of the hydrofoils. During winter testing, the turbine required an external heat source to get up to operating speeds before it was self sustained. When it would stall due to either overloading or ice buildup, it remained stationary until manually restarted. When initially deployed, the gearbox contained a natural oil that, when chilled by the ambient temperature, generated

significant viscous losses. Manual start of the turbine became difficult, thus the turbine's drivetrain above the water was put in a heated and insulated enclosure, and synthetic oil replaced the natural oil. Between January 9 and March 16, 2008, the turbine logged a total of 1632 hours in the water and ran for 1260 hours. The entire rig was removed from the test location on March 18, 2008 before the spring break up.

#### **5.4.1 Power output**

The results of winter testing showed the consistency of this technology. The mean output is steady for all hours, giving hydro power its advantage over other intermittent generation. Flow and power output can be viewed in Figure 38 along with the hourly averaged results in Figures 36 and 37. Throughout the winter, the turbine operated with long term consistency. Given a short enough time scale, the power coming off the generator is oscillatory due to the inherent torque fluctuations of the vertical axis turbine and the minute-to-minute variations in flow. The power output consistency discussed in this section is based on hourly averages because a goal of this analysis was to look at how reliably kinetic turbines can deliver power on the longer time scale.

Using the hourly averaged data, the turbine produced 539.3 VA with a standard deviation of 24.3 VA. The flow held steady with a mean rate of 2.06 m/s, having a standard deviation of 0.02 m/s. There is a noticeable tracing of the flow and power curves as expected; however, a peak in the flow resulted in a decline in power. It is hypothesized that high turbulence levels in the river might have had a significant impact on power output. This theory is currently being explored and is beyond the scope of this thesis.

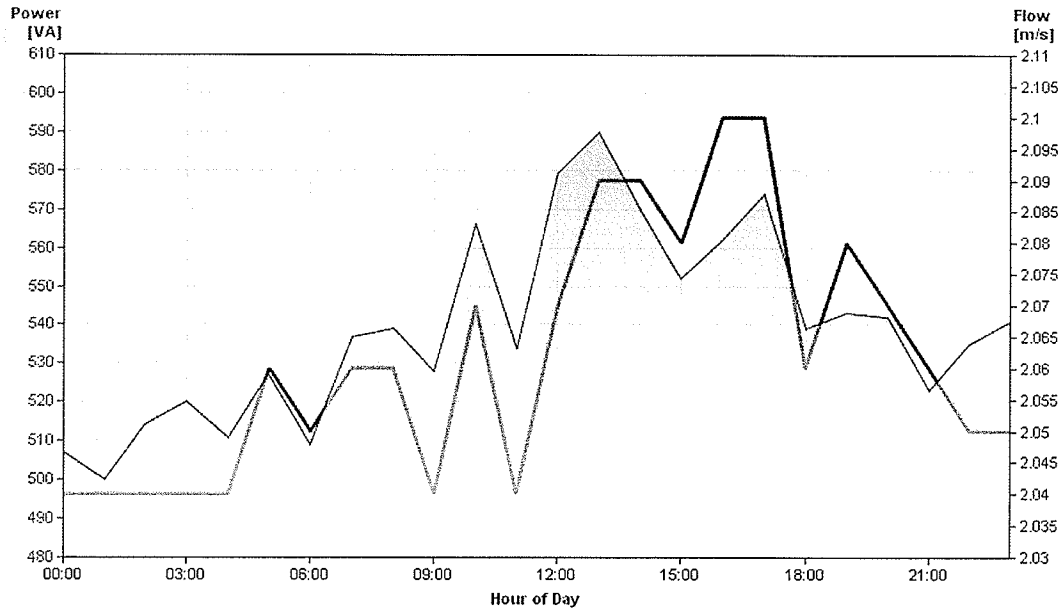


Figure 36: Hourly averaged flow and power data over 1 day

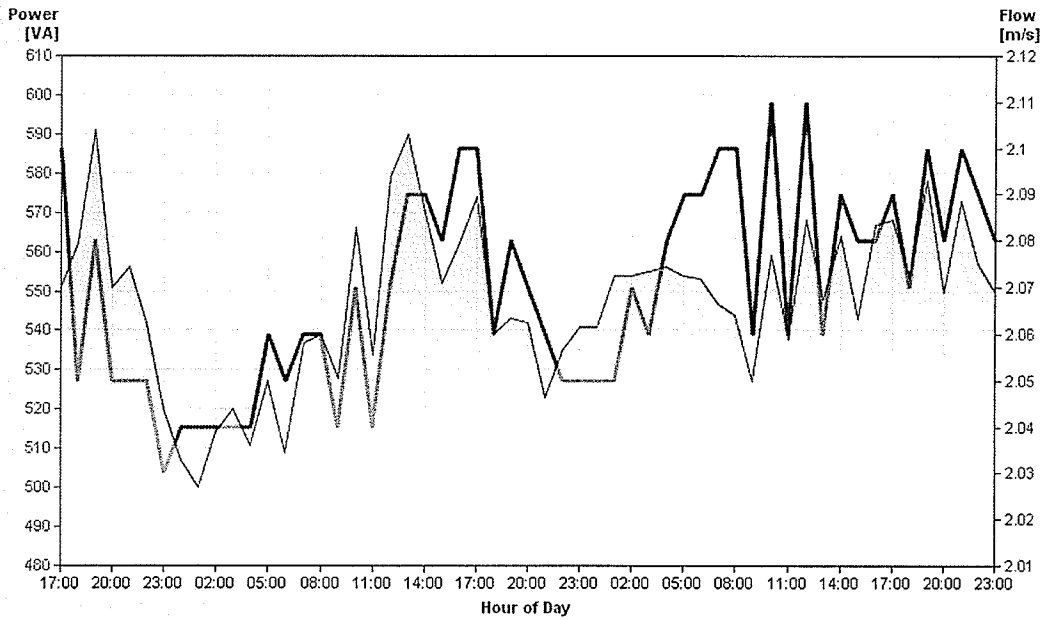
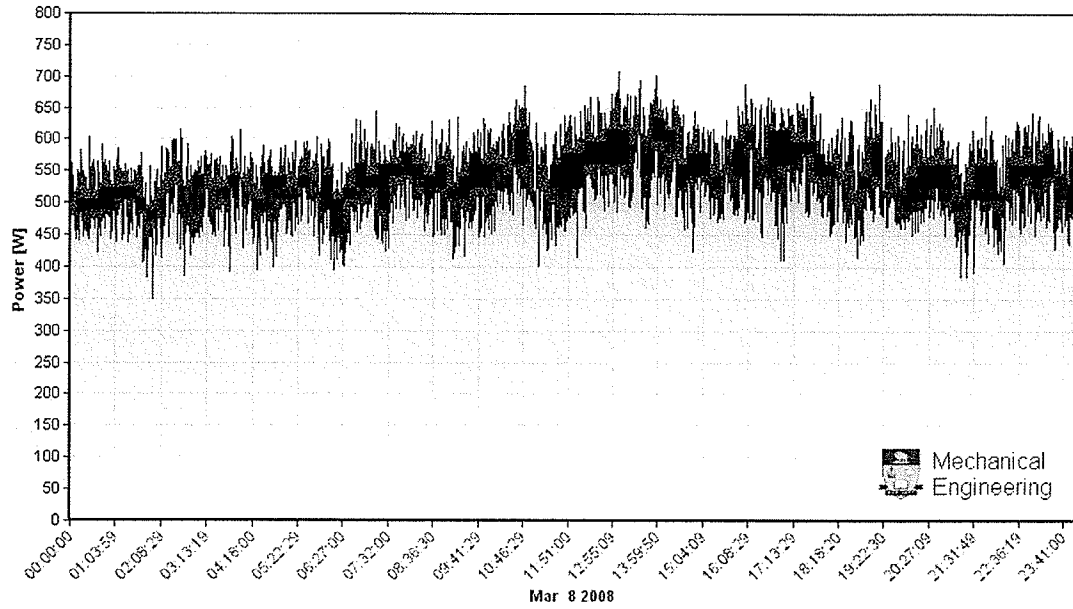
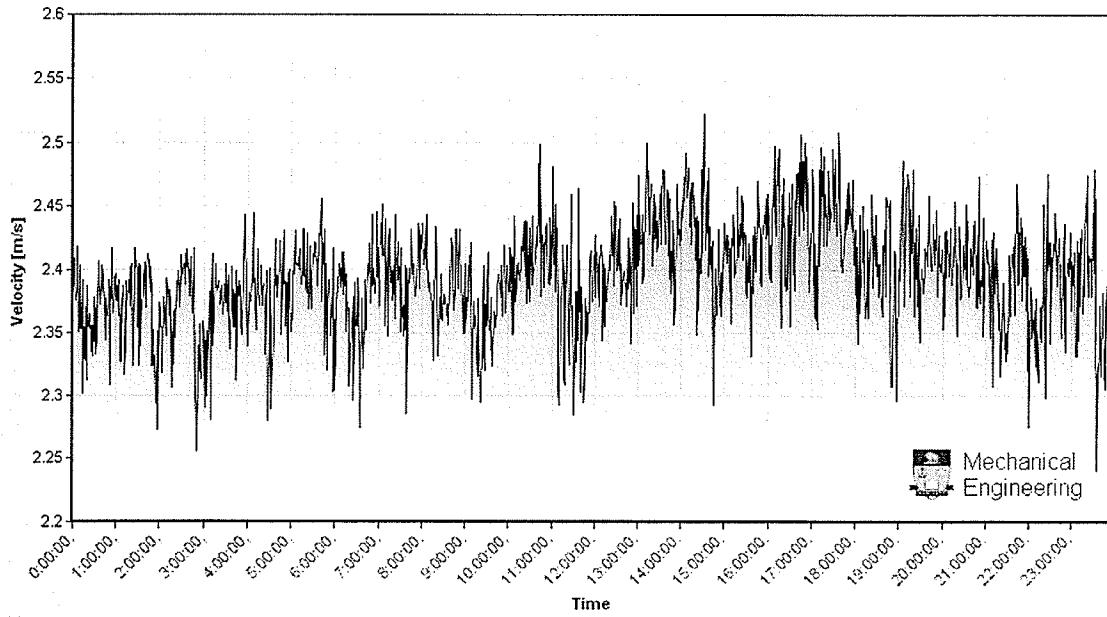


Figure 37: Hourly averaged flow and power over 2 days



a) power



b) free stream velocity

Figure 38: Raw data of the hourly averages presented in Figure 36 (uncorrected data)

The flow conditions at the test site were set by the power dam out flow. The rise and fall of flow rate was determined by the operations manager at the plant and was not adjusted for the purposes of this experiment. Figure 37 shows the hourly trends over 2 days to display the changes incurred during normal dam operations. Throughout winter testing, the turbine operated with efficiencies around 10%, significantly less than the rated performance peaking at 30.3% due to the flat bar support arms.

## 5.5 Modeling power loss due to arms

To examine the effect that the turbine support arms had on overall turbine performance, a mathematical simulation of the arm's drag was performed as a part of the investigation to account for power loss compared to the theoretical performance model. The simulation investigated the power loss in flows ranging from 1.5 to 2.5 m/s and used the turbine's rated RPM in those flows. Therefore only the optimum tip speed ratio was considered for each flow case. A range of drag coefficients from 0 to 1.5 was also incorporated into the program to obtain robust results that are applicable to different arm profiles. The output is a 2-D matrix that represents power lost with respect to a given flow rate and arm drag coefficient. The free body diagram in Figure 39 was used to breakdown the forces that contribute to power production.

By assuming that the hydrofoil acted as a winglet for flow over the arms and neglecting the hydrofoil's contribution to the net torque, the problem of obtaining the net torque on the arms alone becomes a simplified 2-D hydrodynamic problem. The two dimensional approach removes 3-D hydrodynamic effects such as tip vortices and induced drag from

the equation, thus simplifying the model. The 2-D drag force is evaluated using Equation 24.

$$D(r, \theta, \omega) = \frac{1}{2} \rho A V_{rel}^2(r, \theta, \omega) C_d \quad (24)$$

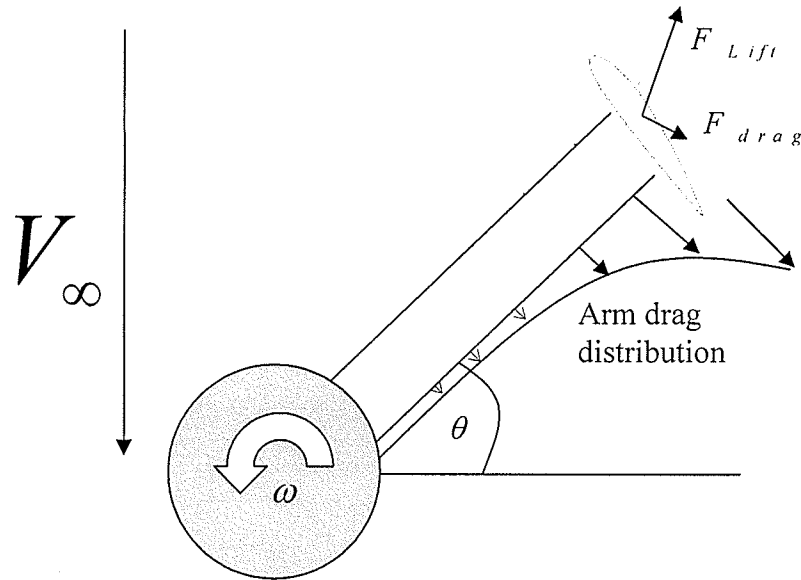


Figure 39: Free body diagram of turbine arm

To calculate the drag on a given section of the arm at radius,  $r$ , and rotational angle,  $\theta$ , the velocity term must be the relative velocity inline with the chord of the arm section. The relative velocity depends on four parameters: the arm's velocity which is dependent on the angular velocity,  $\omega$ , location along the arm, location along its rotation, and the free stream velocity,  $V_\infty$ . Assuming a steady-state, one-dimensional flow, the free stream velocity has only a  $y$  component with a magnitude of

$$V_{\infty} = V_{\infty y} \quad (25)$$

The flow direction and magnitude require some translation onto a reference plan that corresponds to the radial and chord lines of the arm. Therefore the free stream velocity with respect to the chord line of the arm reduces to

$$V_{\infty y'} = V_{\infty y} \cos \theta + V_{\infty x} \sin \theta \quad (26)$$

$$V_{\infty y'} = V_{\infty} \cos \theta \quad (27)$$

The angular velocity of the arm introduces an additional velocity to the relative flow with a magnitude of

$$V_r = r\omega \quad (28)$$

The two relative velocities, the free stream and the rotational motion, superimpose to give the final relative velocity used to calculate the drag at a given point along the radius,  $r$ , angular position,  $\theta$ , and angular velocity,  $\omega$ . Figure 40 shows the relative velocities.

$$V_{rel}(r, \theta, \omega) = V_{\infty y'} + V_r \quad (29)$$



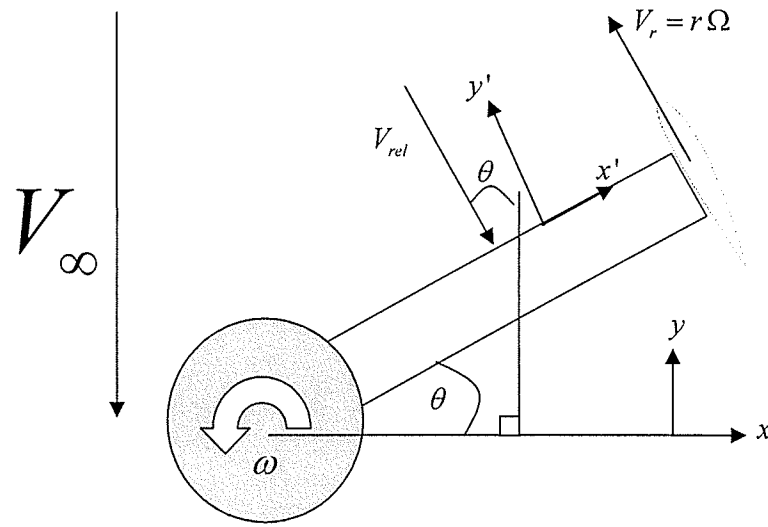


Figure 40: Velocity diagram of turbine arm

For this analysis, the free stream velocity is left as a range of velocities discretized into an array, and the RPM of the turbine is fixed for a given flow rate as per the turbine's optimum design TSR. Thus for each velocity case analyzed, the relative velocity and drag depend on only two parameters as shown in Equation 30.

$$D(r, \theta) = \frac{1}{2} \rho A V_{rel}^2(r, \theta) C_d \quad (30)$$

The drag at any given point multiplied by its radial distance gives the resulting torque for that node. Therefore the net torque of one arm at a given point within its rotation is obtained by integrating the drag along the arm to obtain the net moment about the shaft.

$$T(r, \theta) = D(r, \theta) r \quad (31)$$

$$T(\theta) = \frac{1}{2} \rho A C_d \int_{r_0}^R V_{rel}^2(r, \theta) r \quad (32)$$

where  $A = t dr$

The total power loss due to the rotation of the arms is obtained by integrating the net torque about one rotation, or  $2\pi$ .

$$T(\theta) = \frac{1}{2} \rho t C_d \int_{r_0}^R V_{rel}^2(r, \theta) r dr \quad (33)$$

$$P = \int_0^{2\pi} T(\theta) d\theta \quad (34)$$

The problem is discretized into a finite element problem and is solved as such. The radius and angle of rotation is divided into N and M parts respectively. The model was run with various values for N and M. M was held constant until a value for N resulted in power being accurate within 0.001 of N-1. Next, N was held constant and M was adjusted to have the same accuracy as N. It was found that the optimal discretization of radial and rotational nodes of N and M respectively were 1430 and 11. The nodes where the drag and torque forces are calculated resided in the center of the divisions. The formulas presented above then reduce to the following in discretized form.

$$D(r, \theta) = \frac{1}{2} \rho A V_{rel}^2(r, \theta) C_d \quad (35)$$

$$T(\theta) = \sum_{i=1}^N \left[ D(r, \theta) \frac{r_i + r_{i+1}}{2} \right] \quad (36)$$

$$P = \sum_{j=1}^M \left[ T(\theta) \frac{\theta_j + \theta_{j+1}}{2} \right] \quad (37)$$

After discretization, the numerical integration formula takes on the familiar form of the trapezoidal rule. The area used to obtain the drag is the frontal area of the arm and the radius is taken from the edge of the shaft hub through to the entire length of the arm. The results matrix graphed in Figure 41 shows the power lost due to the arms for a range of drag coefficients and operating flows given that the turbine operates at the optimum TSR.

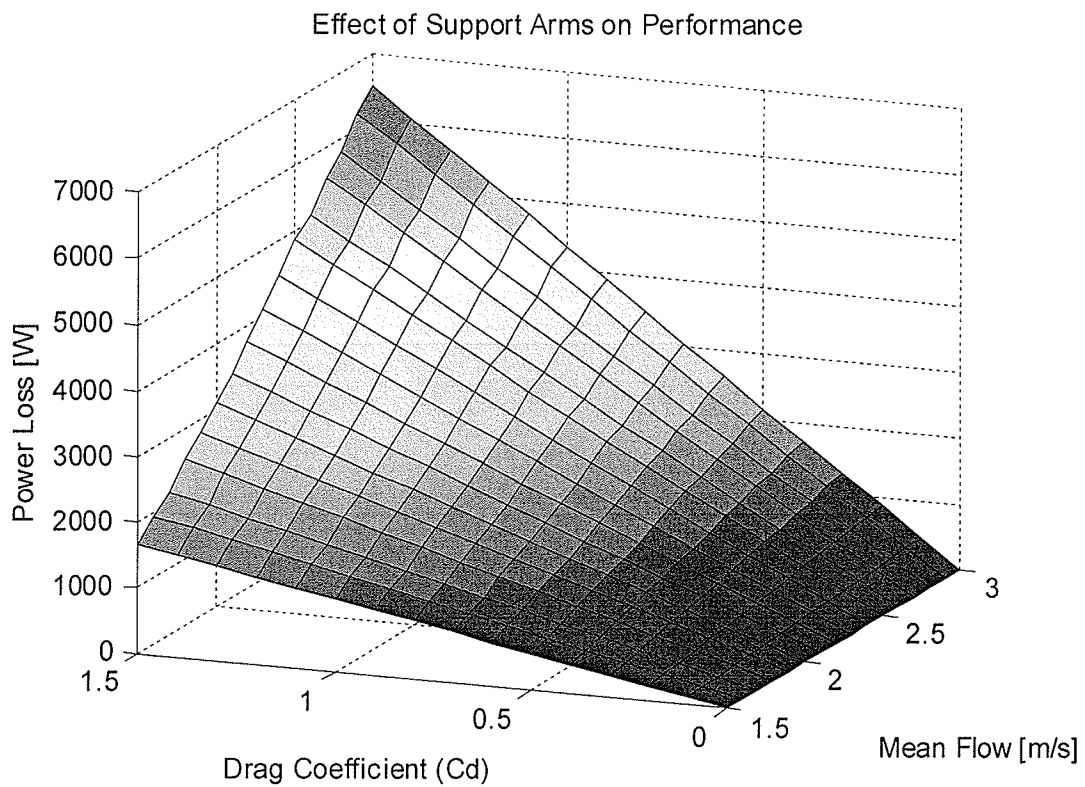


Figure 41: Results from numerical estimation of performance loss due to arm design

The support arms of the vertical axis turbine are found to be a source of significant power loss. It is imperative that to maximize power output, the drag coefficient of the arms be minimized. The power loss varies linearly with drag coefficient and exponentially with increasing velocity, thus more power is lost at higher flow rates. The loss is not found to be constant as the angular position heavily influences the relative velocity. Figure 42 shows a breakdown of the power loss with respect to drag coefficient and Figure 43 shows how the power loss was reduced as the relative velocity changed through one rotation for one arm, both in a 2.3 m/s free stream.

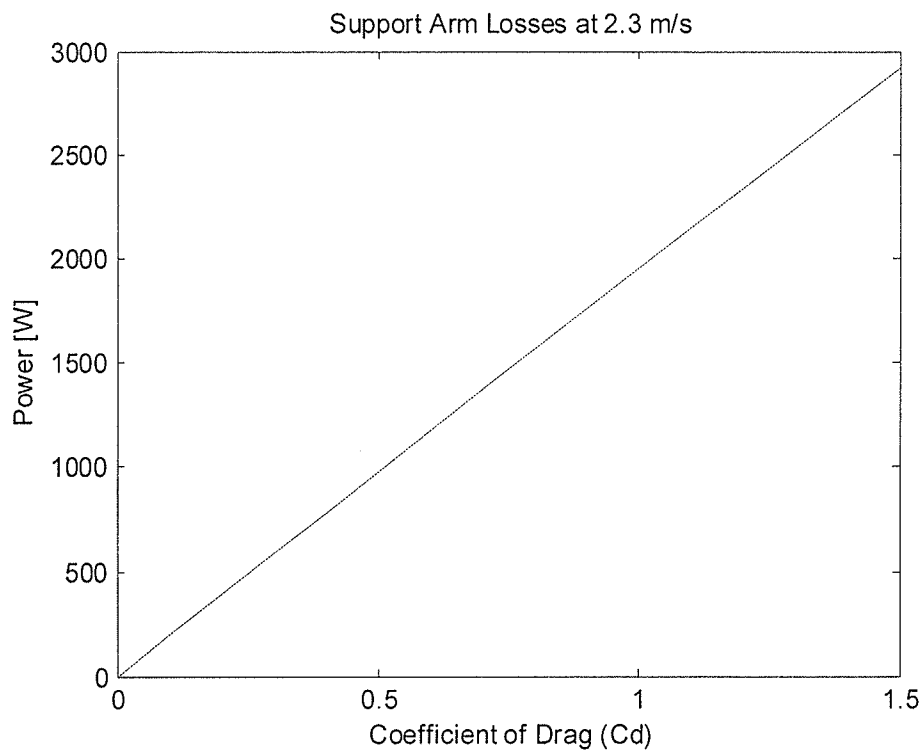


Figure 42: Power loss versus drag coefficient of the arms

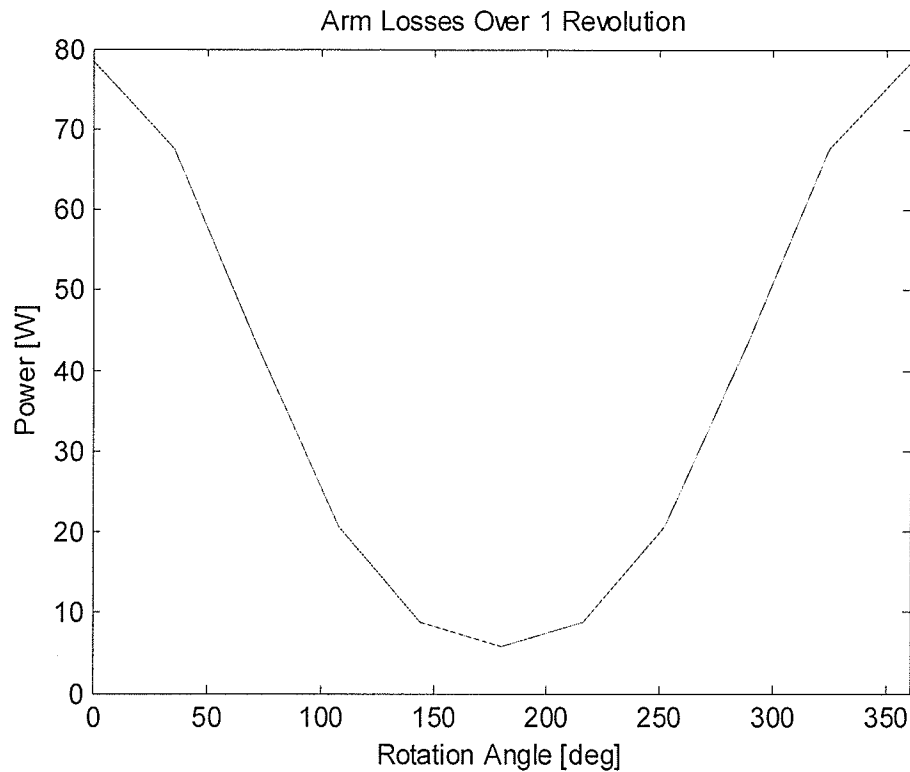


Figure 43: Power loss over one revolution of a single support arm

## 5.6 Arm design tests

This section of the research tests the Darrieus turbine using three different support arm designs. These experiments were carried out to quantify the coefficient of power from each rotor configuration to determine the amount of power lost due to the support arms. Power losses downstream from the rotor were also measured and isolated to a specific source.

The configurations tested were

1. Flat bar arms: These arms were used during the winter test phase.

2. Profiled arms: Flat bars are CNC machined to the general shape of a symmetric airfoil.
3. Profiled arms in front: The turbine location was changed from the rear quarter to the forward quarter to quantify the effect of the wake from the pontoons.
4. Hydrofoil arms: Extruded arms in the shape of hydrofoil blades were used as the supports.

Note that the turbine was initially designed and commercially developed to use the profiled arms. Hence all data that refers to rated turbine parameters are based on the commercial configuration which used the profile support arms. Figure 44 gives the cross-section for each of the arm designs tested.

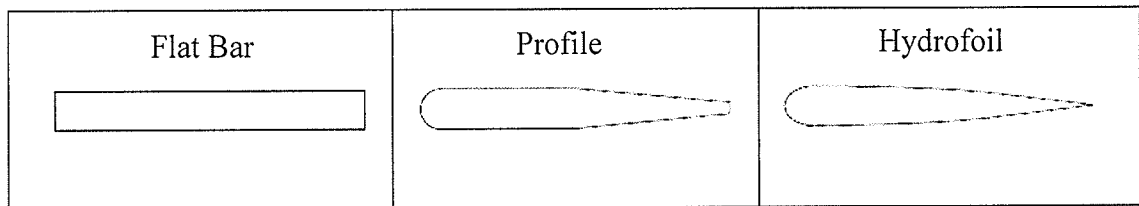


Figure 44: Turbine support arm designs

## 5.7 Summer testing results

Before the 25 kWe turbine was installed, three days of testing with the 5 kWe turbine was performed. Turbine output and efficiencies were combined to describe the overall performance of the unit. Integral to these relations is the instantaneous flow and power output. Figure 45 shows the local flow through the turbine, covering 2 hours of measurements.

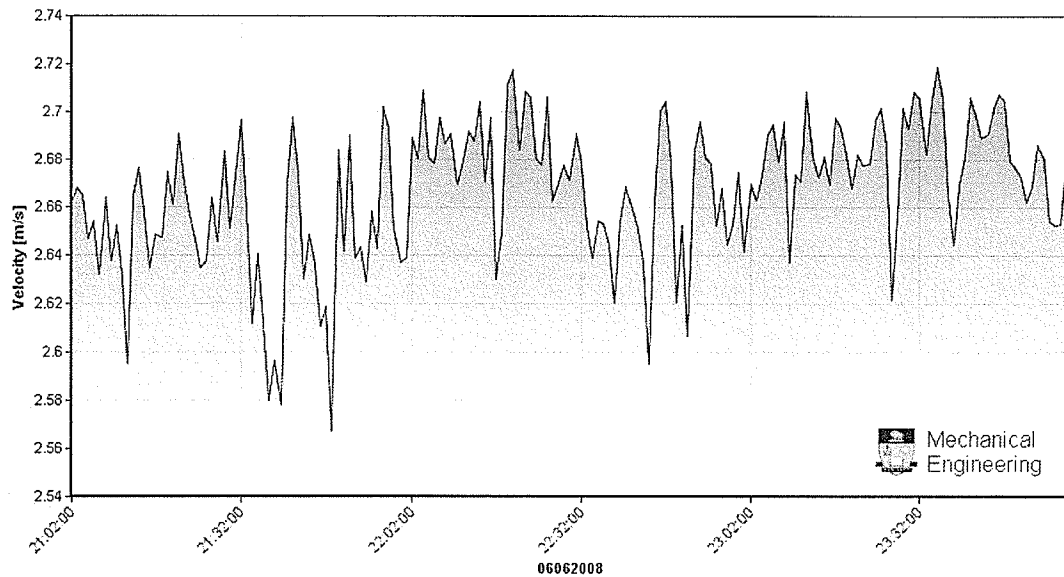


Figure 45: Variations in flow per minute throughout an hour

Averaging the flow data on a per hour basis, the velocity meter recorded a steady flow with a mean of 2.3 m/s over 2 days of testing. On the third day, the flow reduced to an average of 2.1 m/s. Using this average would lead to erroneous efficiencies because the local mean velocities differed from minute to minute. Therefore the flow measurements used throughout the calculations was that of the local mean flow during each test.

Knowing the free stream velocity, the tip speed ratio (TSR) was calculated using the rpm of the rotor obtained by an optical rpm sensor. Testing at Pointe du Bois took a range of TSR points and the performance curves for all testing are presented in Figure 46. These data points depict mostly the back side of the Aurora inverter loading curve. The data

points are taken over several minutes as the programmed load increased until a maximum was reached.

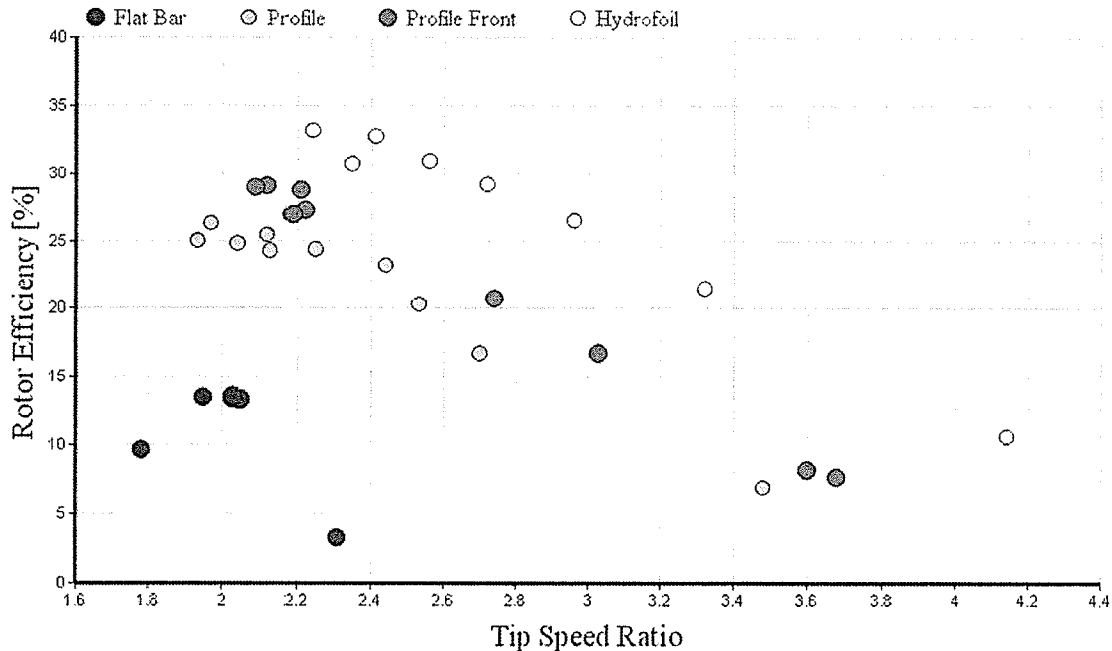


Figure 46: Performance curves for the 5 kWe turbine (courtesy of NECI)

The optimum TSR varies with the different arm profiles. The performance curves shift to the right as the drag on the arms reduces with the various arms tested. Along with the shift there is a broadening of the top peak, translating into efficiencies being less sensitive to TSR fluctuations. The higher drag of the arms makes for a sharp and steep curve.

This can result in unstable power production, which would require a highly sensitive and rapid control system capable of dealing with the sharp slide in performance that occurs with the slightest alteration in flow conditions. The hydrofoil arms perform the best, peaking at an efficiency of 33.2% at a TSR of 2.24. Along with the highest efficiency, the higher level of performance is maintained over a wider range of TSR. The broader



peak gives more leeway for the electronics control system and allows for more stable, high efficiency, power production. During testing it was noticed that the wake off the back side of the turbine was noticeably reduced for the hydrofoil arm. The amount of wake reduction was difficult to qualify as the flow reduced by 7.9% between the profile and hydrofoil arm tests; however, the turbine's overall performance improved, the unit self started, and it ran noticeably smoother.

The arms have a profound effect on the performance of the vertical axis turbine. The drag force of the arms contributes a negative torque applied to the main shaft. This torque causes a performance reduction from the designed values by up to 67%.

Therefore, arms having a minimum drag coefficient dramatically increase the net efficiency. The coefficient of power reduces by 19.4% for the flat bar and the hydrofoil arms output 3.5% less than the rated rotor efficiency. This reduction is due to the many other sources of power loss. Table 6 shows the performance results of the various arm profiles tested.

Table 6: Performance results for the various arm designs

Arm Design	Power to Grid [W]	Water to Wire Efficiency [%]	Rated Rotor Efficiency ( $\eta$ ) [%]	Net Loss [%]
Flat Bar	727	9.6	29.00	66.7
Profile	1449	21.3	29.00	26.47
Profile Front	1599	23.6	30.00	21.5%
Hydrofoil	1410	26.5	30.00	11.6

During testing of the flat bar support arms, the flow was steady at 2.27 m/s (rounded off to 2.3 m/s). For that flow, the turbine was rated to rotate at 70 RPM. The flat bars have a drag coefficient of 0.89 with respect to frontal area (Blevins 2003). With these values, the model presented in Section 5.5 predicts a loss of 1474 W. The results of the arm testing shows that at 2.27 m/s, the turbine rotated at 65 RPM and experienced a loss of 1405 W from its rated power. This result was taken from the inverter DC input power. The RPM was off its optimum point by 7.1%, and the power loss differs by 4.9%. Therefore the model is in good accordance with the data gathered.

The hydrofoil outperformed the other designs. The efficiency gain relative to the profile arms was significant at 5.2%. The delivered power determines the net efficiency; however, the losses incurred by the inverter, the drivetrain (gearbox and generator), and line losses all contribute to reduced efficiency at which the rotor truly operates. Accounting for these losses and adding it to the power output yields the true rotor efficiency.

### **5.7.1 Quantification of power loss**

When the turbine was situated at the rear of the research platform, the wakes from each pontoon had 22 ft to develop. Within the first 10 ft, the wakes off each pontoon met in the center and began interference. The turbulence of the water between the pontoons was an obvious source of loss; hence, the test at the front of the research platform was used to quantify the power lost by the wake. The front location is not entirely wake free; it is not the pure free stream flow. The shaft was located near the intersection point between the

pontoon wakes. Due to physical constraints on the research platform, the turbine was unable to be secured in a purely smooth flow. At the front location, the turbine delivered 2.21% more power, or 150 W. The ratio of the power lost to the velocity was used to extrapolate and estimate the wake effects. Both the front and rear location testing was performed in a 2.27 m/s flow, thus a ratio of the power difference and mass flow was obtained and used to estimate the power loss due to the pontoons for the other test cases.

The drivetrain was another source of significant loss. The inefficiencies in this category encompass the mechanical linkages and conversion to electricity. The bearings, gearbox and generator losses all combined under the overall drivetrain loss. It was measured by NECI by outrigging the drivetrain component on a test stand. The input torque was delivered by a DC motor and the generator's AC output was used to quantify the power lost in the transfer. Running at different RPMs, a curve of the power loss results was developed to calculate the drivetrain losses.

To load to the grid, the power had to be consistent and delivered as single phase 240 VAC at 60 Hz. The Aurora inverter takes the raw generator power signal, rectifies it to DC and then inverts it to the necessary AC specifications. During this process, the unit logs the incoming and outgoing power readings, thus rendering the ability to quantify the loss. Line losses are taken as negligible as the insulated 8-AWG cable length is approximately 100 meters as it runs the length of the bridge from the turbine to the trailer.

Table 7 breaks down the power transfer from generator to grid. The generator to inverter power factor was calculated as the ratio between the real power on the AC output of the inverter and the total power coming from the generator.

Table 7: Breakdown of power from generator to grid

Arm Profile	Generator		Power to Grid [W]	Generator to Grid (PF)
	Total Power [VA]	Reactive Power [VA]		
Flat Bar	1182	931.98	727	0.62
Profile	2216.31	1677.03	1449	0.65
Profile Front	2561.24	2000.79	1599	0.62

The power factor is derived from the phase shift between voltage and current signals. The typical 30 degree phase shift between current and voltage at the generator end increased as the electronics downstream introduced additional reactive loads and real power losses. The net effect of a reactive load does not steal from the real power being extracted from the flow. The reactive energy gets bounced between the generator and the inverter at the frequency of the generated AC signal, giving and taking to keep the generator delivering consistent power. Reactive power does not constitute a loss along the energy path from water to grid and is therefore not a measurement of interest for the mechanical side, but worth knowing on the electrical end. This aspect is part of another research project at Pointe du Bois.

### 5.7.2 Rotor output

Table 8 shows a breakdown of the real power lost due to all sources along the path from generator to grid. Figure 47 gives the complete power extraction breakdown from the available kinetic power in the flow to the power delivered to the grid. It shows the limitation imposed by Betz and the power output after the various sources of loss.

Table 8: Power extraction breakdown

Arm Profile	Velocity [m/s]	Power [W]	Rotor RPM	TSR	Water To Wire Eff. [%]	Losses [W]			Rotor Eff. [%]
						Pontoon	Drivetrain	Inverter	
Flat Bar	2.35	727	59.6	2.03	9.6	166.53	244.7	58.2	15.9
Profile	2.27	1449	56.0	1.97	21.3	150.00	226.3	115.9	28.6
Profile Front	2.27	1599	59.6	2.09	23.6	0.00	244.3	127.9	29.1
Hydrofoil	2.09	1410	58.8	2.24	26.5	117.52	240.4	112.8	35.4

It was anticipated that the maximum rotor output would be within a TSR range between 2.22 and 2.31 yielding a rotor efficiency of 30.3%. The turbine with the hydrofoil arms was the only test case to reside in the optimal TSR zone. The performance of the profile arms in the rear position deviates from the optimal TSR, at most with a difference of 10.5%. Outfitted with the profile arms, as initially designed, the rotor delivers 28.6% of the kinetic energy to the drivetrain. With minimal wake interference at the front, the TSR increased and the rotor output an efficiency of 29.1%, closer to the design mark. The hydrofoil arm exceeds the rated efficiency. This result was expected as the rated design was that of the profile arms with a higher drag coefficient. With far smoother contours,

the hydrofoil reduces the drag enough to see a 5.3% increase in rotor efficiency to deliver a coefficient of power of 0.354, consistent with the findings of Antheaume *et al.* (2008) and Faure *et al.* (1983) who also obtained efficiencies just below this value for a non-ducted Darrieus turbine. The river flow was not constant for all four tests cases. Testing took place over three days and the flow was decreasing over this time. The calculations used the average flow rate during the data sampling time frame. Efficiencies are not dependent on the free stream velocity, but rather there exists an optimal TSR in any given flow where power production will be most efficient.

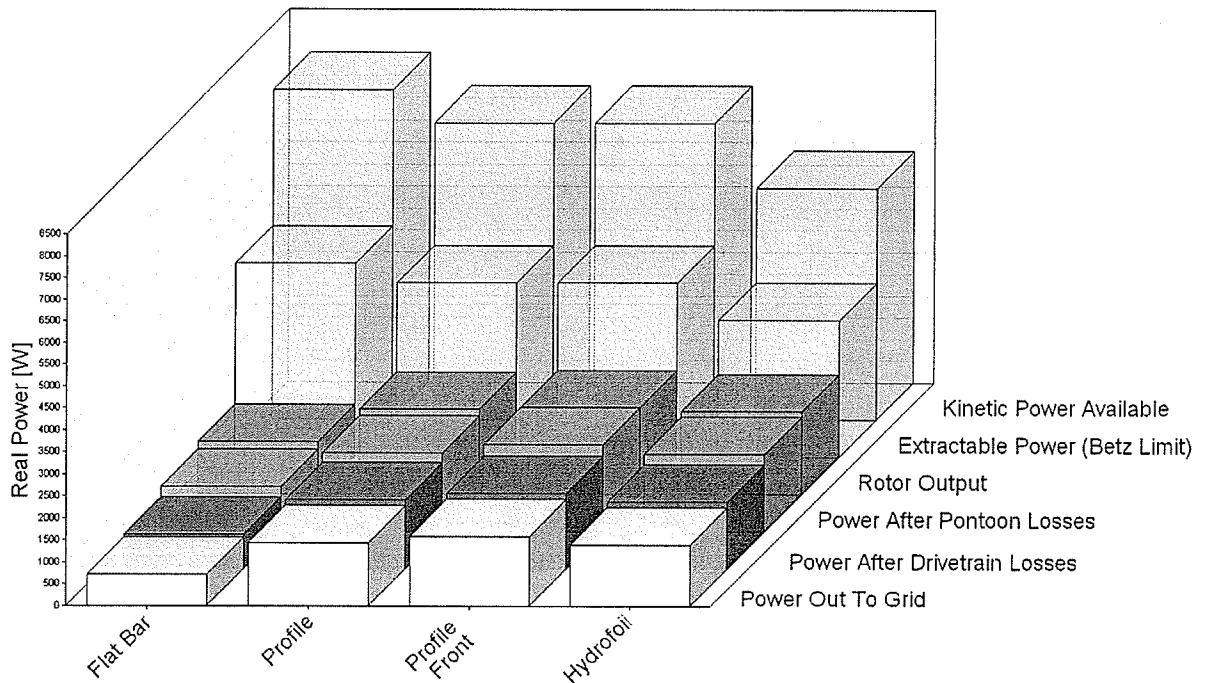


Figure 47: Power extraction, losses, and efficiencies

### 5.7.3 Anchoring loads

The load on the main anchoring line is measured by the load cell. It logs a maximum value per minute of the samples recorded. It must be mentioned that the sampling rate is low, only a few hertz, which is the maximum capacity of the data taker. The results give a good indication as to the loads experienced; however, it does not give the full behaviour of the loading, but rather the data is used to gain a clear picture of the mean load. The results for load and flow are averaged over a few minutes to obtain the average loading on the anchor.

A comparison between the load of the flat bar and the profiled arms showed the amount of drag on the research platform. When the turbine was raised out of the water, the average load value was taken as the baseline load from the research vessel itself. When the flat bar and profile arms were being tested, their drag superimposed onto the baseline load. The baseline research vessel, without any turbine in the water, had an average drag of 836.8 lbs. With the turbine stalled in the water, the results match expected values. The profile arms show a smaller increase from the baseline than the flat bar when the turbine is stationary. During testing of the profile arms, the turbine was loaded immediately upon startup; therefore, freewheel drag was not obtained. Table 9 gives the breakdown of the different loads assessed.

Table 9: Loads on main anchor line

Main Cable Loads [lbs]			
		Flat Bar	Profile
Research vessel		820.3	853.3
Total Drag	Turbine on	1376.4	1474.2
	Turbine off	1015.6	982.5
	freewheel	1120.6	N/A
Rotor Drag	@ 60 RPM	556.1	620.9
	Stopped	195.3	129.2
	freewheel	300.3	N/A

The freewheeling turbine increased the total drag more than a stationary rotor: an increase of 30% over the stationary turbine. When delivering power, the load increased due to the generator loading. The flat bar arm configuration, producing around 700 W, resulted in 10.4% less tension in the main cable than the profile arm configuration producing power in the 1400 W range. However, with the turbine stopped, the flat bar configuration had 51.2% more drag. While extracting rotational power, Newton's third law invoked a counteracting torque which acted about the rotor's axis of rotation. This reaction torque added to the uniaxial loading on the main cable. Although the physical geometry of the profile support arms induced far less drag while in rotation, the reaction torque due to the electrical loading dominated as the main source of additional load on the main cable. From inactive to delivering power, the flat bar configuration increased



the main load by 184.7% while the profile arm, producing 100% more power, increased the load by 380.6%.

Taking only the additional loading caused by the stopped and freewheeling turbine, the coefficient of drag for the rotor was calculated for the flat bar support arms. Taking the frontal planform area of the turbine, this configuration had a coefficient of drag of 0.271 when it was stationary and 0.417 freewheeling. The profile arms configuration yielded a reduction of the drag coefficient to 0.192 when stationary. Therefore, the flat bar support arms contributed a 41.1% increase in the drag coefficient.

The anchors at the Pointe du Bois site were originally designed for a larger 60 kWe unit. The main anchoring line is 1 ¼" steel cable, which has a nominal load of 180,400 lbs. The design load under consideration when designing the anchoring system was a maximum of 50,000 lbs. With the smaller 5 kWe unit in place, which required 1500 lbs of retention force from the anchors, the safety factor was 120.

## **5.8 Conclusions**

The 5 kWe Darrieus turbine performed at a peak efficiency exceeding 35%. This was consistent with the findings of Antheaume *et al.* (2008) and Faure *et al.* (1986) who also tested a non-ducted vertical axis turbine. Winter testing showed a significant loss in power; however, this loss was due to the support arms and not the climate. Summer testing of the turbine's winter configuration showed similar performance values indicating that temperature is not a factor. It must be noted that the turbine drive chain

was heated and enclosed during the winter months to keep the synthetic oil in the gear box at operational temperatures. Manual start of the turbine was difficult when the drivetrain was exposed to cold ambient conditions; however, most of the resistance was not in the oil viscosity but the turbine support arms. The flat bar support arms, which were used during the winter deployment, showed that rotating the 8 arms consumed 67% of the power generated by the rotor. The turbine, equipped with these arms, performed at 9.65% efficiency in the summer. In the winter, an efficiency of 10% was evaluated using a direct connection to a resistive load. Although both data sets were taken at different flow rates, and hence varying TSR, the turbine's performance was unaffected by the winter climate as long as the flow remained unobstructed by ice formation and the drivetrain oil was at operational temperature.

## Chapter 6

### Icing

#### 6.1 Testing in cold climates

The winter of 2008 was one of the coldest winters Manitoba had seen in years. Weather data for the past 10 years (1998 – 2008) quantifies the degree of cold experienced in this year in relation to a typical year. Figure 48 shows the average temperature for each day of the three winter months for this year with the average over the past 10 years.<sup>3</sup>

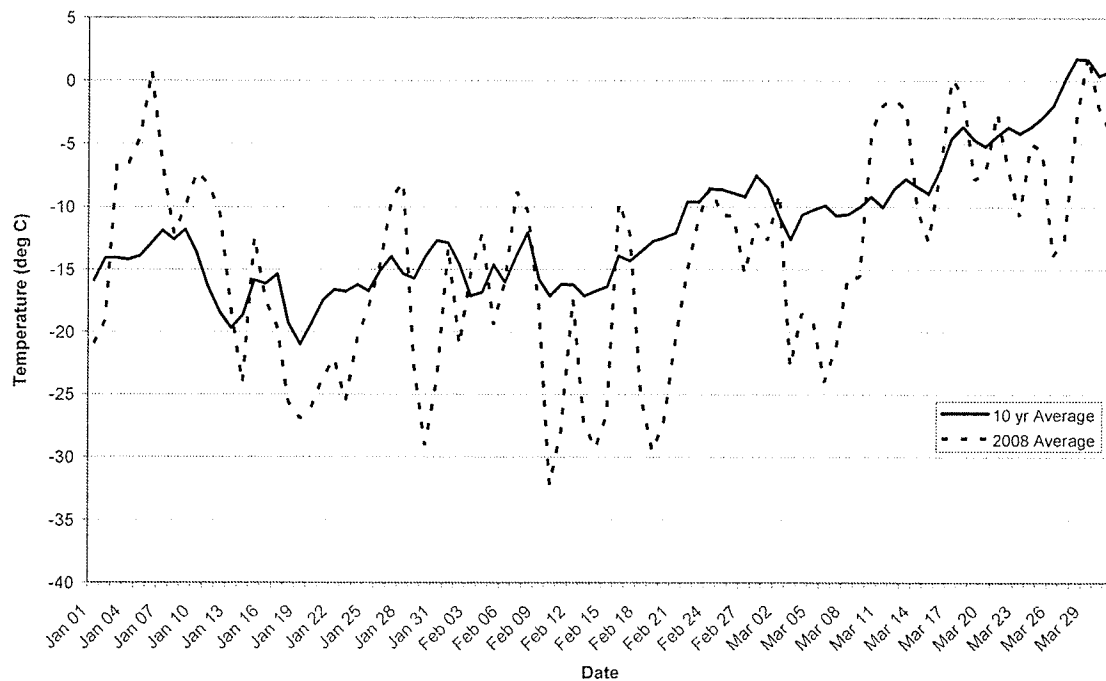


Figure 48: Temperature data at Pinawa, Manitoba for 2008 and the past 10 years

<sup>3</sup> Weather data obtained through the Environment Canada website

The year 2008 was, for the most part, colder than what Manitoba experiences from year to year, so testing in this weather yielded valuable experience of what to expect for a long term installation.

Manitoba saw consistently cold temperatures and many cold weather events throughout the winter of 2008. Launching a research vessel into the river proved to be more difficult than it would have been without the ice on the water. The turbine was deployed in the winter because of previous delays and NECI's readiness to deploy right away. The research teams from both the University of Manitoba and NECI were equipped with Mustang survival suits, which became rather warm during periods of heavy activity on even the coldest of days. Working 16 hour days in -40 degree weather (with the wind chill) proved bearable in those suits provided that warm shoes and gloves were worn; however, with all the necessary protection, the cold climate still had its influence. Tightening bolts, manipulating of small parts, and controlling the data acquisition computer became difficult because it could not be done with gloves on, reducing productivity significantly. Instrumentation would also suffer due to the cold. Many lessons were learned and procedures were adjusted to increase the speed of the work to reduce the amount of time spent in the cold.

The conditions at Pointe du Bois have the potential for frazil ice; however documented observations of its presence are limited. The testing location was at a bottle neck in the river where the vast span of the upstream river flows between the piers of a 200 ft bridge. Aston (1986) noted that at local restrictions in rivers, large and thick frazil pans often

break up or disappear in turbulent flow. Also, the area upstream of the dam was covered by stationary ice all winter long and this keeps the upstream water from being supercooled. Only a few hundred feet before the dam does the flow increase in velocity and is no longer covered by ice. Over this stretch, the flow has a free surface with the frigid air where the surface waters can become supercooled over a short distance. The ice that formed on the research vessel was primarily due to secondary processes and the turbine blades were never observed to be covered in ice during normal operations. Pancake ice consisting of a thin layer of transparent ice floating at the surface and causing no accumulation was observed when temperatures dropped below  $-20^{\circ}\text{C}$ , as shown in Figure 49.

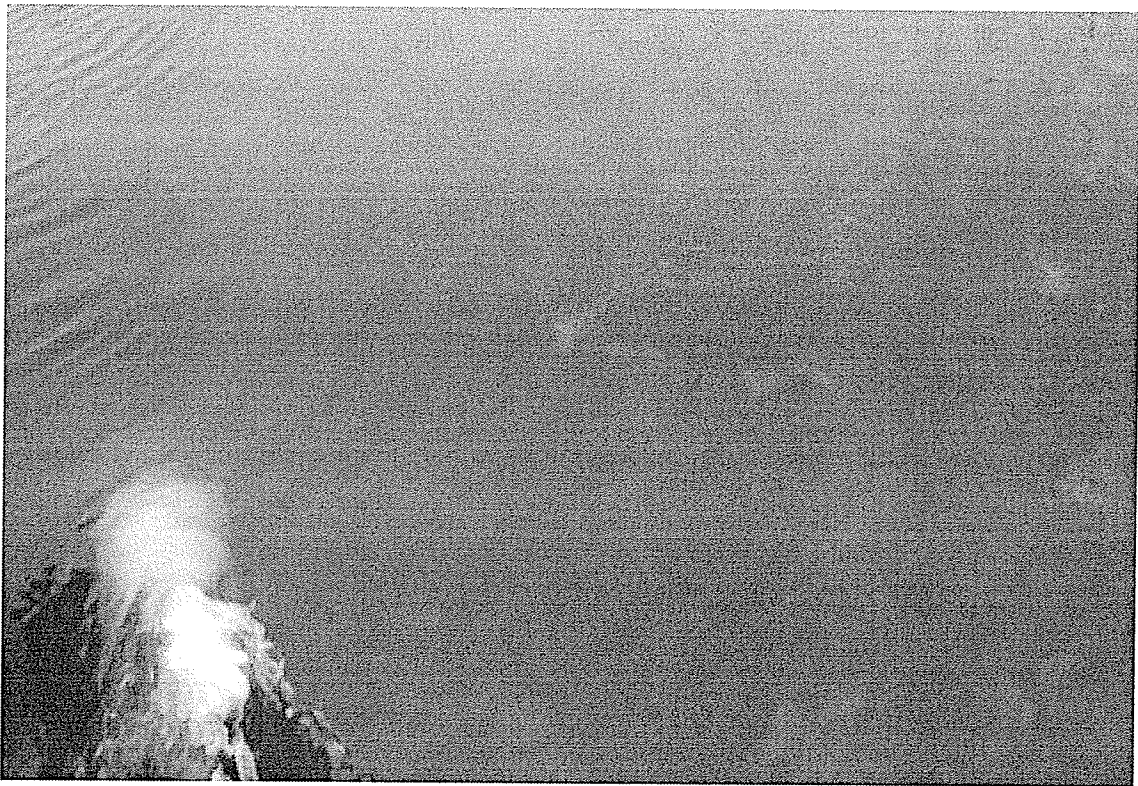


Figure 49: Inactive frazil ice flowing below pancake ice

Observations of frazil ice appeared in its passive form in early February when temperatures were below  $-20^{\circ}\text{C}$ . The frazil ice could be seen floating in the water just below the pancake ice and was observed to be on the order of 0.1 m wide and 0.5 m long. The source was upstream, below the shield of stationary ice that forms over the slower section of the river and is there all winter long. It was hypothesized that active frazil ice upstream passes through the warmer waters under the ice covers and converts into the passive form. This type of frazil ice was not sticky by nature and hence it did not build up on the structures placed underwater, but rather it grouped together at stagnation points and flow restrictions. The ice was very good at retaining its crystals and did not break up easily. It wrapped around objects, and although it did not adhere, it rested on objects and built upon itself. This type of ice builds up rapidly once an initial blockage of passive frazil forms and Figure 50 shows such a collection of passive frazil after one week. Passive frazil was documented during the late winter and early spring (March and April).

## 6.2 Climate effects on instrumentation

The sensors were rated for extreme cold conditions but implementing them in such conditions brought on additional design considerations before installation. Most of the problems occurred in the vicinity of the free surface. Sensors that required to be submerged also did not fare well. Any equipment placed within a foot of the free surface would get encapsulated in ice. Chipping the ice away would either destroy or sever the sensor with the ice. One such instance destroyed the propeller and propeller tube of a flow meter. During the periods when the on-site flow meter was out of commission; a handheld meter was brought in for periodic readings.

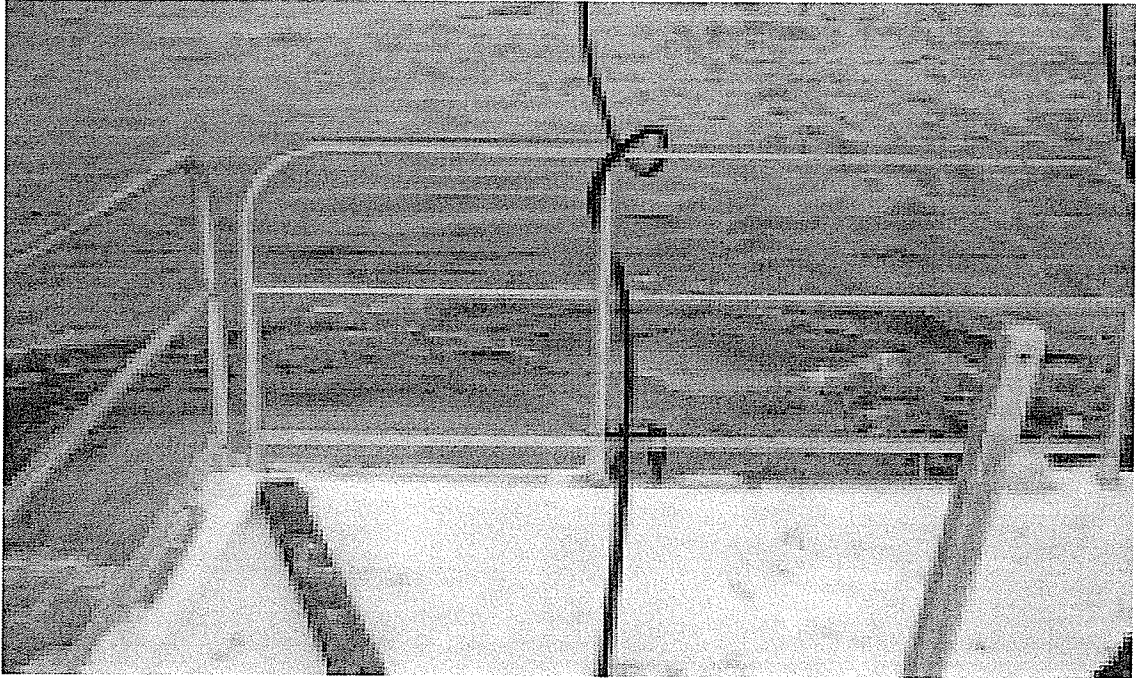


Figure 50: Inactive frazil ice build up

The hand-held instrument froze the instant it was removed from the water and a 15 minute downtime ensued to thaw it out for the next reading. The added drag of the ice accumulation on the load cell wires severed the connection early on during testing and thus that sensor was lost for the remainder of that deployment.

The sensor mounts for the flow meter and underwater camera were designed with ice in mind and thus the sensor wires ran through the inner cavity of a steel tube, thereby protected from severing, and the sensor was placed deep below the level of surface ice. These precautions improved the life span of those sensors; however, the end result was the same: sensors were lost due to harsh environmental conditions. Ice that was chipped off the front of the research vessel traveled under the downstream ice formations and would impact the sensors deep underwater. The impacts were so great that the 1-7/8 inch

steel tube holding the flow meter was bent 20 degrees off vertical. De-icing the vessel resulted in a loss of two flow meters, a load cell, an underwater camera, and a sonar microphone.

The load cell was the first instrument to fail. Although the sensor itself was safe deep underwater, there was a critical design flaw with the sensor. The wire that carried the power and output signals was fastened orthogonally to the load cell, placing the connection of the wire perpendicular to the flow. The drag at 2 m/s induced vibrations in the cable that eventually sheared four metal pins at the connection to the load cell. The vibration sensors, thermocouples, and cameras located above the water fared well and survived winter testing.

The accumulation of ice was found to take place within a small range in height from the free surface of the river. Any physical object that passed through this interface region had to be strong enough to withstand the ice build up and the impact of icebergs or other foreign debris.

### **6.3 Research vessel icing**

The placement of an aluminum pontoon research vessel into sub-cooled water presented a wide array of icing issues. Ice accumulation on the pontoons and anchoring chains not only altered the flow, but encouraged rapid ice growth. This section presents the general observations of ice formation on the research vessel along with the measures taken to mitigate ice formation and the process of removing the build up of ice.



### 6.3.1 Ice formation

Ice forms on any and all surfaces within the water and just above the water line. Within a day, ice a few inches thick would attach itself to the pontoons and anything else that was placed in the water. Metallic objects in the water present a substrate that promotes primary nucleation. With a thin layer of ice formed by the primary nucleation process, a base ice substrate is formed and ice continues to grow until removed by natural or artificial means. The main aggressor of ice formation above the waterline is splashing. Figure 51 shows a picture taken at the same time every day for five days giving a time lapse view of ice growth on the research vessel.



Figure 51: Time lapse ice formation on research vessel

Stagnation points and wakes resulted in a surge of fluid that rose and fell, splashing all surrounding surfaces with a douse of water. When receding, a thin film of water remained on the surface. Exposed to the air, the film of water crystallized instantly and formed a substrate of ice heterogeneously. As the water rose and fell repeatedly, the secondary nucleation process froze more water to the substrate, layer after layer. Splashing allowed the ice to grow out from the water and eventually reached the underside of the research platform. The supercooled temperatures within the boundary layer around the surface ice promoted continuous ice growth underwater as well. The chains that anchor the research vessel at the bow were the most susceptible to ice formed by splashing. Water droplets splashed along the length of the chain that was out of the water. Freezing on contact to the cold steel, ice grew along the chain all the way to the linkage point with the research vessel. The steel chains, which extend into the water, generated wake turbulence that encouraged ice growth by mixing the flow of the supercooled water. The ice that accumulated underwater was attributed to the build up of passive frazil. Slushy underwater ice blocks were found to extend over 2 feet along the length of the chain into the water. When the chain fully iced over, a smooth round surface of ice reduced the severity of the splashing. At this point, a smooth wave sat at the stagnation point where the chain met the waterline. The reduced velocity of the flow encouraged further ice growth that propagated radially creating a flattened area of ice at the water's surface. The massive slabs of ice on the chains grew larger than the 5 kWe turbine itself and weighed heavily on the chains, pulling the bow down towards the waterline.

The pontoons of the research vessel added a new dimension to ice growth because they encouraged thicker sections of ice to form on them. The wakes of the flow around the pontoons caused sizable waves that allowed the water to splash up half way between the waterline and the platform. At times, the ice attached to the pontoons would grow to over 1-½ feet thick. The addition of the ice above the water surface weighed heavily on the research vessel and contributed to pulling the platform lower to the waterline. At its worst, the bow of the platform was only a few inches from the surface of the water and waves from the nose of the pontoons were able to reach above deck. Removing of the ice returned the deck height to its original, non-iced position.

As ice propagates outward, the ice from the port pontoon would eventually connect with the ice from the starboard, creating a flat surface of thick, solid ice under the deck. Figure 52 shows the free surface under the deck frozen from pontoon to pontoon. The thickness of the pontoon ice is also shown as well as the ice that formed on the chains.

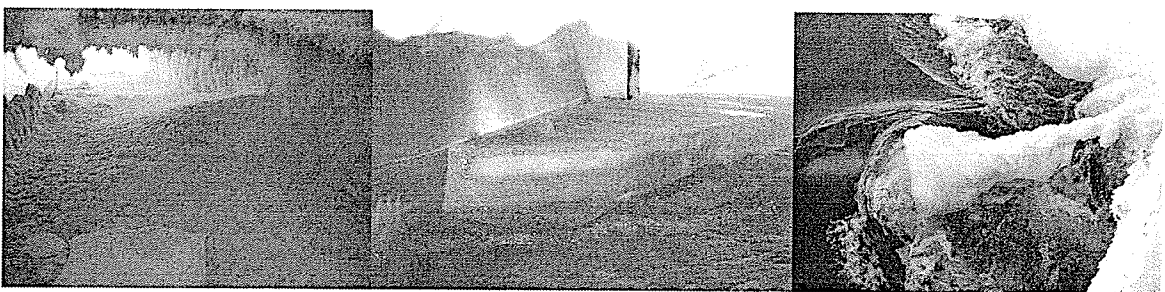


Figure 52: Ice formation between pontoons and on anchoring chain

The rear quarters were the first to ice over completely and there was no free surface aft of the turbine. A rotating shaft kept ice from forming directly on the turbine until the rear

and pontoon ice grew into its way. At the bow of the research vessel, like the rear, ice formed from pontoon to pontoon causing an ice dam. Because of the amount of water rushing in, it took some time for the entire front end to completely ice over. At its worst observation, the entire free surface below deck was covered with ice at a minimum thickness of 8-10 inches, except for a 1-foot wide stream that flowed freely from under the frozen dam at the bow to a foot ahead of the turbine.

A critical situation presented itself when ice accumulation created a dam at the bow. The solid wall of ice posed serious threats to the project. Growth under the surface extended a solid curtain of ice that increased the drag and tested the safety factor incorporated into the anchoring system. Aside from adding significant drag, the ice along the bow allowed the water to reach the deck and drown the nose of the research vessel. Water found its way onto the deck and the bow of the vessel was pulled underwater. A surge wave engulfed the deck, lifting a 600 lb boom that was resting on the deck, and crashed into the data acquisition shed and turbine enclosure. Vital data acquisition equipment was lost but the turbine's generator survived without noticeable damage. Figure 53 shows the extent of the damage.

### **6.3.2 Ice mitigation**

Ice mitigation requires serious design attention early on for a kinetic turbine project in Canada. The winter demonstration at Pointe du Bois was under time constraints and need to get underway, leaving no room for design measures to address ice formation before hand. Heating solutions did not feasibly solve this issue. The amount of energy needed

far exceeded the amount of energy that was available electrically from the turbine. Heat tracers (200 W) within the front section of the pontoon had no effect. A propane torch took minutes to melt the ice that formed. The heat source from the propane flame dissipated in a hurry because the frigid ambient environment was the dominant heat sink. The wind blowing extremely cold air absorbed the heat from the flame and dominated the heat transfer, thus delivering far less energy towards melting the ice. For heat to be a possible ice prevention method, a constant source of gas burners to keep the surface of the aluminum pontoons above freezing would be needed, but this method conflicts with the purpose of this demonstration.

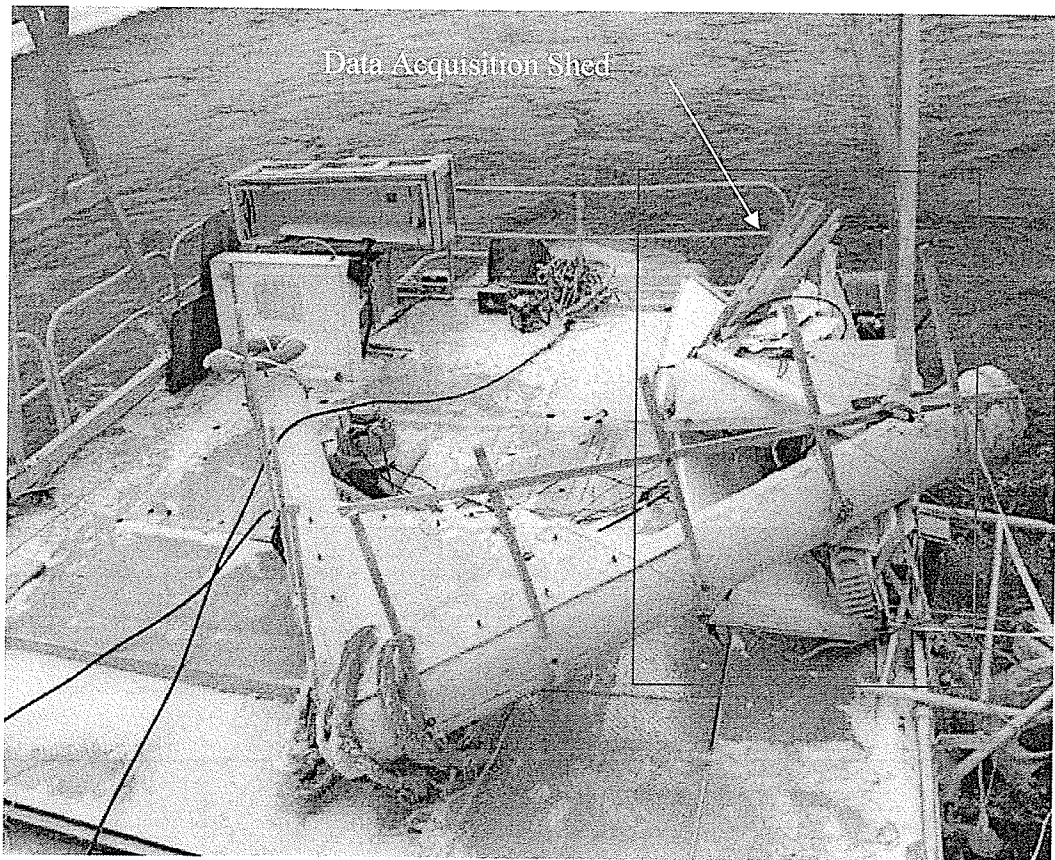


Figure 53: Destruction caused by excessive ice on research vessel

To prevent icing on the anchoring chains, a PVC pipe was placed around the front chains at the waterline. The idea was that a surface that was free to rotate could use the motion to remove any primarily nucleated ice. The PVC device was found a few days later inside a solid block of ice. An inner tube wrapped around the nose of the bow was implemented in an attempt to mask the metallic surface of the nose of the pontoon with a more ice-phobic surface. The ice did not adhere strongly to the rubber and it was easy to detach from its surface. Ice continued to form, however, around the tube and subsequently engulfed the inner tube. It was embedded into the ice but broke loose with a minor force. Rubber-coated pontoons have promise in being a mitigation tool, but this solution needs to be incorporated into the assembly of the research vessel. The only option that remained for this demonstration was ice removal and this took place regularly every few days.

### **6.3.3 Ice removal**

Three tools and a strong flow were all that was needed to de-ice the research vessel. A steel pick and a sledge hammer were essential. The steel pick had a flat edge on one end and a flat top on the other. A large flat top was an excellent surface for a hammer to pound on. The flat edge at the other end concentrated the blow to a sharp edge. These two tools were used to de-ice the outside perimeter of the research vessel in minutes. Picking at the ice/pontoon interface broke the bond that the ice had with the aluminum pontoons. Hammering not only separated the ice from the pontoon, but more importantly it sent strong vibrations down the interface encouraging the crack to propagate down the length of the pontoon. After some work, water began to flow into the crack, eroding any

remaining bonds. Once free of the pontoon, the free stream ripped the large slab of ice from the exterior of the research vessel.

The inner ice between the pontoons required the third tool. An 8-ton jack was used to lift the entire research platform and separate it from the solid ice sheet. The shear force around the base of the jack cracked the ice in all directions. The jack was raised until the sheet of ice dropped below the water line, flooding the cracks and allowing it to erode into wider passages until finally the flow grabbed the ice and it all broke off instantaneously. The large blocks of ice on the chain were the simplest to remove due to the flexibility of the chain. Tapping the chain sent a large wavelength of motion that traveled down the length of the chain and into the water. The motion of the chain shook the ice off while tapping at the interface broke the bond that the ice had on the steel outside the water. The submerged ice, with its slushy and soft composition, was much more difficult to remove because it absorbed the pick's energy, but it was not bonded to the chain as rigidly as the surface ice and could be scraped off.

## 6.4 Conclusions

Operating a kinetic turbine in the winter can involve extensive maintenance on a regular basis to remove ice build up. The economics of constant care would outweigh the benefits of micro hydro. Ice was a constant challenge for this installation because the research vessel employed was aluminum and the installation was at the surface of the water. Any structure within a foot of the water's free surface was susceptible to rapid ice growth. The pontoon design of the research vessel used for this project created a unique

dimension of ice growth that allowed solid ice sheet to form between the two pontoons. Encasing the vessel in a block of ice not only stalled the turbine, but could critically damage the rotor while removing of the ice block. Precautions had to be taken when removing the ice from the encased rotor because it needed to be removed in sections strategically to minimize impacts on the rotor blades. The rotation of the vertical axis shaft prevented ice accumulation during operation. Ice built up around the turbine, between the pontoons, until it slowly closed in on the shaft. When friction from the encroaching ice stalled the turbine only then would ice encase the shaft.

Frazil ice was only observed in its passive form. This type of frazil ice led to build up on the anchoring chains and affected the incoming free stream flow by causing a blockage. The build up, however, did not show any deterioration to turbine output as it was cleared on a regular basis.

The advantages of a kinetic turbine installation at the river's surface are numerous, including but not limited to easy access was possible for maintenance, waterproof seals for the drivetrain were not necessary, and installation costs were minimal. For a year round installation, preventive designs would need to be employed to mitigate the issue of icing. Using a platform constructed of ice phobic materials and incorporating automated ice breaking machines may be the best solution. It was found that an 8-ton jack did very well in removing the ice by separating the ice block from the pontoons. A hydraulic press would work well in removing ice around and between pontoons.



Figure 54 shows more pictures of the severity of the ice growth on the vessel at the Point du Bois site. After chipping away sections of ice, the thickness of the ice accumulation on the pontoons can be seen. The pictures taken through the access hatches on the vessel's deck show the early stages of ice propagation, encasing a pipe onto which the underwater camera was mounted. The photos taken below deck show the end result when ice grows from one pontoon to the next. Ice grew extensively on the exterior of the pontoons as well. Clearing these sections of ice required extra care with regard to safety. The use of lanyards and harnesses were mandatory for any trip onto the research vessel. Along with photos of ice buildup along and between the pontoons, this figure shows the size of the icebergs that break off from the ice sheets in the spring. The size of the detached ice sheets are larger and have more mass than the research vessel.

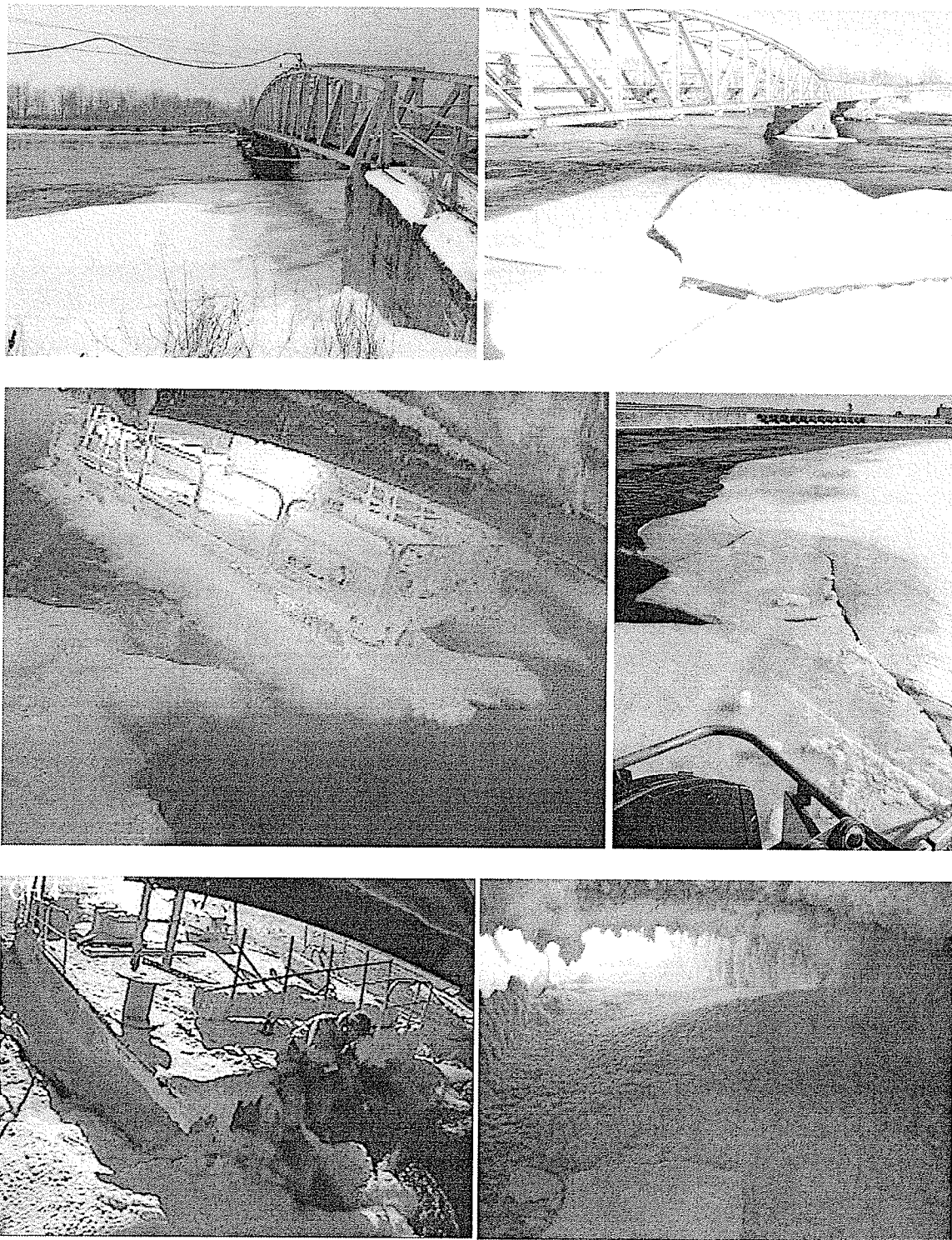


Figure 54: Additional photos of icing

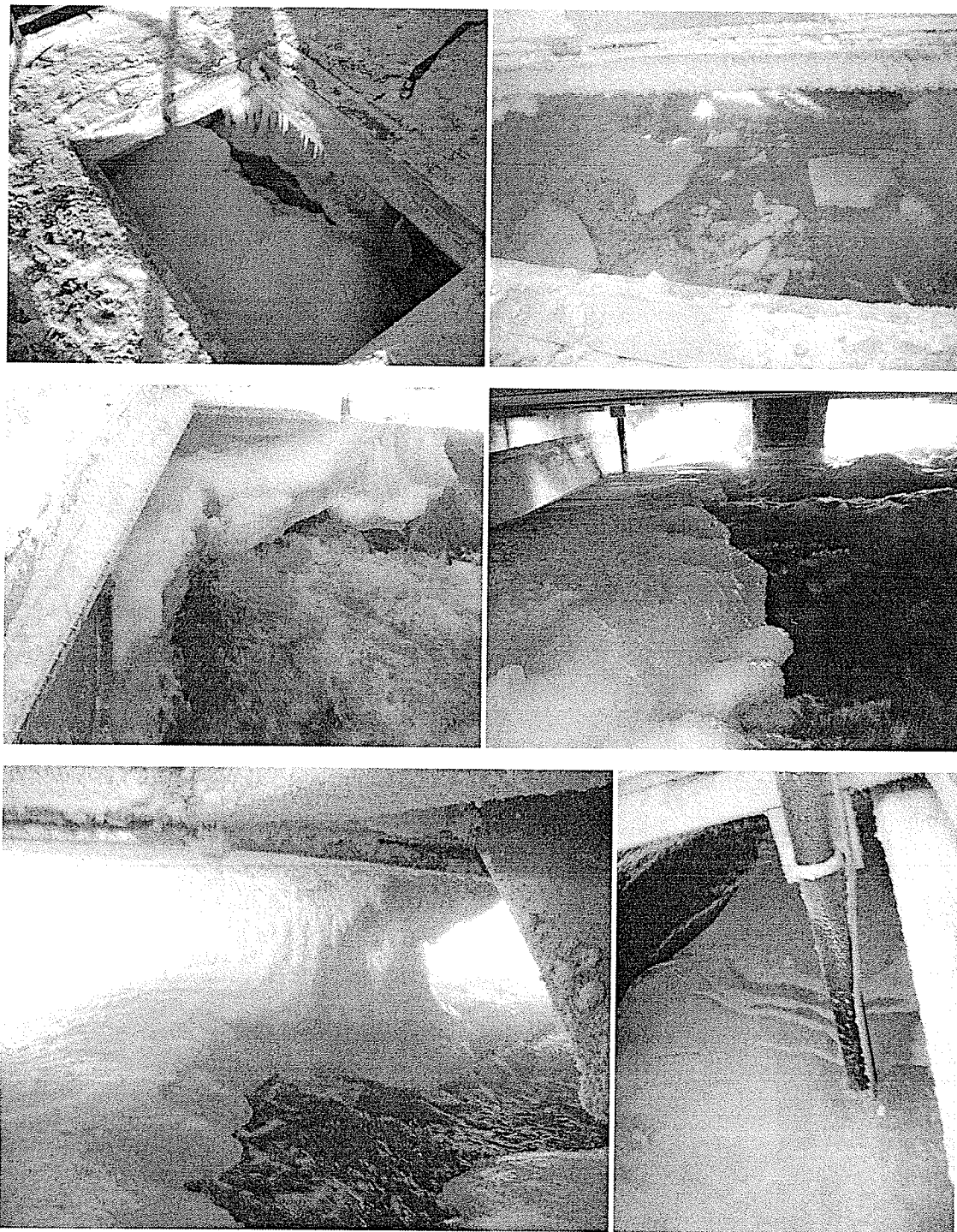


Figure 54: Additional photos of icing (cont'd)

## Chapter 7

### ADV Flow Measurements

#### 7.1 Acoustic Doppler velocimetry

The Acoustic Doppler Velocimetry (ADV) was used to characterize river flows upstream of the turbine. This device was designed to be an accurate method of acquiring flow data because it used a more precise method that involved transmitting an acoustic signal and measuring the Doppler shift from the moving particles embedded within the flow. To obtain an adequate signal, the flow must be seeded with enough particles of adequate size to reflect the acoustic signal. The relatively high frequency for flow meter, sampling at 200 Hz, allowed for the direct measurement of turbulence within the flow. While the flow meter was used to obtain the general mean flow rate of the water at all times, the ADV offered a snapshot of a few minutes, which details not only the mean velocity, but the turbulent fluctuations as well.

#### 7.2 ADV tests

Thirteen flow measurements were taken with the ADV at various locations. Samples were taken at 2 locations along the research platform. At each location, measurements were taken at 3 levels. Locations 1 and 2 sampled the flow 1 foot and 7 feet upstream of the turbine respectively. Levels 1, 2 and 3 respectively correspond to samples taken at

42, 52, and 62 inches below the deck of the vessel. Note that the midpoint of the turbine was approximately 45 inches below the deck. Particles were introduced to the flow to obtain a reliable signal from the unit. Milk was used as the particle-laced fluid and it was injected into the flow using a pressurized tank. The milk was diluted with river water for various ratios of milk-to-water as discussed in Section 7.5.1. Table 10 gives the ADV test matrix with respect to location, depth, milk-to-water seeding ratio, and the data set sample size.

Table 10: ADV test matrix

Test	Location	Depth Level	Milk-to-Water Ratio	Sample Size
1	1	2	1:0	30000
2	2	1	2:1	14030
3	2	2	3:2	3404
4	2	2	3:1	1173
5	2	1	2:1	4721
6	2	1	1:1	1000
7	2	3	1:1	10000
8	2	3	1:1	50000
9	2	2	1:1	50000
10	2	1	1:1	50000
11	1	2	2:1	46799
12	1	3	2:1	11738
13	1	3	2:1	50000

### 7.3 ADV test apparatus

The ADV recorded fluid velocities on a frame of reference that is relative to itself. Therefore, an apparatus for the ADV needed to be adjustable and precise to align the ADV's local reference with a global reference. Setting up the ADV was a quick task in laboratory settings, but the field presented a league of challenges all its own. The requirements for the frame were that it must be removable and lightweight so that it could be installed and operated by two people. The field apparatus was designed to span streamwise on the research platform. A 2" angle bar was the main support with a smaller length angle bar bolted orthogonally at one end. The smaller length bar was used to fasten the unit against one of the deck panels. From the main support, a small pipe extended half above and half below the base. It was supported using 1/2" angle bars. This 4-foot pipe was a sleeve for the main pipe, which held the ADV mounting plate to allow the ADV to be positioned anywhere up to 6 feet deep. The ADV mounting plate was an aluminum flat plate designed to act as a small rudder to help align it within the flow. The pipe was fastened at a set depth by a bolt tensioned through the sleeve and onto the pipe. To seed the flow with particles, a pressurized tank injected the particle laced fluid into a plastic tube that ran down the inside length of the main pipe. At the mounting plate, the tube was brought out of the pipe and fastened to a steel tube that delivered the particles directly into the ADV sampling control volume.

## 7.4 ADV deployment

The ADV was not a sensor that was constantly in operation. It was used intermittently for direct sampling for specific testing. The ADV test apparatus could have been erected on the deck of the research vessel within 5 minutes for temporary deployment. Leaving the ADV deployed at all times presented a safety concern while working around it. The deck of the research vessel consisted of 5 panels that were removable. The turbine occupied one of these panels at any time it was deployed. An additional panel was removed exposing a 32 ft<sup>2</sup> gap on the deck where the ADV was to be inserted. The stand was placed across the open gap and fastened to the aluminum panels on both sides of the gap using self-tapping screws. The screws kept it from being pulled into the water by the drag on the pole. The ADV was subject to the vibration of the deck. The free standing pole, onto which the ADV was mounted, was restrained in the streamwise direction by design and the lateral sway was dampened by ratchet straps from each side of the research platform. Figure 55 shows the apparatus as it was deployed on the deck of the research vessel.

## 7.5 ADV flow analysis

The ADV returns a signal that required post-processing to obtain pertinent information from it. This section outlines the issue with the signal and the two methods used to filter it.



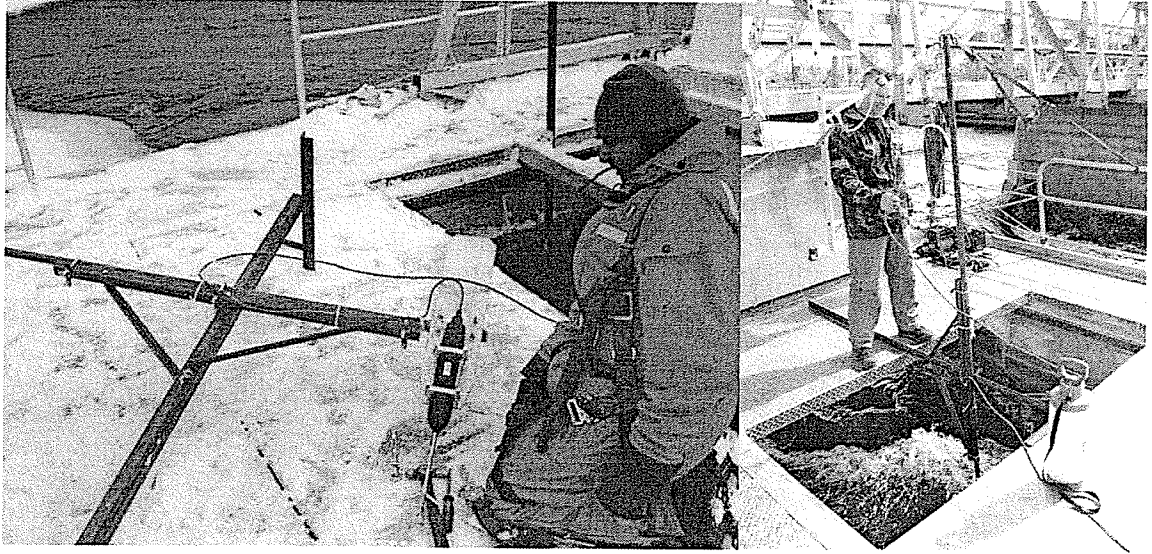


Figure 55: ADV stand deployed on deck

### 7.5.1 Seeding

The ADV worked by measuring the reflection of an acoustic signal from particulates within the flow. The velocity of the particles were calculated by analyzing the Doppler shift in the frequency of the return signal picked up by the four prongs, compared to the transmitted signal emitted from the center stem. The number of particles in the flow related directly to the intensity of the backscatter of the reflected acoustic signal. The ADV had a probe check option that displayed the strength of the signal being acquired in terms of signal amplitude. Figure 56 shows the screen of the probe check during the early summer months of the 5 kWe testing. The  $198 \text{ mm}^3$  control volume of the ADV, located 10 cm from the transmitting signal at the stem of the probe, received a signal that ranged between 50 and 60 counts in amplitude. During the winter months, the signal was flat because there were not enough particles in the water to obtain a signal. The snow and ice cover during the winter months froze particles into place and prevented them from



seeding the flow. In the spring, rain water run-off introduced a large number of suspended particles into the flow and the warm summer months encouraged the growth of small organisms, which may have also been a part of the particles that the ADV picked up.

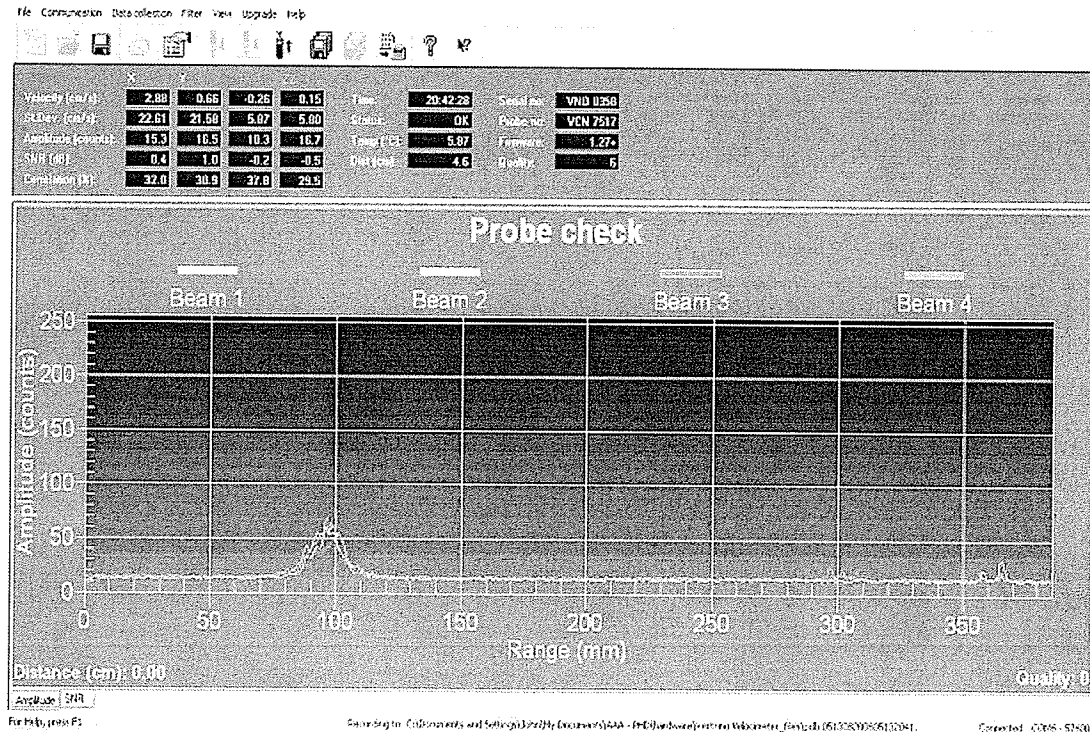


Figure 56: ADV probe check

Since the ADV operations manual recommended a signal over 40 counts, because this was the threshold for noise, it was put into practice to obtain the highest amplitude counts for the most reliable and accurate flow measurements. Therefore, a method of seeding the flow was developed and implemented. Introducing particulates to the environment poses many limitations because the goal of this demonstration was to prove this technology's ability to be implemented with a minimal ecological footprint. Therefore an

organic substance was injected into the flow, upstream of the probe and directly into the ADV control volume. Milk was the liquid used to seed the flow because it is organic and contains large particles that the ADV signal can reflect off. Figure 57 shows the stream of milk as it entered the flow



Figure 57: Milk injected into the control volume of the ADV

A 12 gallon pressurized tank was used to inject the milk into a series of tubes that delivered the milk upstream and inline with the control volume. This method provided enough particles to run the ADV to obtain 100,000 samples, or 8.33 minutes of flow data. The natural turbulence within the flow dispersed the milk in and the flume of milk got sparse as it traveled downstream. The flow was sampled using different milk-to-water ratios to obtain an adequate signal with minimal injection of a foreign fluid. The

amplitude was not consistent throughout the sampling period because turbulence would break up the steady stream of milk. There were times when the flow led the milk away from the control volume (CV) and/or the turbulence dispersed the milk, leading to a temporarily lower amplitude signal. A breakdown of the maximum and average amplitudes for the different milk to water ratios is presented in Table 11.

Table 11: ADV tests using milk to seed the flow

Test #	Milk to Water Ratio	Sample Size	Max Amplitude	Mean Amplitude	NOTES
1	1:0	30000	173	87	
2	2:1	14030	168	96	
3	3:2	3404	150	65	Milk nozzle was off center
4	3:1	1173	158	72	Milk nozzle was off center
5	2:1	4721	112	47	Milk nozzle was off center
6	1:1	1000	171	159	
7	1:1	10000	170	157	
8	1:1	50000	173	139	
9	1:1	50000	172	157	
10	1:1	50000	171	149	
11	2:1	46799	174	118	Turbine producing 1.2 kWe
12	2:1	11738	169	61	Turbine at 1.2 kWe and then stopped
13	2:1	50000	170	73	

The 1:1 ratio produced the largest amplitude counts and maintained it for most of the samples. The 2:1 was also adequate with lower mean amplitude indicating that there

were pockets of lower counts caused by the water mixture. It is difficult to pinpoint a single reason for lower amplitudes, but rather there could be one or more mechanisms at play. Turbulence dispersing the milk within the flow, flow deviations that pushed the milk away from the control volume, or larger than acceptable particles within the milk all contributed to an undesirable signal that was full of erroneous spikes.

### 7.5.2 Signal

The signal obtained by the ADV that characterized the flow depended on the conditions in which the signal was obtained. In-situ testing introduced many uncontrollable variables such as particle sizes and naturally occurring air bubbles in the flow. The ADV apparatus and research vessel vibrations also had a direct effect on the results. Richards *et. al.* (1996) discussed the performance of sound attenuation underwater for shallow rivers because particle size and bubbles presented many issues for that particular setting. They concluded that the effects of suspended particulate matter on acoustic absorptions are significant. They also stated that air bubbles within the flow pose a resonance issue when the bubbles are of radii in the  $\mu\text{m}$  magnitude. These bubbles would become the dominant absorption process. The nozzle of the milk delivery system could have also introduced bubbles within the wake that it created.

The main disadvantage of ADV technology were the spikes found in the resulting signal. Figure 58 shows the signal from Test 7.

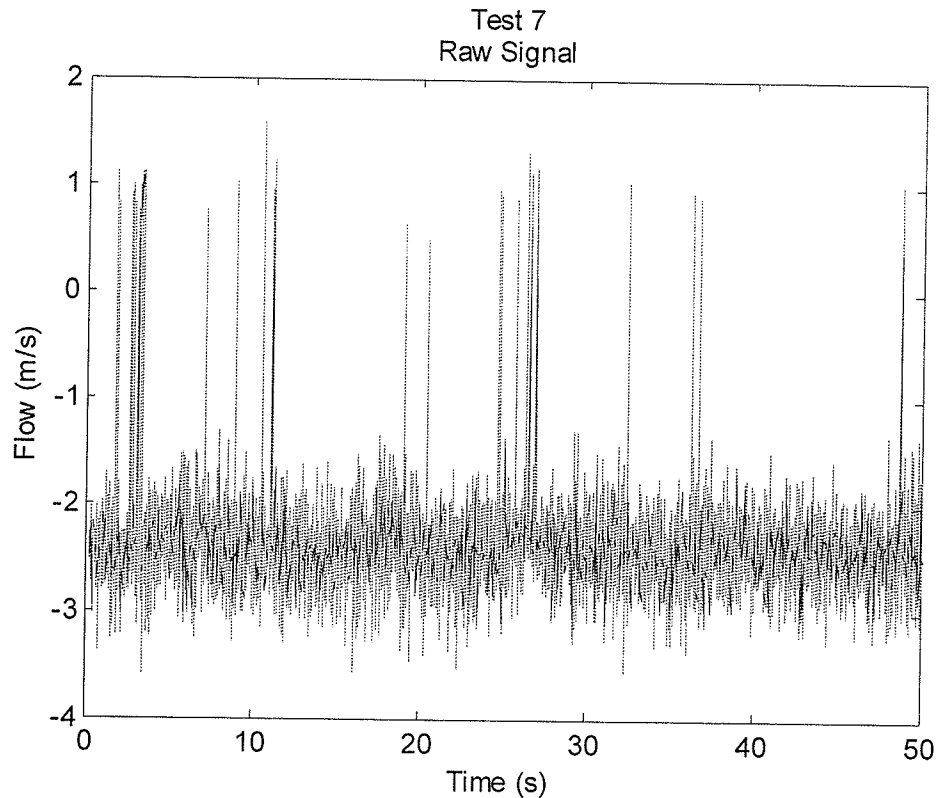


Figure 58: ADV Test 7 raw signal full of spikes

Goring and Nikora (2002) attributed these spikes to “aliasing of the Doppler signal”. The phase shift between source and received signals was outside the range of  $\pm 180$  degrees and thus there was ambiguity causing spikes in the record. Goring and Nikora (2002) presented a few methods for de-spiking the ADV signal for an accurate measure of the flow. Using a bubble generator, Mori *et al.* (2007) conducted seven experiments to test the validity of current de-spiking methods and the relationship between spike noise and air bubbles. Applying the method presented by Goring and Nikora (2002), it was concluded that the 3-D phase space method is the most efficient algorithm for de-spiking ADV data. The filtered data was valid for void fractions of 1 to 3%. For the purposes of this thesis, another method presented by Goring and Nikora (2002) was used. The

Acceleration Thresholding Method (ATM) was used to filtering out the erroneous data from the ADV signal to calculate an accurate mean flow. Figure 59 shows the filtered signal from Test 7.

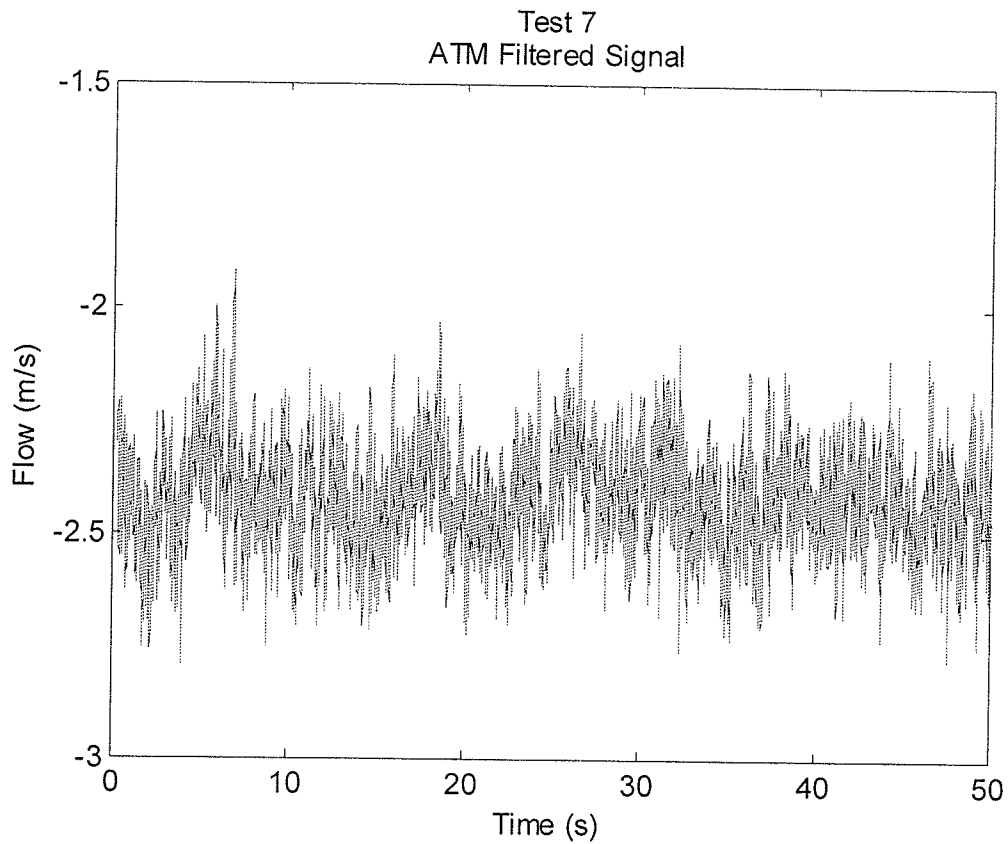


Figure 59: ADV Test 7 filtered signal using the ATM method

The ATM is based on the postulate that under normal flow conditions, the instantaneous acceleration in a stream must be in the same order or less than gravity,  $g$ , ( $9.81 \text{ m/s}^2$ ).

This criterion was used to filter the spikes to obtain a reliable mean flow reading.

Therefore, the iterative process of eliminating spikes based on the acceleration threshold was employed until the mean velocity of the signal converged to a solution within  $0.001 \text{ m/s}$  of the previous iteration.

#### 7.5.4 Acceleration thresholding method

To obtain an adequate mean velocity from the ADV, the signal required filtering. The ATM approach was applied to the ADV data to remove the spikes caused by large particles or air bubbles embedded within the flow. This method scanned each signal and analyzed the acceleration of the fluid particles between two measurements. Numerous iterations were made until the acceleration at any time did not exceed  $9.81 \text{ m/s}^2$ . The algorithm calculated the acceleration from Equation 38.

$$a = \frac{\text{abs}(V(i) - V(i+1))}{\Delta t} \quad (38)$$

When the 1 g criterion was exceeded,  $V(i+1)$  was flagged as a spike. With a spike detected within the signal, there were numerous options with which to replace the spike value. Two options were assessed: replacement with a running mean and replacement with linear interpolation as represented by the Equations 39 and 40 respectively.

$$U(i+1) = \frac{\sum_{j=1}^i U(j)}{i} \quad (39)$$

$$U(i+1) = \frac{U(i) + U(i+2)}{2} \quad (40)$$

The resulting estimate of the mean flow rates were presented in Table 12. The difference between the two methods was found to have a negligible difference in mean velocity. All but one of the cases had mean velocities that differed by less than 1%.

Although the mean velocities varied insignificantly, the signal itself was different.

Figure 60 shows the filtered signal using the two methods of replacing spikes. It was evident that replacing the spikes with a linear interpolation of the two surrounding points led to a more realistic data set of the flow characteristics. Replacing the spike with the mean flow flattened out the signal because the spikes were forced to the mean value. The interpolation method preserved more of the tendencies expected from a velocity sample. Fluctuations in the local mean velocity were visible in higher detail using interpolation replacement; therefore, it is deemed to be the best method for estimating the true flow.

Table 12: ADV results using two spike replacement methods

Test	Sample Size	Flow [m/s]		Difference [%]
		Mean Replacement	Interpolation Replacement	
1	30000	2.1537	2.1585	0.222
2	14030	2.3840	2.3826	0.059
3	3404	2.4156	2.4122	0.141
4	1173	2.3189	2.3775	2.465
5	4721	2.4040	2.4030	0.042
6	1000	2.0593	2.0630	0.179
7	10000	2.4263	2.4258	0.021
8	50000	2.3493	2.3531	0.161
9	50000	2.3436	2.3491	0.234
10	50000	2.1795	2.1836	0.188
11	46799	2.1113	2.1187	0.349
12	11738	2.2502	2.2490	0.053
13	50000	2.2613	2.2640	0.119



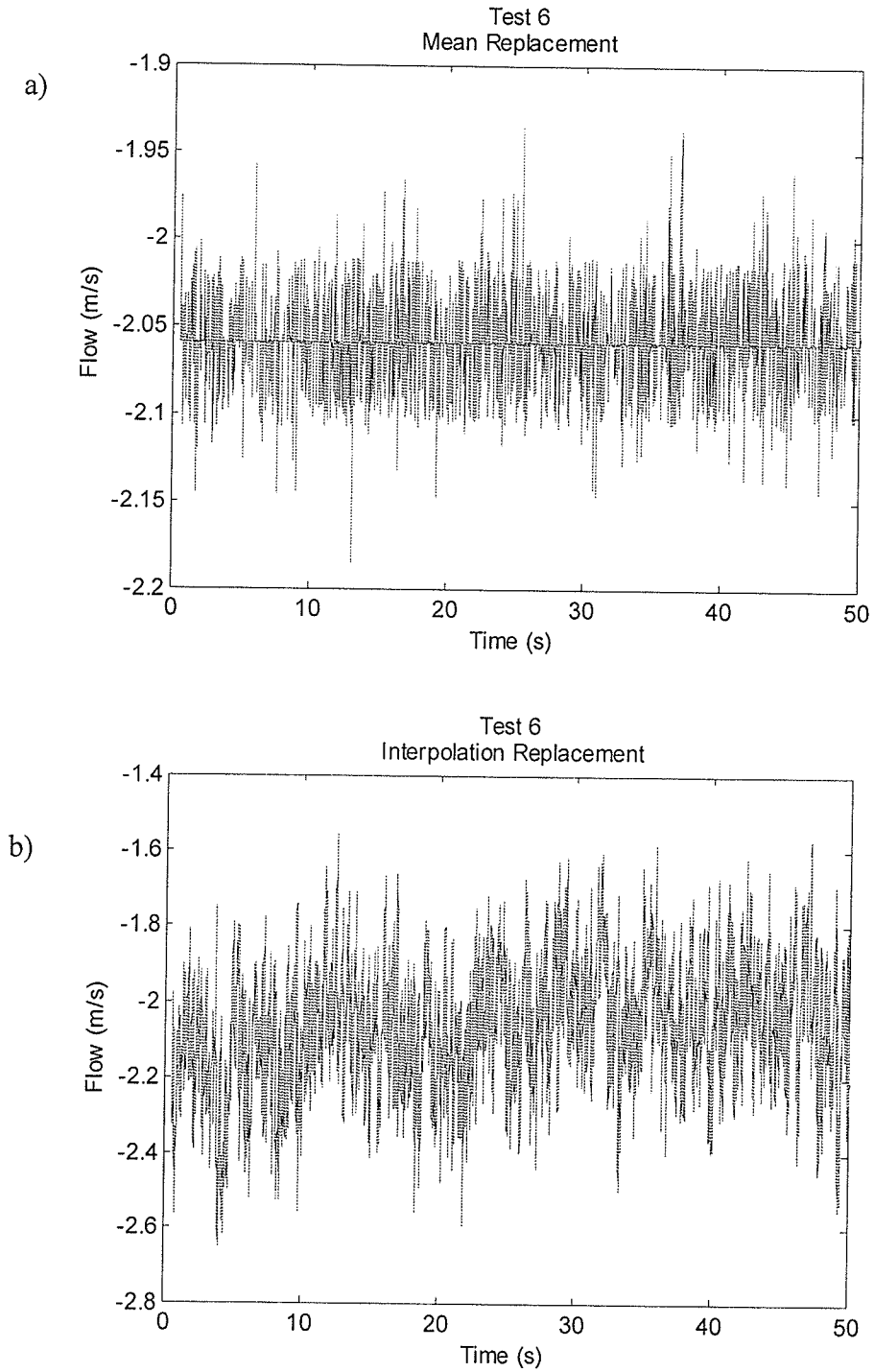


Figure 60: ADV Test 6 signal after a) Mean replacement filtering, and b) Interpolation replacement filtering

## 7.6 ADV field measurements

Table 13 presents the details of all 13 ADV tests that were carried out with the resulting mean flow rate found using the ATM approach.

Table 13: ADV final results

Test	Location	Depth Level	Milk to Water Ratio	Sample Size	Flow (m/s)	Notes
1	1	2	1:0	30000	2.15	
2	2	1	2:1	14030	2.38	
3	2	2	3:2	3404	2.41	Milk nozzle was off center
4	2	2	3:1	1173	2.37	Milk nozzle was off center
5	2	1	2:1	4721	2.40	Milk nozzle was off center
6	2	1	1:1	1000	2.06	
7	2	3	1:1	10000	2.43	
8	2	3	1:1	50000	2.35	
9	2	2	1:1	50000	2.35	
10	2	1	1:1	50000	2.18	
11	1	2	2:1	46799	2.12	Turbine producing 1.2 kWe
12	1	3	2:1	11738	2.25	Turbine @1.2 kWe and then stopped
13	1	3	2:1	50000	2.26	Turbine off

Although there were differences depending on location and depth, the average flow for all tests that day was 2.29 m/s within a range of  $\pm 10\%$ . The river fluctuated throughout the day, hence testing of the 5 kWe system required concurrent power and flow readings to ensure that the most accurate performance data could be produced. The flow data used to calculate turbine performance agreed with the ADV data. Table 14 arranged the results by location and depth for additional insight.

Table 14: ADV results by location and depth

Location	Depth Level	Flow [m/s]	Increase
1	2	2.14	
1	3	2.26	5.51%
2	1	2.26	
2	2	2.38	5.38%
2	3	2.39	0.41%

Location	Depth Level	Flow [m/s]	Reduction
1	2	2.14	10.13%
1	3	2.26	5.56%
2	2	2.38	
2	3	2.39	

The free surface interactions, and the pontoon wake, worked to reduce the flow close to the surface. As the probe sampled at deeper points in the flow, the mean velocity increased. The flow also increased as the ADV measured farther from the turbine. The

rotation of the turbine produced a situation similar to a uniform streamline flow superimposed over a dipole, creating a cylindrical wall. Hence the mean flow rate was reduced close to the turbine due to the cylindrical rotation of the fluid around the rotor. Level 2 had a 10% reduction from location 2 to location 1, and level 3 had a 5% reduction in mean flow.

Another point of interest was how the turbine affected the flow characteristics upstream of the turbine. Test 12 took ADV measurements while the turbine was delivering 1.2 kWe to the grid. Midway through sampling, the turbine was stopped and the flow was allowed to return to its free-stream state between the pontoons. Figure 61 shows a plot of the ATM filtered ADV signal for Test 12.

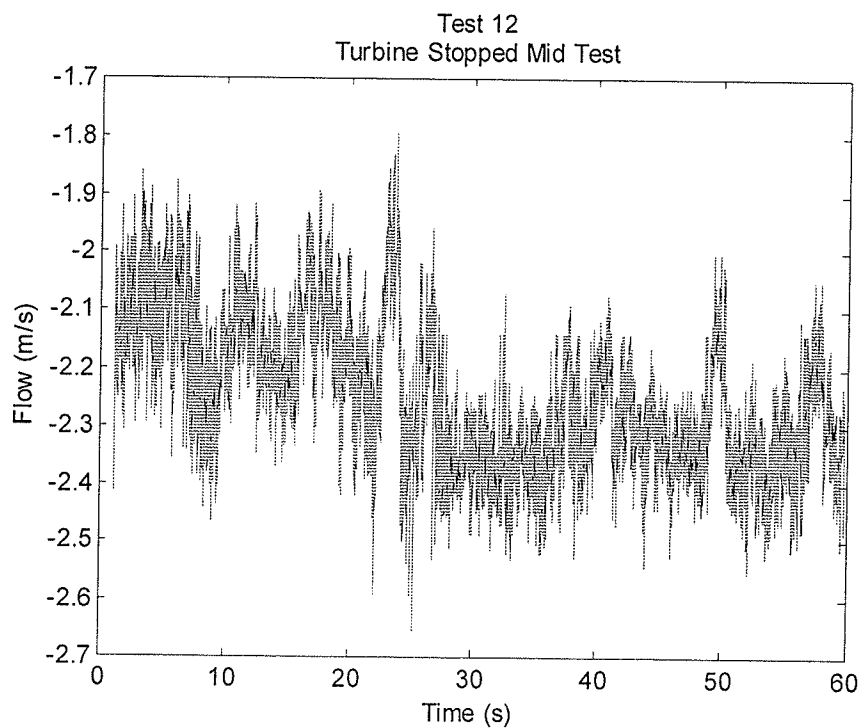


Figure 61: Test 12 ADV data as turbine was stopped

The turbine was stopped close to mid way through the sampling period. The velocity of the water with the turbine had a mean of 2.16 m/s. When the turbine shut off, the cylindrical rotation of the flow obstructing the free stream dissipated, the free stream became uniform, and the mean velocity increased to 2.32 m/s. When the turbine was running, the free stream velocity measured by the ADV reduced by 6.82%.

## Chapter 8

### Turbine Durability

#### 8.1 Overview

To address the issue of operational risks for a kinetic turbine installation, a study was launched into the hazards of floating debris. Floating objects pose a risk for any installation at the surface of the water all year round. Icebergs during winter pose their greatest threat at the end of the season during the spring break up. With the ice cover gone, dead logs, which wash off the shores and into the river, pose yet another risk of impact all summer long. This chapter investigates the frequency of impacts experienced during the summer and comments on the threat of icebergs. During testing in both the winter and summer, the turbine was hit by icebergs and floating logs. Performance of the turbine with pristine blades and impacted blades are presented as well.

#### 8.2 Hazardous floating debris

This section examines the risk of impact from floating debris. This type of hazard included a wide range of objects that could be in the river at any time. The objects of primary concern, and potential danger to an installation of a kinetic turbine, were ice floes and logs. These objects were not easily identified because many objects travel with the flow, from a few inches, up to a few feet, below the water's surface.

Icebergs and ice floes presented the most dangerous scenario because their size and mass can easily dwarf the turbine itself. Although they were easier to identify, they were far more difficult to protect against. Protection designs called for a boom to be placed upstream of the turbine to deflect the ice. This option may hold some benefits, however the difficulty of maintaining the research platform throughout the winter was analogous to what the boom would face. During the winter, much of the ice that had accumulated on the research vessel was chipped free on a regular basis. Each trip to de-ice the research vessel would see a slab of the ice, recently chipped away, being accelerated by the flow and impacting instrumentation and the turbine itself. Although the ice did not have much time to accelerate before impact, the results were devastating for many sensors. The flow meter, for instance, was mounted at the end of a 1-7/8" diameter steel pipe with 1/8" wall. When ice chipped off the front of the research vessel collided with the pipe approximately 10 ft downstream, it was bent by 20 degrees as seen in Figure 62.

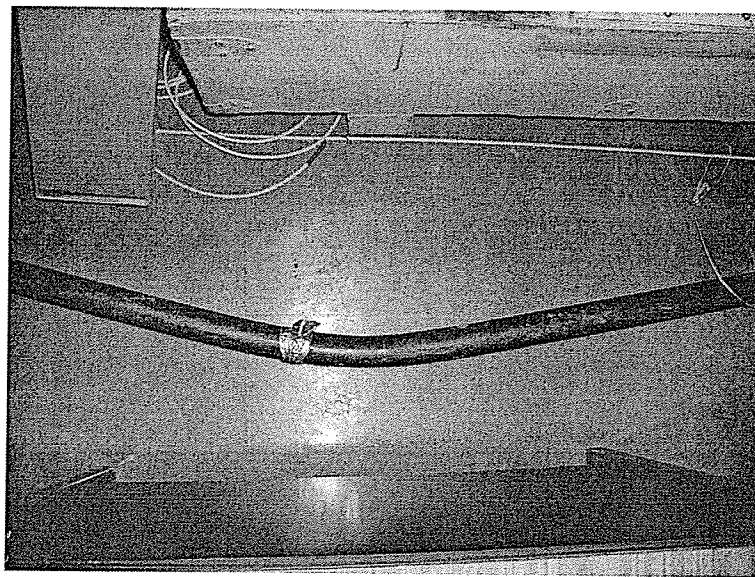


Figure 62: Pipe holding the flow meter after iceberg impact

The minimum force required to bend that pipe was calculated, indicating that the iceberg measuring roughly 8 ft x 3 ft x 1 ft impacted this pole with at least 5089 lbs force. For this demonstration of the 5 kWe NECI turbine, the unit was removed before spring break up since the risk to the research vessel and turbine was too great.

Floating debris, typically logs, are numerous outside of the winter months. During the winter, the upstream inlet to the Pointe du Bois test site is frozen over, preventing any floating debris from making its way down the river. The trash racks at the power dam, which operated just downstream of this installation, gave clear indication as to the debris that flows in the Winnipeg River.

Besides man-made garbage, such as crates, foam insulation, 2 x 4's, etc, the debris consisted of logs. Logs of many different sizes were found, most being logs cut down by beavers. There were tree stumps, tree trunks, and branches, indicating that natural cycles of forestry inject debris into the flow. There were logs as small as a foot with diameters of mere inches to logs ten feet tall and 8 inches in diameter found in the trash racks and even wedged between the arms of the turbine itself. Figure 63 shows a picture of one such log removed from the 5 kWe unit placed behind the 25 kWe turbine (not shown). To assess the risk these objects pose, an investigation into the frequency of impacts was conducted within the scope of this thesis. This analysis was carried out during July and August of 2008, which serves as an adequate cross-section of the summer months. Debris was present within the flow throughout the months when there was no ice cover upstream. Typically, this timeframe encompasses 7 months of the year from May until



November in Manitoba; thus, the results of the 2 month survey were used to extrapolate probabilities for the 7 months.

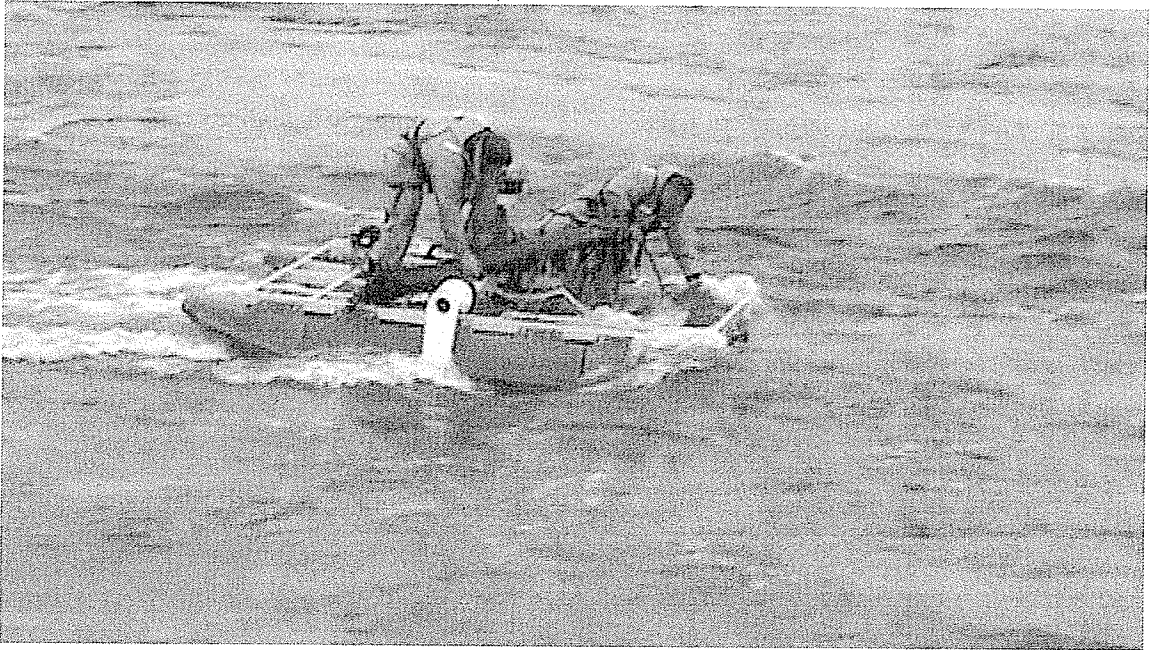


Figure 63: Log jam being cleared

This investigation was performed after the 5 kWe unit was removed from the research platform and exchanged with the larger 25 kWe unit. The 5 kWe unit was then mounted onto a tailor-made platform, also shown in Figure 63. This was the first trial of the platform that was designed for the 5 kWe commercial unit. The platform was tied to the back of the research vessel and sat 40 feet downstream. Impacts on this unit caused much lower vibration readings, while direct hits to either pontoon recorded much larger readings. The vibration data was analyzed qualitatively. When sampled, the sensor gave an RMS reading of the vibrations between samples. The data taker logged only the maximum reading logged for each minute. The result was clear to assess. Figure 64

shows a graph of August 14, 2008 when three different magnitude impacts were recorded. People were working on-site that day and their work caused minor disturbances between the times of 10:00 and 14:00. These peaks were not recorded as impacts; however, the three impacts which were recorded as impact events are the spikes at 01:00, 13:00, and 15:00. The spike at 13:00 was a result of removing debris on the front anchor line, which floated downstream hitting the 25 kWe unit and finally became jammed in the 5 kWe rotor.

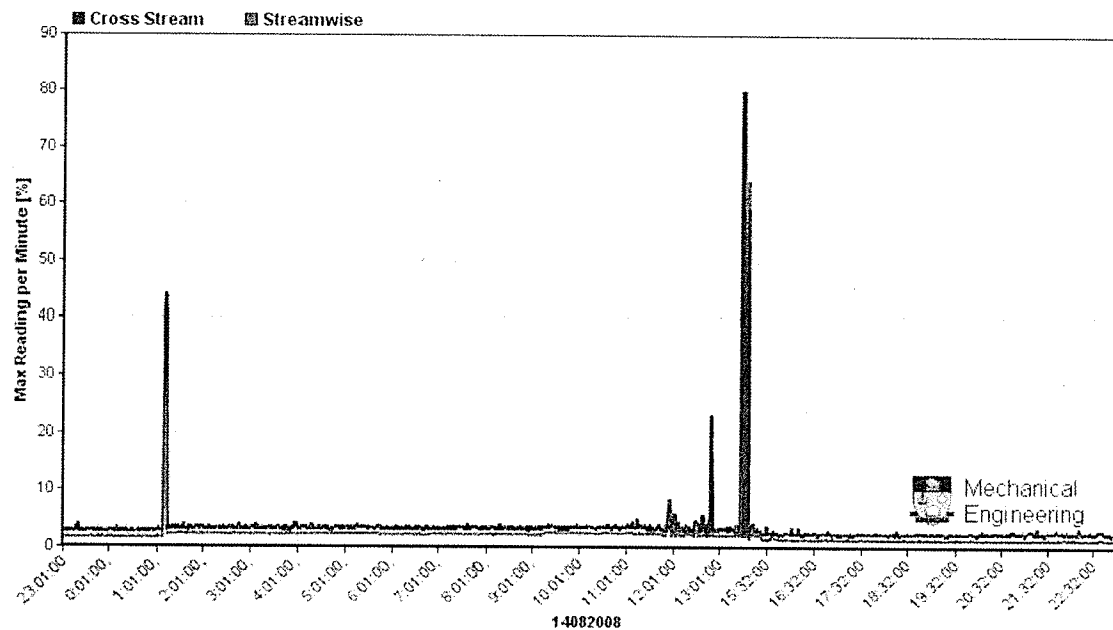


Figure 64: Peaks in the vibration data indicating an impact

To classify the impacts, no quantitative means were available to calibrate impact strength. Therefore, magnitudes were qualitatively separated into minor, small, medium, and large impacts. They corresponded to vibration peaks of less than 10%, 10% to 30%, 30% to 50% and over 50%, respectively. The results of the analysis are presented in Table 15.

For the 71,207 minutes that were recorded over the two months, 38 spikes were tallied in the data. Small impacts were most frequent with 23 occurrences while only 2 large impacts were observed. More important than the quantity would be the mean time between impacts to quantify the frequency of these events. Minor impacts occurred within a mean time of 148.35 hours. Small and medium impacts struck with a mean time of 51.60 and 237.36 hours respectively. The least common and most violent impacts frequent every 593.39 hours.

Table 15: Assessment of the risk of impact

Type of Impacts	Number of Impacts	Mean Time [hours]
minor	8	148.35
small	23	51.60
medium	5	237.36
large	2	593.39

Extrapolating to encompass the entire open flow season for one year, assuming that the mean time between impacts stays constant, it was estimated that 34 minor, 99 small, 22 medium and 9 large impacts could occur. The minor and small impacts were of least concern because they were most likely to be either light brushes along the pontoon sides or small objects that were deflected or impacted, and passed through the rotor. The medium and large impacts were of more importance because they were large objects that

hit the rotor and/or pontoons directly. These objects were more likely to be lodged into the turbine and damaging it.

### **8.3 Effect on performance**

After multiple impacts during research vessel de-icing in the winter, the 5 kWe unit was removed in the spring. The turbine was removed, placed on the deck of the research platform and moored to shore. Before removing the research vessel, the turbine was producing 500 W when running with a TSR of 2.27 in a flow of 2.02 m/s. Using the blades that endured the punishment of winter impacts, the turbine operated at 10.4% efficiency. The low efficiency was due to the support arms because they were the flat bars. The toll of the impacting icebergs was observed. The trailing edge of each hydrofoil was no longer crisp, sharp, or straight. The tips of the foils were dented and one hydrofoil was slightly bowed. The observations were photographed and are presented in Figure 65. The hydrofoils were then swapped out for a new set. When the flat bar support arms were tested in 2.35 m/s flow, the turbine ran with a TSR of 2.03 and produced 727 W. Although it performed at only 9.6% efficiency, the difference of 0.8% was within a reasonable range since the TSR differed.

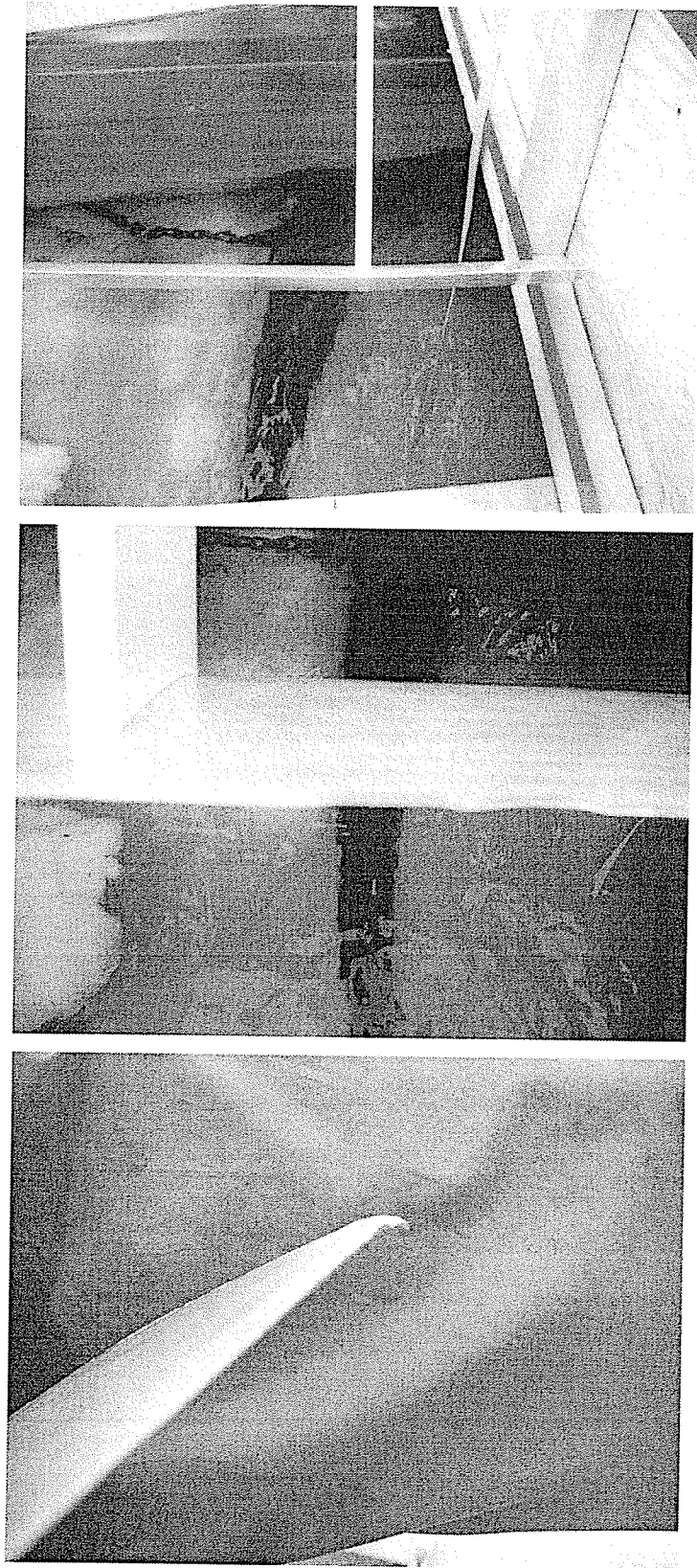


Figure 65: Turbine blades after winter testing

## 8.4 Conclusions

Impact from floating debris is a year-round threat to a water surface installation. Over the course of testing, the vertical axis design had proven itself to be durable in this environment. The rotation of the blades helped reduce the impact on the major components as it pushed the debris around it rather than absorb the brunt of the impact. When comparing pristine rotor blades with ones that have been impacted several times by objects of varying magnitude, the performance variation was found to be minimal.

## Chapter 9

### Conclusions and Recommendations

#### 9.1 Conclusions

The 5 kWe vertical axis turbine performed well during the year at Pointe du Bois. Peaking with rotor efficiencies over 35% and delivering power with consistency for days, this technology proves itself to be versatile and most likely competitive. With minimal cost infrastructure, a research vessel was launched into a fast flowing river location where it produced clean, renewable power. The advantages of this unit were numerous. Its ability to deflect impacts and continue to produce consistent power proved its durability and reliability. Hydrofoil support arms performed the best because they contributed the least amount of drag to the rotor's dynamics. With these support arms, the turbine was able to self start in a flow of over 2 m/s, contrary to some literature, which listed the Darrieus as unable to self-start.

The turbine performed well during the winter as long as it was not frozen in. Flat bar support arm test showed that the power output was consistent from winter to summer, even with slightly dented and lightly bowed hydrofoil blades. The cold climate did not affect power production as long as the free stream and turbine remained unobstructed by ice cover. Ice was a major concern for northern operations. During the coldest days of the winter of 2008, the entire research vessel would be encased in ice within a week's

time. This situation proved itself to be dangerous to the equipment, so ice was cleared on a regular basis. The research vessel was removed for spring break up of the ice sheets because it had been seen that ice floes could impact the unit with catastrophic results. There was potential for impact all year round with ice in the winter and logs in the summer.

This technology has proven potential to extract the gigawatts of power that flow through rivers. There have been numerous sites identified and many more yet to be found where the kinetic turbine would be used for power extraction. Faure *et al.* (1986) outlined that one of the best applications for this technology was in the river where deployment could be made easily and cost effectively with mooring lines and/or bridges. Since the size of the rotors would be limited to the range of tens or hundreds of kWe by the river cross-section, these locations could accommodate an array of small turbines contributing to a sizable amount of total power extraction.

## 9.2 Recommendations

Kinetic turbine technology has potential to provide reliable and consistent power in remote locations. Minimal construction was necessary to anchor and deploy a turbine at the river's surface. Locating the turbine at the surface reduced installation and maintenance costs. To maximize output, a ducted design would be optimal. By reshaping the flow, the local velocity through the rotor is increased. This option was thoroughly examined and optimized but it increases overall project cost and complexity. A low cost approach was to design contoured pontoons that created a duct for the flow



into the turbine. With this option, construction costs of a shaped, hollow, aluminum pontoon would be far less costly than any concrete form. This alternative, however, is primarily viable for kinetic turbine installations at the water's surface.

Having the generator at the surface was a great advantage for the vertical axis turbine; however, having any power extraction device at the free surface would not fare well in the winter unless ice-resistant materials or other ice mitigation design features were incorporated. It would not be viable to operate this technology with the upkeep of de-icing the unit throughout the winter. If the icing issue could be avoided entirely, this technology would work well in controlled environments all year round; locations such as sewage and water treatment plants or any other industrial location where water flows on a large enough scale would work well. For this technology to prosper in the field for a year-round installation, it is recommended that any power extraction unit be fully submerged, well below the free surface and above the boundary layer of the river bed; however, this increases costs, complexity, maintainability, and may affect operational reliability.

An alternative to the submerged turbine would be to design impact safeguards and ice breaking devices. Automated hydraulic jacks would break ice once it forms to a significant size. Ice-phobic materials would eliminate the issue of ice formation entirely. This solution would raise costs but not overall project complexity or maintainability. The addition of a trash rack would deflect all sizable objects which could endanger a kinetic turbine of any scale.

Further study is required into many issues such as the long term effects of frequent impacts on the rotor, mooring lines, the vessel itself, the output of turbine arrays, ice mitigation designs, and submersible solutions.

### **9.3 Contributions**

The majority of the work described in this thesis was done in collaboration with others. Assembly of the unit, deployment, grid connection, and support arm testing was performed New Energy Corporation and students from the University of Manitoba working with this project under the supervision of Dr. Eric Bibeau. John Woods played an integral role on this project with his work on anchoring, deployment, de-icing of the research vessel, testing of the turbine and ADV, and analysis and understanding of electrical data.

This author's independent contribution to this research was primarily in the data acquisition system and numerical analyses. Configuring, testing and maintaining of the DAQ hardware and software were major components of this project. The modeling of power loss due to support arms, filtering of the ADV signal, and the impact frequency analysis were all independent studies.

---

## References

- Antheaume, S., Maître, T., and Achard, J. (2008), "Hydraulic Darrieus Turbines Efficiency for Free Fluid Flow Conditions Versus Power Farms Conditions," *Renewable Energy* Vol. 33, pp. 2186–2198.
- Arden, R.S. and Wigle, T.E. (1972), "Dynamics of Ice Formation in the Upper Niagara River," *Proc., The Role of Snow and Ice in Hydro.* Banff, Alberta, Canada.
- Aston, G.D. (1986), "River and Lake Ice Engineering," *Water Resources Publications.* Littleton, Colorado, USA.
- Bahaj, A.S., Batten, W.M.J., McCann, G. (2007), "Experimental Verifications of Numerical Predictions for the Hydrodynamic Performance of Horizontal Axis Marine Current Turbines," *Renewable Energy*, Vol. 32, pp. 2479–2490.
- Bahaj, A.S. and Myers, L.E. (2006), "Power Output Performance Characteristics of a Horizontal Axis Marine Current Turbine," *Renewable Energy* Vol. 31, pp. 197–208.
- Bahaj, A.S. and Myers, L.E. (2003), "Fundamentals Applicable to the Utilization of Marine Current Turbines for Energy Production," *Renewable Energy* Vol. 28, pp. 2205–2211.

- Batten, W.M.J., Bahaj, A.S., Molland, A.F., Chaplin, J.R. (2008), "The Prediction of Hydrodynamics of Marine Current Turbines," *Renewable Energy* Vol. 33, pp. 1085–1096.
- Batten, W.M.J., Bahaj, A.S., Molland, A.F., Chaplin, J.R. (2006), "Hydrodynamics of Marine Current Turbines," *Renewable Energy* Vol. 31, pp. 249–256.
- Bergander, B.B. (1988), "Small Scale Hydro Power in Cold Climates," *Waterpower '87: Proc., International Conference on Hydropower*. Portland, Oregon, USA, pp. 1210–1217.
- Bibeau E.L., Kassam S., Woods J., Vauthier P., Molinski T. and Golé A. M. (2007), "Design of in-situ river kinetic turbines in cold weather," *CDEN/C2E2 2007 Conference*. Winnipeg, Manitoba, Canada.
- Blais, J. (2006), "Cold Weather Wind Turbine Generation Curtailment Study" Presentation Slides from the CanWEA Conference. Winnipeg, Manitoba, Canada.
- Blevins, R. (2003), "Applied Fluid Dynamics Handbook," Krieger Publishing. Malabar, Florida, USA.

- Clark, S and Doering, J. (2008), "Experimental Investigation of the Effects of Turbulence Intensity on Frazil Ice Characteristics," *Canadian Journal of Civil Engineering*, Vol. 35, pp. 67–79.
- Cornett, A. (2006), "Inventory of Canada's Marine Renewable Energy Sources," National Research Council – Canadian Hydraulic Centre. CHC-TR-041.
- Daly, S.F. and Ettema, R. (2006), "Frazil Ice Blockage of Water Intakes in the Great Lakes," *Journal of Hydraulic Engineering* Vol. 132 Issue 8, pp. 814–824.
- Daly, S.F. (1987), "Frazil Ice in Rivers and Streams," *The Northern Engineer* Vol. 19 No. 3, pp. 19–25.
- Doering, J.C., Bekeris, L.E., Morris, M.P., Dow, K.E., and Girling, W.C. (2001), "Laboratory Study of Anchor Ice Growth," *Journal of Cold Regions Engineering*. March 2001.
- Faure, T.D., Pratte, B.D., and Swan, D. (1986), "Darrieus Hydraulic Turbine–Model and Field Experiments," *Fourth International Symposium on Hydro Powered Fluid Machinery*. Anaheim, California, USA, pp. 123–129.

- Fonseca, F. and Roberts, S. (1987), "Frazil Ice Observations at Rivière-des-Prairies Power Plant," CEA/EPRI/HQ Hydro Operations and Maintenance: Winter Operation - Ice Problems Workshop. Montreal, Quebec, Canada.
- Gaden, D. and Bibeau, E.L. (2008), "Velocity Profile Enhancements Using an Anchoring System," Submitted to the Journal of Renewable Energy.
- Gaden, D. (2007), "An Investigation of River Kinetic Turbines: Performance Enhancements, Turbine Modeling Techniques, and an Assessment of Turbulence Models," M.Sc Thesis, University of Manitoba.
- Gemperline, E.J. (1991), "Frazil Ice Problems and Solutions at Hydro-Power Intakes," Waterpower '91: Proc., International Conference on Hydropower. Denver, Colorado, USA, pp. 1744-1753.
- Gilbert, B.L. and Foreman, K.M. (1983), "Experiments with a diffuser-augmented model wind turbine," J. Energy Resources Technology, Trans ASME Vol.105, pp. 46-53.
- Goring, D.G. and Nikora, V.I. (2002), "Despiking Acoustic Doppler Velocimeter Data," Journal of Hydraulic Engineering Vol. 128 Issue 1, pp. 117-126.

- HATCH Energy (2008), "Natural Resource Canada - Low Head Hydro Market Assessment," Report for Natural Resource Canada, HATCH Energy. March 2008.
- Khan, M.J., Iqbal, M.T., and Quaicoe, J.E. (2008), "River Current Energy Conversion Systems: Progress, Prospects, and Challenges," *Renewable and Sustainable Energy Reviews* Vol. 12, pp. 2177–2193.
- Kiho S, Shiono M, Suzuki K. (1996), "The Power Generation from Tidal Currents by Darrieus Turbines," *Proc. of the world renewable energy congress* Vol. 2. Denver, Colorado, USA. pp. 1242–1245.
- Kirke, B. (2003), "Developments in Ducted Water Current Turbines," University of South Australia, Mawson Lakes, Australia. Online resource available at [www.cyberiad.net](http://www.cyberiad.net). Date accessed: 02/25/2009.
- Martin, S. (1981), "Frazil Ice in Rivers and Oceans," *Annual Review of Fluid Mechanics* Vol. 13, pp. 379–397.
- Mori, N., Suzuki, T., Kakuno, S. (2007), "Noise of Acoustic Doppler Velocimeter in Bubbly Flows," *Journal of Engineering Mechanics* Vol. 133 Issue 1, pp. 122–125.
- Ponta, F.L., and Jacovkis, P.M. (2008), "Marine Current Power Generation by Diffuser-Augmented Floating Hydro-Turbines," *Renewable Energy* Vol. 33, pp. 665–673.

- Qu, Y.X., and Doering, J. (2007), "Laboratory Study on Anchor Ice Evolution Around Rocks on Gravel Beds," *Canadian Journal of Civil Engineering* Vol. 34, pp. 46–55.
- Radkey, R.L. and Hibbs, B.D. (1981), "Definition of Cost Effective River Turbine Designs," Technical Report AV-FR-81/595 (DE82010972), Report for The Department of Energy, Aerovironment Inc., December 1981.
- Riegler, G. (1983), "Principles of energy extraction from a free stream by means of wind turbines," *Wind Engineering* Vol.7 Issue 2, pp. 115–126.
- Richards, S.D., Heathershaw, A.D., and Thorne, P.D. (1996), "The Effect of Suspended Particulate Matter on Sound Attenuation in Sea Water," *Journal of the Acoustical Society of America* Vol. 100 Issue 3, pp. 1447–1450.
- Terada, K., Hirayama, K., and Sasamoto, M. (1998), "Field Measurement of Anchor Ice," Proc., 14<sup>th</sup> IAHR Symposium on Ice, pp. 697–702.



---

## Appendix A

### DAQ Start-Up Sequence

There were four main components to the data acquisition system: the power analyzer, data taker, Digipro video software, and Perl scripts. They each functioned in unison but required independent start-up regiments. Data could be logged locally using only the boat computer or it could be combined with the ATCO computer to utilize the alarm, analysis, graphing, and web posting functions.

#### A1.1 Boat computer operation

The boat computer was operated as follows:

1. Start up the boat computer and log into the 'Kinetic Turbine' user account, password 'pdb'. There were three scheduled tasks that the computer ran on predefined timed intervals. These tasks include deload, Power Copy, and Power Copy Day.
2. To find these tasks go to Start→All Programs→Accessories→System Tools→Scheduled Tasks. Figure A-1 shows the tasks on screen.
3. Ensure that all three are active. Unless previously disabled, they should remain active upon reboot.

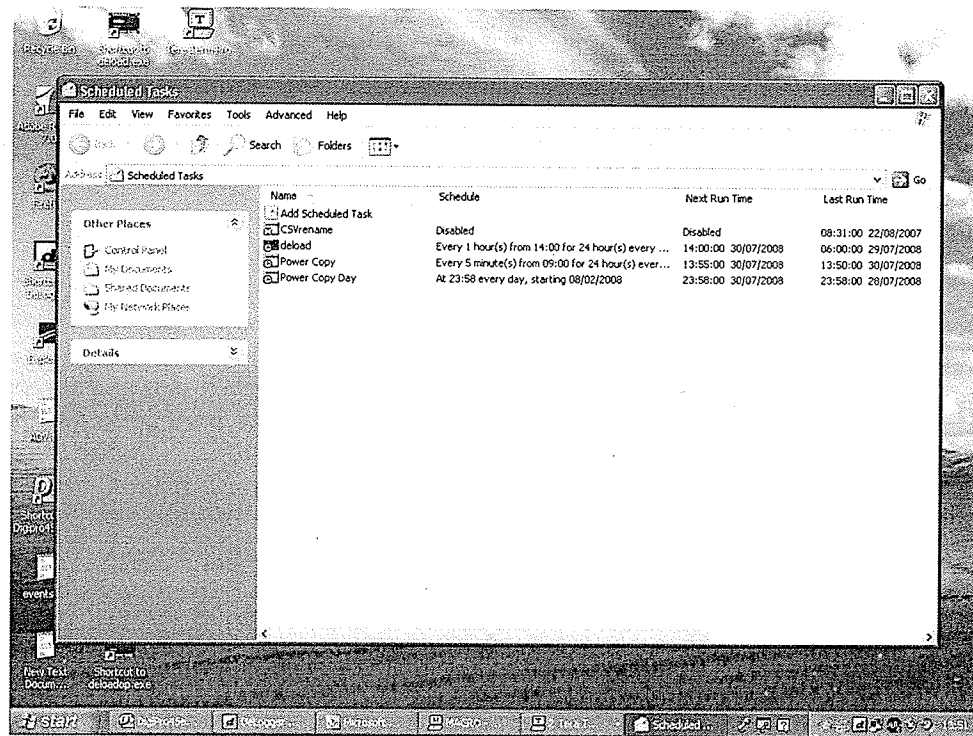


Figure A-1: Scheduled tasks

4. Start up the video software: Digipro Server. This was the only software that cannot be activated or manipulated remotely. Any attempt to access this program using remote desktop results in its failure and termination.
5. To start this program, double click on the Digipro Server icon. Once on, it will run as usual. With a 200 GB hard drive dedicated to video storage, the hard drive can hold up to 2 weeks of video before it deletes the oldest records.
6. Once initialized from the boat computer, minimize the program so that remote desktop to the boat computer can function normally.

With video running and the scheduled tasks active, the rest of the data logging systems may be initiated.

## A1.2 Power analyzer operation

The 930-A power analyzer operates as follows:

1. To start logging the power parameters, turn on the 930-A power analyzer.
2. Initiate the correct settings via the 930-A input panel. This cannot be done remotely. Figure A-1 shows the layout of the interface. Once the power analyzer is set up to display the desired data, the rest of the data logging set up can be done remotely.

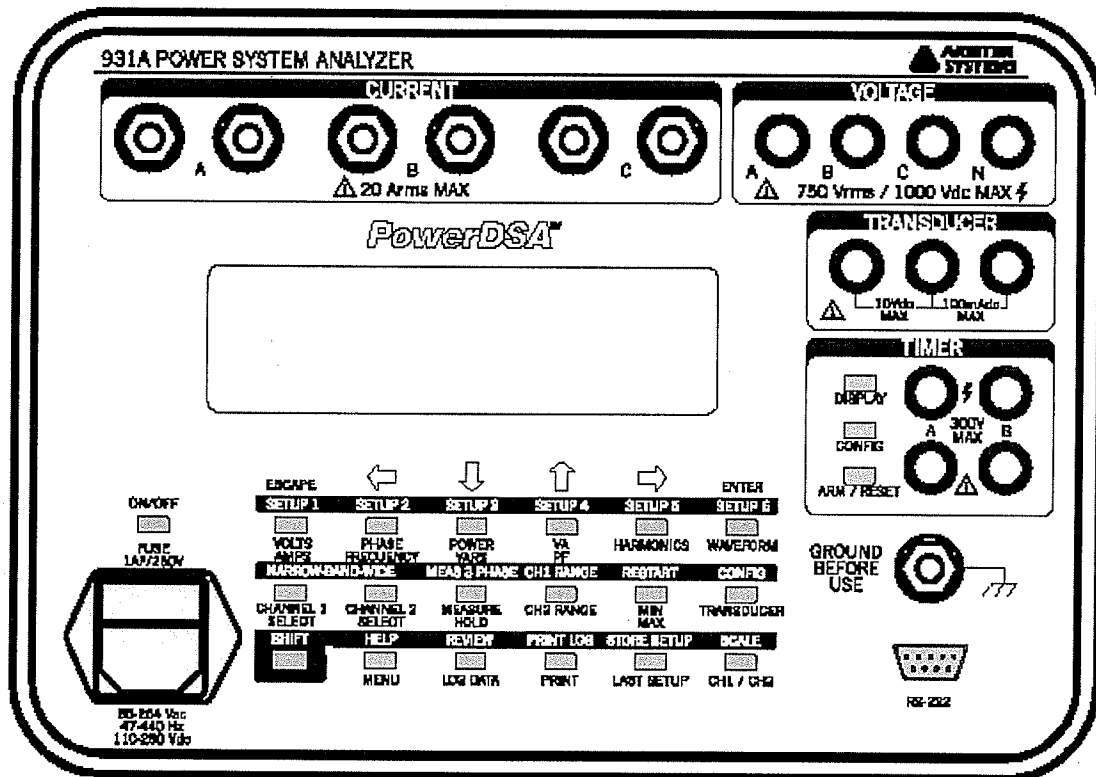


Figure A-2: Power analyzer input panel

3. Set the meter to measure 3-phase power.

4. To access the 3-phase menu, press SHIFT and the MEAS 3 PHASE button. The screen in Figure A-3 will be displayed.

```

3 PHASE MEASUREMENT SELECTION
+1Ph 3W 2E: (Split; VanIa, VcnIc)
3Ph 3W 2E: (UabIa, UcbIc, 'Uac, Ib')
3Ph 3W 3E: (UasIa, UbsIb, UcsIc)
3Ph 4W 3E: (VanIa, UbnIb, VcnIc)
3Ph 4W 2.5E: (VanIa, 'Ub' Ib, VcnIc)
              (connect Ub to Un)

```

Figure A-3: Power analyzer display screen for 3-measurement set up

5. If this display does not appear, press the ESCAPE key (do not press SHIFT first).  
If it still does not display, continue to press ESCAPE and then try the sequence again.
6. Using the top arrow keys, scroll down to the desired wiring set up and hit ENTER. The 3Ph 3W 3E, tabular with power will give a phase to neutral reading for the voltage. For more information on the settings please refer to the 930-A manual. Note that the 930-A and 931-A manuals are identical. When successfully activated, the 3 phase data will appear on the screen as shown in FigureA-4. This setting was saved as SETUP3, so pressing SHIFT -> CONFIG -> SETUP3 will also bring up these settings.

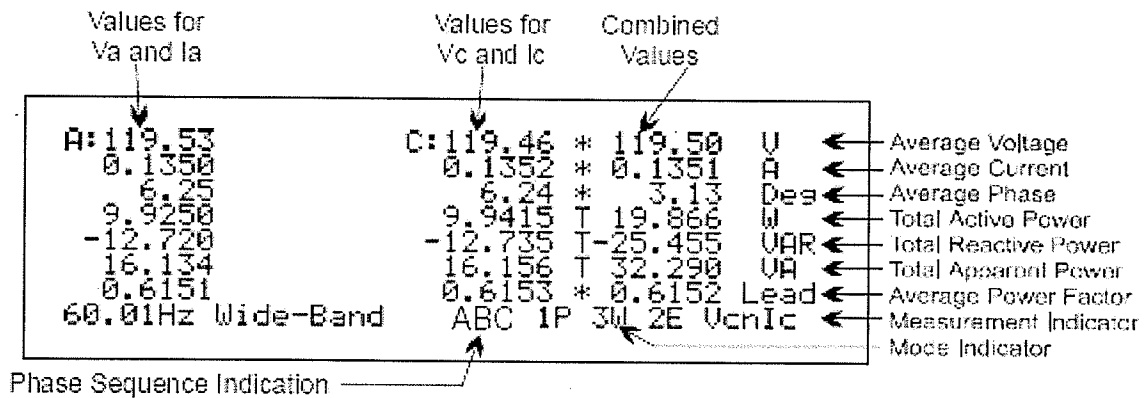


Figure A-4: Display when measuring 3-phase power

It may take a few seconds for the screen to fill with numbers and they should update every 10 seconds. At this point the data is only displayed, it is not being logged.

7. To log the power data use a program called Tera Ter. A macro for this program was created to connect and start the logging process. This macro is called Connect.ttl and is located on the boat desktop and under the data drive in the DT800/Data subfolder. NOTE: this software must be started in sync with the computer clock.
8. Initialize the Connect.ttl macro by double clicking the file. Start this program a few seconds after any 5 minute interval, so start it at 5:05:02 or 10:25:04. The program will display 3 windows and all three must be active or the data will not be logged. One of the windows shows the terminal that displays the raw data coming from the power analyzer. Figure A-5 shows the data as displayed by the Tera Term terminal. The data is so large that it wraps around when the screen is filled. This poses a problem for post processing because the data is written as

viewed in this terminal. If left as is, a single line of data will be recorded over 4 or 5 lines in the log file.

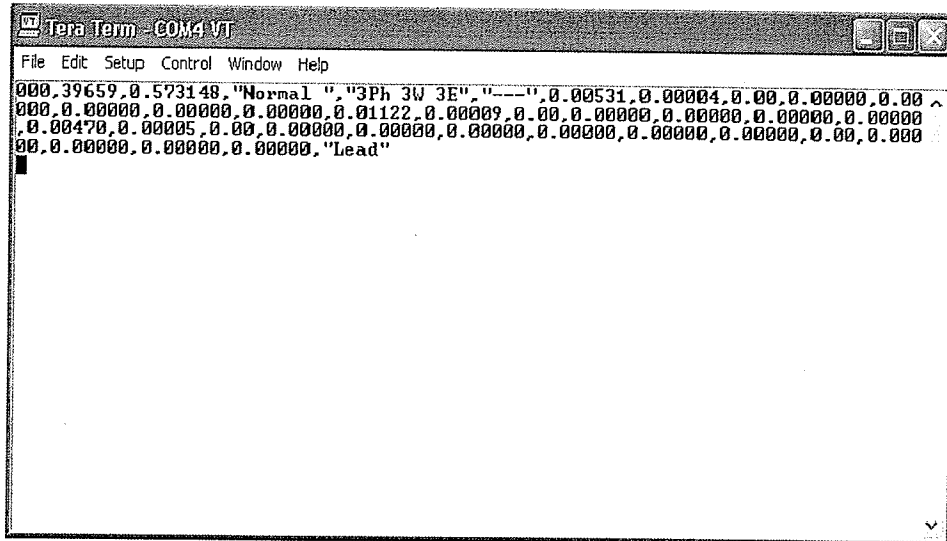


Figure A-5: Tera Term data display window

9. To put all of the data for one time onto one line, increase the size of the terminal. Go to Setup→Terminal and change the first dimension so that it is large enough to accommodate all of the characters being logged. The width of the window size is adjusted in the terminal setup as seen in Figure A-6. A size of 300 will work fine. When done correctly, the data will output one string per line as shown in Figure A-7

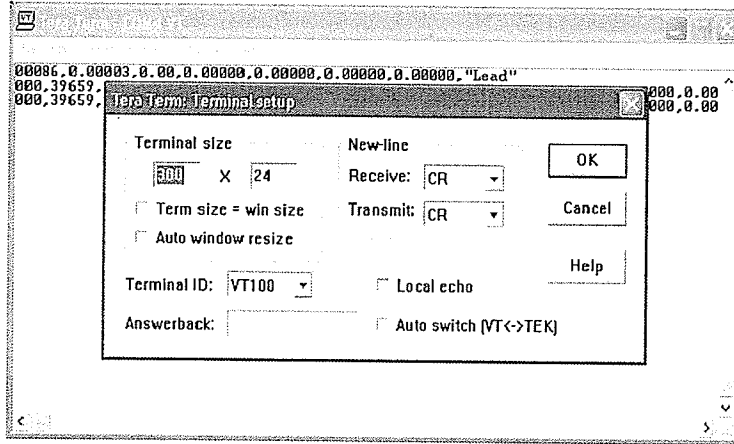


Figure A-6: Tera Term terminal setup

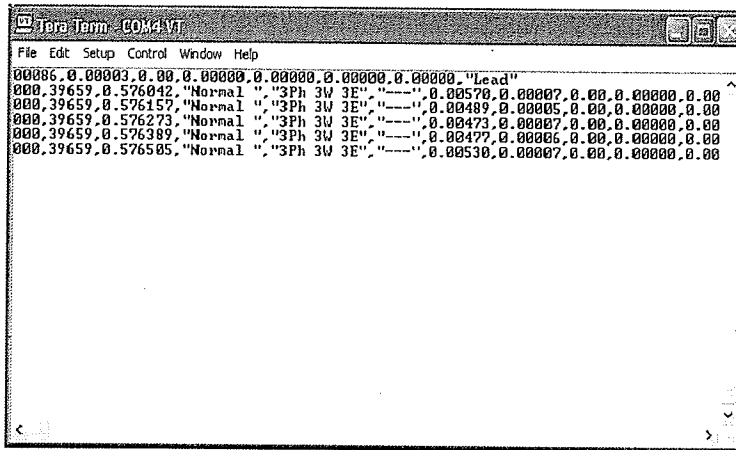


Figure A-7: Tera Term window of adequate width

### A1.3 Data taker operation

Operate the data taker as follows:

The data taker emits a clicking sound when it is actively logging data.

1. To view the data, the software program DeLogger is used.
2. If there is no sound coming from the DT85, then restart it through the DeLogger software.

3. Open the program; it can be found on the boat desktop.
4. Use the connections tab to connect to “DT&x Com1”. The software will search for the correct baud rate but it may not find the data taker on the first try. It usually connects on the second successive attempt.
5. Try repeatedly until connected. There is a message window at the bottom of the DeLogger screen (Figure A–8) that will indicate if you are connected. Just above the message window, where all of the commands are displayed, there is a task bar with several tabs. The tab “Prog1.d80” is the tab in which all of the sensors are assigned to a channel. The first tab, “Form1.dlf” is where the real time results are displayed.

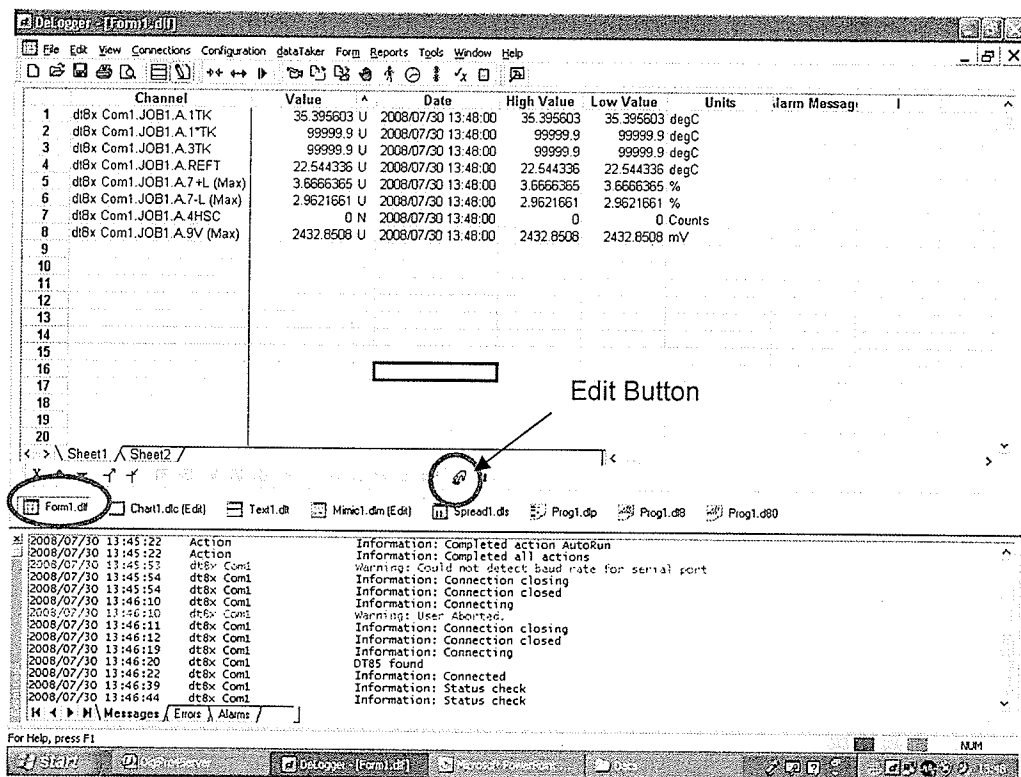


Figure A–8: DeLogger screen



6. Click on this tab to view the readings.
7. To start the data logging process, click on the green jogging icon next to the red hand icon (stop). A pop up window will give you further options to start specific jobs.
8. Start all jobs and the DT85 should begin logging data and emitting clicking noises as it samples.

The program used for this project logs data every minute. Each minute the values in the display above will be updated with the most recent data set logged. If the values do not change, it may be in edit mode.

9. Click the edit button shown in Figure A–8 to enter and exit the edit mode.
10. In edit mode add the desired channels to display; however, you cannot see the real time data unless you exit from edit mode.
11. Once the data taker has been activated, disconnect it from the DT85. The DeLoad software cannot access the data on the DT85 unless it is free of other connections. You can run the DeLoad at any time by double clicking the executable icon on the desktop. It will run automatically every hour as per the scheduled task. The unloaded data is stored under boat computer's data drive, under the DT85 subfolder.

## A1.4 ATCO computer operation

On the ATCO computer, the Scanfile software is the only program that must be running to post the data online and to have the email alarm system in place. Without this program running, the data will still be logged on the boat computer, but no data will be analyzed, posted online, or backed up onto the ATCO computer.

1. To start this script, locate the file under the C:\ drive of the ATCO computer.
2. Locate the most recent version (the highest sequence of numbers) and activate it.
3. The script is in a .txt format and must be opened with the Perl Command Line Interpreter.
4. Right mouse click on the file and select "Open with". This will bring up a new list of programs,
5. Choose the Perl Command Line Interpreter. A small, black window will appear. This is the program running. It runs on an infinite loop, therefore minimize the window and allow it to run continuously.

The DAQ system should now be up and running independently. Within an hour, graphed data for the recent data will appear online. The graphs that appear online are also saved on the ATCO computer's C:\ drive. Back up copies of the power and sensor data will also be found on the ATCO computer.

# Appendix B

## Sensor Specifications

### B1 Load cell

#### B1.1 4-wire

# Honeywell

Honeywell  
Sensotec Sensors  
2080 Arlinggate Lane  
Columbus, Ohio 43228 U.S.A.

Phone: 614-850-5000  
Fax: 614-850-1111  
URL: <http://www.sensotec.com>  
E-mail: [service@sensotec.com](mailto:service@sensotec.com)

## Certificate of Calibration

### Product Identification

Product Type: Load Cell  
Serial Number: 1136592

Model: RGF  
Part Number: 060-K853-01-01  
Order Code: AL428EP,6I 50FT.

### Product Specifications

Full Scale Range: 50000 lbs  
Calibrated At: 50000 lbs  
Tension

Excitation: 10 VDC  
Input Impedance: 703  $\Omega$   
Output Impedance: 703  $\Omega$   
Electrical Leakage: 8 Meg $\Omega$

### Calibration Data

Calibration Factor: 1.3694 mV/V

Shunt Cal Factor: 0.8770 mV/V  
Shunt Cal Resistor: 200k $\Omega$

### Wiring Code

UNAMP#3,4-COND,CBL,SMS

COLOR	DESIGNATION
RED	(+)EXCITATION
BROWN	(-)EXCITATION
YELLOW	(-)OUTPUT
ORANGE	(+)OUTPUT

001-0333-03

### Certification Information

Type of Calibration: Standard  
Calibration Date: 09/14/2006

Certificate Number: 086-0000-00  
Calibration Procedure: 072-LC75-10

## B1.2 3-wire

**Honeywell**

Honeywell  
 Sensotec Sensors  
 2080 Arlingate Lane  
 Columbus, Ohio 43228 U.S.A.

Phone: 614-850-5000  
 Fax: 614-850-1111  
 URL: <http://www.sensotec.com>  
 E-mail: [service@sensotec.com](mailto:service@sensotec.com)

**Certificate of Calibration****Product Identification**

Product Type: Load Cell  
 Serial Number: 1136593

Model: RGF  
 Part Number: 060-K854-01-01  
 Order Code: AL42SEP.2K.61 50FT.

**Product Specifications**

Full Scale Range: 50000 lbs  
 Calibrated At: 50000 lbs  
 Tension

Supply: 15-40 VDC  
 Output: 4-20 mA  
 Electrical Leakage: 8 Meg $\Omega$

**Calibration Data**

Calibration Factor: 15.9873 mA

**Wiring Code**

AMP(NS),3-COND,CBL,GND,SMS

COLOR	DESIGNATION
RED	(+)SUPPLY
BROWN	(+)OUTPUT
ORANGE	CASE GROUND

001-0962 01

**Certification Information**

Type of Calibration: Standard  
 Calibration Date: 09/12/2006





Certificate Number: 086-0000-00  
 Calibration Procedure: 072-LC75-10

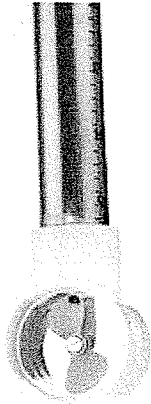
## B2 Vibration sensors

### Technical Specification

Output Current	4-20mA DC proportional to RMS velocity (mm/s)
Velocity Range	See table below
Frequency Response	2 Hz to 1 kHz $\pm 10\%$
Dynamic Range	50 g peak
Mounted Resonance	5 kHz min
Isolation	Base isolated
Operating Temp Range	-25 to 90 °C
Temperature Sensitivity	0.08 %/°C
Transverse Sensitivity	Less than 5%
Supply Voltage Range	12-32 Volts DC (4-20mA)
Case Material	Stainless steel
Weight	140 gms (nominal)
Sealing	IP67
Mounting Torque	8 Nm
Mating Connector	MTN/MH008
Options	Ranges, filters, mounting threads, mating cable assemblies, high temperatures.

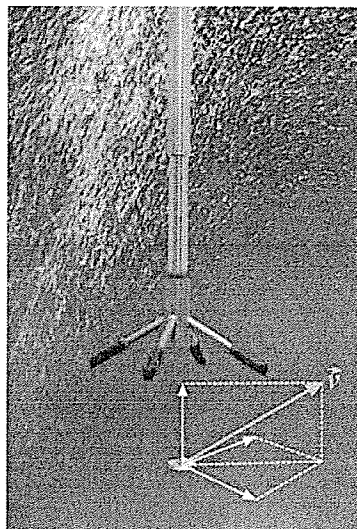
## B3 Thermocouples

ANSI Code	Alloy Combination		Color Coding  		Maximum Useful Temperature Range ++
	+ Lead	- Lead	Thermocouple Grade	Extension Grade	
<b>K</b>	CHROMEAL® NICKELCHROMIUM Ni-Cr	ALOMEGA® NICKEL-ALUMINUM Ni-Al (magnetic)			Thermocouple Grade: -328 to 2282°F -200 to 1250°C Extension Grade: 32 to 392°F 0 to 200°C
Maximum Thermocouple Grade Temperature Range	EMF (mV) Over Max. Temperature Range	Standard Limits of Error*** (above 0°C)	Special Limits of Error*** (above 0°C)		
-454 to 2501°F -270 to 1372°C	-6.458 to 54.886	greater of 2.2°C or 0.75%	greater of 1.1°C or 0.4%		

**B4 Flow meter****Specifications**

Range:	0.3-15 FPS (0.1-4.5 MPS)
Accuracy:	0.1 FPS
Averaging:	True digital running average. Readings taken once per second.
Display:	LCD
Sensor Type:	Protected Turbo-Prop propeller with electro-magnetic pickup.
Weight:	2 Lbs (10 lbs. U.S., 14 lbs. international shipping weight)
Size:	Length: FP101 3' to 6'; FP201 5' to 15'
Materials:	PVC, anodized aluminum, stainless steel bearing
Power:	Internal watch type batteries/1 year life
Operating Temperature:	0° to 120° F
Carrying Case:	The Flow Probe is shipped in a padded carrying case.

## B5 ADV specifications



Power  
 DC Input 12–48VDC  
 Peak current 2.5A at 12VDC (user selectable)  
 Max. consumption, 200Hz 1.5W

Connectors  
 Bulkhead Splash proof connector or MCBH-12-FS, bronze (Impulse) – see also options below.  
 Cable Splash proof or PMCIL-12-MP – see also options below.

Environmental  
 Operating temperature  $-5^{\circ}\text{C}$  to  $45^{\circ}\text{C}$   
 Storage temperature  $-15^{\circ}\text{C}$  to  $60^{\circ}\text{C}$   
 Shock and vibration IEC 721-3-2

### Water Velocity Measurements

Range  $\pm 0.01, 0.1, 0.3, 1, 2, 4\text{ m/s}^{\dagger}$   
 (user selectable)  
 Accuracy  $\pm 0.5\%$  of measured value  $\pm 1\text{ mm/s}$   
 Sampling rate (output) 1–25Hz  
 1–200Hz (Vectrino<sup>®</sup> firmware)

<sup>†</sup> The velocity range is not the same in the horizontal and vertical direction. Please refer to the configuration software.

### Sampling Volume

Distance from probe 0.05m  
 Diameter 6mm  
 Height (user selectable) 3–15mm

### Echo Intensity

Acoustic frequency 10MHz  
 Resolution Linear scale  
 Dynamic range 25dB

### Sensors

Temperature Thermistor embedded in probe  
 • Range  $-4^{\circ}\text{C}$  to  $40^{\circ}\text{C}$   
 • Accuracy/Resolution  $1^{\circ}\text{C}/0.1^{\circ}\text{C}$   
 • Time response 5 min

### Data Communication

I/O RS232. The software supports most commercially available USB–RS232 converters.  
 Baud rate 300–115200  
 User control Handled via Vectrino Win32<sup>®</sup> software, ActiveX<sup>®</sup> function calls, or direct commands.  
 Analog outputs 3 channels standard, one for each velocity component. Output range is 0–5V, scaling is user selectable.  
 Synchronization SynchIn and SynchOut

## Appendix C

### Journal Entries

**Dec.10, 2007** - New Energy Arrives in Winnipeg

**Dec.14, 2007** - Boat ready for launch

**Dec.18, 2007** - Boat anchored into final position

**Jan.10, 2008** - Turbine started. Ice caused load cell cable to break off. The load cell is now out of commission until retrieval in spring. Cameras are up and running.

**Jan.15, 2008** - Ice formation deemed excessive and hazardous (ice was chipped away). Ice formed across front creating an ice dam. This dropped the nose of boat to point where water was 1 ft away from splashing onto deck. The ice was broken off the front to allow flow to continue through the pontoons. The flow meter was damaged during deicing. The front bracket holding flow meter tube was broken and the entire tube was removed for repairs.

**Jan 16, 2008** - Ice was chipped away. The bow of boat rose back to ice free level. The hull was completely cleared except in rear quarters where there was no access to be able to chip at the ice. Major chunks of ice were sent directly into the turbine. The turbine stalled by a medium (3'x2'x1') iceberg (2:55pm) and once again on a large (5'x2'x1') iceberg (3:59pm). Heat trace (200W) was placed inside the pontoon nose piece. The flow meter was destroyed by ice formation or ice removal. Video captured during these two events. Pictures were taken. Flow was measured to be 2.6 m/s using handheld meter. Turbine was producing less than 1 kWe (suspiciously low).



**Jan 18, 2008** - Ice formed quickly. The 200W heaters were ineffective. A propane flame torch was bought to melt the ice. The blast of heat worked on thin sections of ice but not even a dent on major ice around the pontoons. Thermo couples were positioned and data started logging. Turbine stalled and took a half hour to warm up before restart attempt. It took considerable effort to restart (drill start for a few minutes). Video and sound of the turbine turning was captured.

**Jan 20, 2008** - The Scanfile program was started up for the thermocouple data. Data was transmitted online. Thermocouple #3 (gearbox) was suspect, giving larger than expected readings.

**Jan. 22, 2008** - Turbine stalled and froze into place. The unit would not turn under starter (drill). We continued to clear ice around the outside of the pontoons. While clearing ice at the front, large chunks flowed into the turbine and knocked it free. Turbine re-start was attempted, but would not get up to operating speed. Suspect friction with surface ice.

**Jan 23, 2008** - Continued de-icing. The outer perimeter was removed of ice and the rear was cleared except for the ice attached to motor. Ice between the pontoons remained. A jack was used to break the ice under the deck. It worked great in breaking the ice, but not removing it. Require a larger jack (longer stroke). Thermocouple #3 was removed from gearbox and placed in ambient to verify accuracy. Reads over +20C when ambient thermocouple (proven) reads -17C. Need to replace thermocouple and investigate further. Scanfile was found to have an error and stopped analyzing for almost a day.

**Jan 24, 2008** - Hardware Failure: underwater camera.

**Jan 25, 2008** - Underwater camera is fine, just a loose connection at the computer end. Purchased a 2 ton farmer's jack but was found to be ineffective. Ice had completely taken over the under side of the boat except for a small stream which passed through the front about halfway down the pontoon in the center of the boat. Ice was stubborn and would not crack. All day was spent on the front starboard quarter of ice which was successfully removed. The iceberg hit the camera and turbine at about 3:45pm. Camera was

knocked to a different view and needs to be adjusted once freed from ice. Flow was allowed to enter the front of the boat to encourage ice erosion. Heat trace was placed around the shaft of the turbine within the housing on deck.

**Jan 28, 2008** - New Energy arriving to see the situation first hand. They will attempt to clear the ice, restart turbine, and diagnose the low power output.

**Jan 30, 2008** - Ice cleared, Inner tubes were placed at the front of the pontoons to help with the icing issue. Thought is that the surface will encourage large formations of ice to break off and/or make removal easier. New Energy assessed the inverter settings and took flow reading of 1.7 m/s.

**Jan 31, 2008** - Started uploading power data; set up synchronization with data taker. Vibration sensors were mounted and recorded at an independent frequency (1 Hz).

**Feb. 3, 2008** - Turbine stalled at approx 23:43 Feb. 3, 2008.

**Feb 5, 2008** - Turbine started around 4:20 pm. Power meter (3phase, 3wire, 2Element) is being logged and software is being updated to enhance power data capabilities (Scanfile 7.2.2). Underwater camera was pummeled while testing in the frigid tundra of Manitoba. May it rest in peace, united with its crowbar comrades at the bottom of the river. Inner tube was ineffective in preventing the formation of ice, but made it easier to remove. Inner tube was replaced by white boat bumper. PVC pipe was sliced and placed onto the chain so that the flow was smooth around the tube instead of splashing around the chains.

**Feb 5-7, 2008** - Program was updated in an attempt to control the graphing situation as there are some bugs in the program causing bad graphs. The raw data is logging fine but graphs are giving problems. Remote desktop can be a slow connection so this is a slow process.

**Feb. 7 2008** - Noticeable jump in power. Inquire with hydro as to their flow for the day. Power jump occurred around 6pm.

**Feb. 8 2008** - Chipped away minor ice build up. PVC pipe froze over as well as white boat bumper. Data was unloaded from boat computer onto backup hard drive. Data system was restarted, programmed to download power data per day and delete old log every night at 11:58pm. It was unsuccessful, logging continuously. Also, the power meter would log partial data every now and then. This would cause distortion and false values in the power graph.

**Feb. 10 2008** - It was found that the data is being logged quicker than it can be processed. There is a back log of data. Need to up the intervals from 5 min to 10 min and see if that works. Scanfile was updated to eliminate power data abnormalities. If voltage or current was less than zero, data was replaced with older data for graphing purposes. Raw data remains untouched.

**Feb. 11, 2008** - lost communication with boat. Last data acquired at 8:25pm. Status: unknown.

**Feb. 12, 2008** – The bow of the boat submerged briefly with catastrophic consequence. Boat was dragged under water level, boom was floated and pushed back, destroying data shed as well as taking out some rails of the boat. Some equipment was salvaged and boat sustained a heavy hit. Boat was de-iced and heaters were re-established to warm the turbine for possible restart or removal.

**Feb. 13, 2008** - New data taker, wireless transmitter, and monitor are needed. Boat computer was found to be operational. New cameras were ordered.

**Feb. 15, 2008** - New aluminum lock box (DAQ box) was purchased to house computer and data taking equipment. Power meter was found to be non operational. New wireless transmitter received from Manitoba Hydro. DAQ box was fitted with insulation and cut holes for cables. Operational status of the data taking equipment (cpu and power meter) was checked. Power meter was non operational.

**Feb. 16, 2008** - Ice removal took 5-6 hours. An ice pick was lost into the river near the turbine and the pick's safety line got snagged on the turbine blade and shaft. Wire was unwound around the shaft. Underwater camera was used to precisely pick out the wire which was wrapped around the airfoil. Turbine was restarted and turning normally. It was easy to start, minimal effort to get free wheeling, and then started with drill quickly. All Ice was removed from front, sides, and most of the underneath. One camera was operational and started recording continuously. Camera feed was online but with intermittent access due to poor connectivity between boat and trailer (20%).

**Feb. 19, 2008** - Antenna extension requested to improve connectivity between boat and ATCO computers. It may take some time to be received.

**Feb. 20, 2008** - Power meter was found to be once again operational, unexplainable other than warm indoor climate helped. Power lines were reestablished on the boat from generator to power analyzer, no load on turbine yet. Power cable not connected to inverter in the trailer. Second camera was found to be non operational when set up. Software re-programmed to collect, copy, and upload power data. Flow taken at 5pm found to be 2.5 m/s. No load voltage was around 90 V. Ice was removed from most of the exterior and around the turbine. Power data was found to have random sets of zeros for phase data of B and C. All three phase Voltages are logged consistently. DAQ system is to be free of timing error.

**Feb. 21, 2008** - Power data suggests that turbine stalled at 12:18:40 am on this date.

**Feb. 26, 2008** – Turbine was restarted and a load was added while power measurements were taken directly. Power output was connected to heaters on board. 600 W of load stalled the turbine. New data taker arrived and was missing vital components (power supply, serial cable). The ice from the stern was removed and the tail end rose out of the water by at least a foot.

**Feb. 29, 2008** - Data taker was connected on board. Temperature sensors were connected and logging, however issue with deload became apparent. Turbine continued to turn at no load rpm.

**Mar. 4, 2008** - Boat was de-iced. Steel pipes holding underwater camera and flow meter were re-installed. Flow started logging. The vibration of the camera and flow meter poles dominate the vibrations felt on the boat. You can feel the vibration of the poles while standing on the boat. Efforts were made to tighten and secure the pipes to reduce vibration but the depth of the poles coupled with the force of the water, elasticity of the pipe and more importantly the simplicity and under design of the pipe clamps to the boat, the poles vibrate significantly. The turbine was found stalled and was restarted. Lanyard found caught in turbine.

**Mar. 7, 2008** - Boat was de-iced and inverter was turned on. Turbine was found to be stalled and was re-started.

**Mar. 11, 2008** - ADV measurement taken. Issue with communications between ADV and computer hindered the attempt to take readings, hence none were taken. Communication issue was due to incompatibility between RS-232 and USB. Digimerge interfered with COM1 so DT85 was not de-loaded since around 2pm. Data is being stored locally on the data taker but is not being downloaded onto computer.

**Mar. 14, 2008** - Data logging was restarted. ADV take 2 was unsuccessful due to low density of particles in the water. Too little back scatter resulted in only noise being recorded. Communications issue before was resolved.

**Mar. 17-19, 2008** - Boat was removed from the water. 25 kWe unit arrived on-site. All data taking has halted for spring break up.

**Mar. 20, 2008** - Boat computer data was backed up.

**Mar. 21, 2008** - Video cameras back online to capture ice break up and look at the size of the icebergs which float down river.

**Mar. 27, 2008** - Cameras repositioned to view boat on shore. When setting up camera an oil leak was spotted to come from the gearbox housing.

**Mar. 30, 2008** - Got MSDS for oil and found that it was non-toxic. Clean up of site took place.

**Apr. 11, 2008** - Digipro server was shut off by unknown reason. System was restarted.

**Apr. 15, 2008** - Ice floated by and was captured on video. Time: 11:53:55 caught by Craig of NECI. Today generator was removed and brought back to shop. It will be fitted to a motor and tested at HVDC.

**April 21, 2008** - Ice spotted at 15:23, 15:26:55, and 15:28:20. There appears to be small chunks almost slushy like, but not big icebergs as anticipated. It was believed to be passive frazil ice.

**May 8, 2008** - Spring break up data was deleted by software when over-writing the HD. 1 Month of video was lost. Icebergs found on April 21 were captured

**May 20, 2008** - DAQ box was modified to have easy connection to instruments on the exterior of the box. The internal equipment was organized so that the computer and DAQ system may be accessed with minimal opening of the box to avoid rain exposure.

**June 2, 2008** – Hydro plant shut down offered perfect opportunity to re-claim the anchoring chains from off the river bed. The 9/16" line upstream of the load cell was snagged on large jagged rocks. A winch was required to pull it up. The load cell was recovered and found the connection severed at the junction with the load cell. The right angled wired connection plug was sheared off. Decision was made to swap with the second load cell for summer testing.

**June 5, 2008** - Load cell was retrofitted with additional support. A PVC pipe was used to encase the right angle junction and protect the weak connection. The pipe was filled with foam and the exiting wire was passed through a heavier duty plastic wire conduit. The boat was anchored back into position and turbine was lowered and started (free-wheeling).

**June 6, 2008** - Instrumentation was reconnected and data started logging. Power data started logging. The turbine was CONNECTED TO THE GRID at 7:30 pm. Max power was found to be around 700 W as expected; flow was around 2.6 m/s before flow meter correction. ADV flow measurements were taken.

**June 7, 2008** - Turbine support arms were changed to steel profile blades. Output increased to 1.5 kWe. Data was logged. In evening Turbine was moved to the front of boat and flow meter stopped working. Power continued to log. A log got jammed on the turbine around 16:20 pm.

**June 8, 2008** - Turbine was put back into rear position and aluminum profiled arms were installed. Turbine had a significantly reduced wake, but power output remained similar as steel profiled arms. Flow was found to be lower, thus improving efficiency.

**June 9, 2008** - Boat re-docked and turbine removed and research vessel was prepped for 25 kWe system.